THESIS DEFENDED BY

**Laura Lizeth López de la Torre**

AND APPROVED BY THE FOLLOWING COMMITTEE


Dr. Miguel Avalos Borja
*Supervisor*

Dr. Björn Winkler
*Co-supervisor*


Dr. Karsten Knorr
*Committee Member*

Dr. Armando Reyes Serrato
*Committee Member*


Dr. Noboru Takeuchi Tan
*Committee Member*


Dra. Laura Cecilia Viana Castrillón
*Graduate Studies Coordinator of
the Physics of Materials Department*

Dr. Raúl Ramón Castro Escamilla
*Director of Graduate Studies*

May 5th, 2006.

CENTRO DE INVESTIGACIÓN CIENTÍFICA Y DE EDUCACIÓN SUPERIOR DE ENSENADA



Graduate Program in Science
in Physics of Materials

RELATIONS OF ELECTRONIC STRUCTURE AND MACROSCOPIC PROPERTIES ON BINARY TANTALUM COMPOUNDS

**Thesis**

submitted in partial fulfillment of the requirements for the degree of
**DOCTOR IN SCIENCE**

presented by:

Laura Lizeth López de la Torre

Ensenada, Baja California, México. May, 2006.

**ABSTRACT** of the thesis of **LAURA LIZETH LÓPEZ DE LA TORRE**, submitted in partial fulfillment of the requirements for the degree of **DOCTOR IN SCIENCE** in **PHYSICS OF MATERIALS**. Ensenada, Baja California, México. May 2006.

RELATIONS OF ELECTRONIC STRUCTURE AND MACROSCOPIC PROPERTIES ON BINARY TANTALUM COMPOUNDS

Abstract approved by:

<table>
<tr><td>Dr. Miguel Avalos Borja</td><td>Dr. Björn Winkler</td></tr>
<tr><td><em>Supervisor</em></td><td><em>Co-supervisor</em></td></tr>
</table>

## ABSTRACT

This thesis describes studies regarding some mechanical properties of several binary tantalum compounds through *ab initio* calculations. In this work, tantalum carbides TaC and $Ta_2C$, as well as tantalum nitrides $\delta$-TaN and $\epsilon$-TaN, were chosen due to the unusual combination of physical and chemical properties that they exhibit. Although these compounds contain the same elements, Ta and C, and Ta and N, the differences in stoichiometry or crystal structure conduct to different mechanical behaviour. Studies on crystal tantalum and diamond were also performed.

Elastic properties, such as bulk and Young moduli, Poisson ratio and the elastic stiffness coefficients, for TaC, $Ta_2C$, $\delta$-TaN and $\epsilon$-TaN, were determined, along with phonon dispersion curves for tantalum, diamond, TaC and $Ta_2C$. In addition, the phonon density of states and heat capacity for tantalum, diamond, TaC and $Ta_2C$ were obtained. For the TaC case, the elastic stiffness coefficients $c_{11}$ and $c_{44}$, as well as the heat capacity curve, were obtained experimentally.

*Ab initio* total-energy plane-wave pseudopotential calculations were performed based on the Density Functional Theory (DFT). The exchange-correlation potential has been determined using the Local Density Approximation (LDA) and the Generalized Gradient Approximation (GGA). The code ABINIT, which uses norm-conserving pseudopotentials, was used to determine the phonon dispersion curves. On the other hand, elastic properties were determined with the CASTEP code, that uses ultrasoft pseudopotentials.

Results of elastic properties were compared with early published data, when available, and sets of predicted values are given of properties not studied yet or with notorious discrepancies in their published values. The phonon dispersion curves and specific heat curves for Ta, diamond and TaC agree within a few percent with experimental values already published and with those measured here for the specific heat of TaC. For $Ta_2C$ no experimental data is available and its phonon dispersion curve and specific heat curve can be seen as a prediction for future measurements.

## Relaciones entre la estructura electrónica y las propiedades macroscópicas de compuestos binarios de tantalio

En esta tesis se describe el estudio de las propiedades mecánicas de algunos compuestos binarios de tantalio mediante cálculos *ab initio*. Para este trabajo se seleccionaron los carburos de tantalio TaC y $Ta_2C$, así como los nitruros de tantalio $\delta$-TaN y $\epsilon$-TaN, dada la combinación de propiedades físicas y químicas que poseen. A pesar de que estos compuestos contienen los mismos elementos, Ta y C, o Ta y N, las diferencias en su estequiometría o en su estructura cristalina conducen a diferentes comportamientos mecánicos. De la misma manera que los compuestos antes mencionados, se estudiaron también el tantalio y el diamante.

Entre las propiedades elásticas en estudio se encuentran los módulos de volumen y de Young, la razón de Poisson y los coeficientes de elasticidad, que se determinaron para los compuestos TaC, $Ta_2C$, $\delta$-TaN y $\epsilon$-TaN. Además, se obtuvieron las curvas de dispersión de fonones para el tantalio, diamante, TaC y $Ta_2C$, así como la densidad de estados de fonones y el calor específico. En el caso del TaC, se determinaron experimentalmente los coeficientes elásticos $c_{11}$ y $c_{44}$ y la capacidad calorífica utilizando un monocristal.

Este estudio se realizó mediante cálculos *ab initio* de la energía total basados en la teoría del funcional de densidad (Density Functional Theory, DFT), utilizando pseudopotenciales y una base de ondas planas. El potencial de intercambio y correlación se calculó mediante las aproximaciones de la densidad local (Local Density Approximation, LDA) y del gradiente generalizado (Generalized Gradient Approximation, GGA). Las curvas de dispersión se calcularon utilzando el programa ABINIT, el cual utiliza pseudopotenciales que conservan la norma, mientras que las propiedades elásticas se calcularon con el programa CASTEP, que utiliza pseudopotenciales ultrasuaves.

Los resultados obtenidos correspondientes a las propiedades elásticas han sido comparados con valores reportados en la literatura. En los casos en que no se encontraron valores reportados, o que éstos muestran notorias discrepancias, los valores obtenidos del cálculo se consideran como predicciones de dichas propiedades. Las curvas de dispersión de fonones y del calor específico para Ta, diamante y TaC concuerdan razonablemente con los valores experimentales reportados en la literatura y, en el caso del TaC, con los valores experimentales de capacidad calorífica determinados aquí. Por otra parte, no se encontraron valores reportados de dispersión de fonones ni del calor específico del $Ta_2C$, por lo que los resultados obtenidos del cálculo se consideran como una de las mencionadas predicciones a estos valores.

Palabras clave: cálculos *ab initio*, calor específico, carburos, fonones, funcional de la densidad, nitruros, propiedades elásticas.

*Resumen Ejecutivo*

# Relaciones entre la estructura electrónica y las propiedades macroscópicas de compuestos binarios de tantalio

## Introducción

El presente resumen describe el trabajo de tesis doctoral sobre el estudio de las propiedades mecánicas de diversos compuestos binarios de tantalio, determinadas mediante cálculos de primeros principios de la energía total, utilizando la teoría del funcional de densidad (DFT, por sus siglas en inglés), pseudopotenciales y una base de ondas planas.

Los compuestos estudiados son los carburos TaC y $Ta_2C$ y los nitruros $\delta$-TaN y $\epsilon$-TaN. Estos compuestos fueron seleccionados para su estudio ya que presentan una combinación poco usual de propiedades físicas y químicas. A pesar de que estos compuestos están formados por los mismos elementos, Ta y C, y Ta y N, las diferencias en estequiometría o en estructura cristalina los hacen presentar diferentes comportamientos mecánicos.

## Descripción general de los compuestos en estudio

Los carburos y nitruros de los metales de transición de los grupos IV (Ta, Zr y Hf) y V (V, Nb y Ta) poseen propiedades que los mantienen en el interés de la investigación científica básica y del área tecnológica. En el caso de los carburos, sus principales aplicaciones comerciales son como abrasivos, como materiales de corte y en superficies duras, debido a la alta dureza y durabilidad que presentan [1, 2, 3]. Muchos carburos binarios de metales de transición muestran valores de microdureza entre 2000 y 3000 kg/mm$^2$ [1], lo que los hace comparables a la dureza del diamante de 9000 kg/mm$^2$ [4], que es el material más duro que se conoce actualmente. Su alto punto de fusión, su excelente resistencia al esfuerzo a altas temperaturas y su buena resistencia a la corrosión los convierte en materiales idóneos para la fabricación de filamentos y cabezas de impresión en ciertos aparatos [5]. Por otra parte, los carburos y nitruros de metales de transicion son utlizados como recubrimientos ópticos, contactos eléctricos y barreras de difusión en las áreas de electrónica, ingeniería eléctrica y en las ciencias de materiales a altas temperaturas [6, 7].

### TaC

El carburo de tantalio, TaC, es uno de los compuestos más representativos de los carburos de metales de transición y existe en un amplio intervalo de estequiometrías. Muestra una

estructura cristalina del tipo cloruro de sodio (ver figura 5.1) correspondiente al grupo espacial $Fm\bar{3}m$ (225). Tiene una parámetro de red de $a$=4.454 Å (ver tabla 5.1) y una densidad de 14.498 g/cm$^3$ [8]. Posée propiedades muy sobresalientes tales como una alta dureza a temperatura ambiente, un alto punto de fusión (3880 °C) y resistencia al ataque químico y al choque térmico [3, 9]. Además, el TaC muestra una excelente conductividad electrónica (42.1 $\mu\Omega$ cm a 25 °C), buena conductividad térmica (cerca de 22 Wm$^{-1}$C$^{-1}$) y alta resistencia a la oxidación [3, 10, 11]. Sus notables propiedades físicas y químicas son atribuidas a los enlaces tipo covalente-metálico que muestra [12, 13, 14].

Varios autores han estudiado las propiedades elásticas y los coeficientes elásticos de rigidez del TaC mediante diferentes métodos, tanto experimentales como teóricos, desde la década de los 60's. [12, 15, 16, 17]. Sin embargo, los valores de los coeficientes elásticos de rigidez publicados anteriomente muestran diferencias entre sí de hasta un 50%. Por otro lado, las curvas de dispersión de fonones para el TaC han sido medidas por Smith y Gläser [18] y Smith [19], y reproducidas con buena corcondancia mediante diversos modelos teóricos tales como la aproximación de la respuesta dieléctrica [20], el modelo de capas [21, 22] y el modelo de capas de fuerza entre tres cuerpos [23]. Sin embargo, no hay ninguna referencia a estudios donde se determinen las frecuencias fonónicas del TaC utilizando cálculos de primeros principios con DFT.

## $Ta_2C$

El Ta$_2$C presenta una estructura del tipo CdI$_2$ basada en una red hexagonal compacta formada por los átomos de tantalio, mientras que los átomos de carbono ocupan la mitad de los sitios octaedrales [24, 25]. Además, muestra una simetría triagonal correspondiente al grupo espacial $P\bar{3}m1$ (164). La figura 5.2 muestra la celda convencional del Ta$_2$C con parámetros de red de $a$=3.1059 Å y de $c$=4.946 Å, y una densidad de 15.02 g/cm$^3$ [26]. A diferencia de los monocarburos de tantalio, cuyas propiedades electrónicas y mecánicas han sido investigadas experimentalmente y teóricamente, el Ta$_2$C no ha sido estudiado todavía [9].

## $\epsilon$-TaN y $\delta$-TaN

La fase más estable de los nitruros de tantalio es la fase $\epsilon$-TaN, con una composicón química de la forma Ta$_{1.0}$N$_{1.0}$ y con simetría hexagonal [27]. Tiene parámetros de red de $a$=5.1918 Å y de $c$=2.9081 Å, una densidad de 14.306 g/cm$^3$ y pertenece al grupo espacial $P6/mmm$ (191) [28]. La fase $\epsilon$-TaN cambia, a través de una transición de fase a altas temperaturas y altas presiones, de una estructura hexagonal a una estructura tipo cloruro de sodio conocida como la fase $\delta$-TaN [29, 30]. Sin embargo, la fase $\delta$-TaN es más utilizada en aplicaciones comerciales que la fase $\epsilon$-TaN.

La fase $\delta$-TaN es un compuesto comúnmente no estequiométrico [31] con un parámetro de red de $a$=4.339 Å (ver figura 5.3). Al igual que el TaC, pertenece al grupo espacial $Fm\bar{3}m$ (225) y tiene una densidad de 15.842 g/cm$^3$ [32]. Es un material superconductor con una temperatura de transición de 6.5 K in bulto [33] y 4.8 K como película delgada [29].

## Objetivos

En el presente trabajo se determinaron algunas propiedades mecánicas macroscópicas de los carburos y nitruros de tantalio TaC, $Ta_2C$, $\delta$-TaN y $\epsilon$-TaN, mediante cálculos de primeros principios. Se determinaron, además, las propiedades estructurales así como las propiedades elásticas para el tantalio y el diamante.

Entre la propiedades mecánicas estudiadas se encuentran los coeficientes elásticos de rigidez ($c_{ij}$), el módulo de volumen ($B$) y su primera derivada ($B'$), el módulo de Young ($E$) y la razón de Poisson ($\nu$). También se calcularon la curvas de dispersión de fonones para el tantalio, el diamante y los carburos TaC and $Ta_2C$. A partir de las relaciones de dispersión de fonones calculadas, se determinó la densidad de estados de fonones y la capacidad calorífica para estos mismos compuestos. Dado que el TaC es el compuesto considerado de mayor relevancia en este estudio por sus aplicaciones comerciales, además de ser el más fácil de obtener como monocristal, sus coeficientes elásticos de rigidez y su capacidad calorífica, fueron determinados experimentalmente.

## Métodos

En este estudio se realizaron cálculos *ab initio* de la energía total basados en la teoría del funcional de densidad (Density Functional Theory, DFT) [34, 35], utilizando pseudopotenciales y una base de ondas planas. La energía de intercambio y correlación se calculó mediante la aproximación de la densidad local (Local Density Approximation, LDA) [35] y la aproximación del gradiente generalizado (Generalized Gradient Approximation, GGA) [36]. Las curvas de dispersión se calcularon utilizando el código ABINIT [37], el cual utiliza pseudopotenciales del tipo Hartwigsen-Goedecker-Hutter (HGH) [38] que conservan la norma para cálculos con LDA, y del tipo Troullier-Martins [39], para cálculos con GGA. Las propiedades elásticas se calculan utilizando el código CASTEP [40], el cual utiliza pseudopotenciales ultrasuaves [41]. Los cálculos se efectuaron considerando cristales perfectos en bulto y a una temperatura de 0 K.

Las mediciones realizadas de los coeficientes elásticos de rigidez se hicieron mediante una técnica de resonancia de ultrasonido aplicada a un monocristal de TaC. Por otra parte, las mediciones de la capacidad calorífica de una muestra de TaC, en forma de polvo, se llevaron a cabo con un calorímetro de barrido diferencial.

## Resultados y Discusiones

### Tantalio y Diamante

Previo a los estudios de los carburos y nitruros de tantalio se llevaron a cabo cálculos de las propiedades mecánicas del tantalio y el diamante, con la finalidad de determinar los parámetros esenciales y la precisión de los cálculos. Los resultados y las discusiones en referencia a estos compuestos se presentan a continuación.

*Tantalio*

El tantalio es un metal de transición que se cristaliza en una estructura tipo cúbica centrada en el cuerpo (*bcc*), con un parámetro de red de $a$=3.305 Å y pertenece al grupo espacial $Im\bar{3}m$ (229). Con la finalidad de determinar los parámetros óptimos para los cálculos, se realizaron pruebas de convergencia para la energía de corte de las ondas planas (figura 4.2) y del número de puntos $k$ (figura 4.3) necesarios para el muestreo de la zona de Brillouin. Los valores obtenidos para estos parámetros, y utilizados en los siguientes estudios, son de 1360.5 eV (50 Hartree) para la energía de corte y una malla de $6 \times 6 \times 6$ de puntos $k$. La relación de la energía total con el parámetro de red se muestra en la figura 4.4. El parámetro de red correspondiente a la energía mínima se determinó por un ajuste con un polinomio cúbico a los datos anteriores, obteniendo el valor de $a$=3.255 Å. También se utilizó el procedimiento de minimización de energía encontrado en el código y con el cual se obtuvo un valor de $a_0$=3.251 Å.

La relación de la presión con el volumen, obtenida mediante un ajuste con la ecuación de estado Birch-Murnaghan a 3er orden, se muestra en la figura 4.5. Los valores a presión cero encontrados son de $v_0$=34.39(2) Å$^3$ para el volumen, $K$=221(9) GPa para el módulo de volumen y $K'$=4(1) para la primera derivada del módulo de volumen (los números entre paréntesis indican la incertidumbre en los datos). El parámetro de red asociado a este volumen es de $a_0$=3.25(2) Å. La tabla 4.1 muestra los valores publicados y obtenidos aquí de los cálculos del parámetro de red, el módulo de volumen y su primera derivada para el tantalio. Los parámetros de red concuerdan en un 2% con el valor experimental publicado de $a_0$=3.305 Å [42]. Por otra parte los valores para el módulo de volumen y su primera derivada muestran una concordancia razonable con respecto a los valores de Cynn y Yoo [43] así como también con los valores de Katahara *et al.* [44]. La figura 4.7 muestra la curva de dispersión de fonones calculada para el tantalio donde se observa que los valores de dicha curva son 0.5 THz más grandes que los valores experimentales publicados por Woods [45].

*Diamante*

El diamante se seleccionó por ser un material a base de carbono, poseer una estructura cúbica y mostrar el valor más alto conocido de dureza. Pertenece al grupo espacial $Fd\bar{3}m$ (227) [46] y tiene un parámetro de red de $a$=3.5668 Å. Los parámetros óptimos utilizados en los cáclulos fueron una energía de corte de 1360.5 eV (ver figura 4.9) y una malla de puntos $k$ de $10 \times 10 \times 10$ (figura 4.10). La relación de la energía total con el parámetro de red se muestra en la figura 4.11. Los valores encontrados para el parámetro de red son de $a$=3.536 Å, utilizando un ajuste con un polinomio cúbico, y de $a$=3.531 Å utilizando el código ABINIT.

La variación del volumen de la celda del diamante a diferentes presiones, obtenida mediante un ajuste a la ecuación de estado de Brich-Murnhagan a 3er orden, se muestra en la figura 4.12. Los valores obtenidos del ajuste para el volumen a presión cero es de $v_0$=43.62(2) Å$^3$, para el módulo de volumen es de $B$=471(8) GPa, y para la primera derivada del módulo de volumen es de $B'$=3.7(2). El parámetro de red asociado a estos valores es $a_0$= 3.52(2) Å. La tabla 4.3 muestra los valores obtenidos del cálculo y los valores publicados del parámetro de red, módulo de volumen y su primera derivada. El valor de $a$=3.531 Å es menor en un 1% respecto al valor reportado por Straumanis & Aka [46] de $a_0$=3.5668 Å. Además, el valor de

$a$=3.52(2) Å obtenido por el ajuste a la ecuación de estado, y el de $a$=3.536 Å obtenido por el ajuste al polinomio cúbico concuerdan en un 2% y en 1%, respectivamente, al compararlos con dicho valor experimental. Por otra parte, el módulo de volumen de $B$=471(4) GPa obtenido en el ajuste a la ecuacón de estado concuerda en un 6.5% con el valor de $B$=442 GPa reportado por McSkimin *et al.* [47]. La figura 4.14 muestra la curva de dispersión de fonones calculada para el diamante, donde se observa una excelente concordancia con los valores experimentales publicados por Warren *et al.* [48] y Warren *et al.* [49].

**Carburos y Nitruros de Tantalio**

Las propiedades elásticas de los carburos y nitruros de tantalio se estudiaron utilizando los códigos ABINIT y CASTEP. Los detalles de los cálculos, los resultados y sus correspondientes discusiones se presentan a continuación.

*TaC*

Los cálculos para el TaC utilizando el código ABINIT se hicieron utilizando las aproximaciones de la densidad local (LDA) y del gradiente generalizado. En el caso de LDA, se utilizaron pseudopotenciales del tipo Hartwigsen-Goedecker-Hutter para el C ($4\,e^-$) y para el Ta ($13\,e^-$). Para GGA se usaron pseudopotenciales del tipo Troullier-Martins para C ($4e^-$) y Ta ($5^-$). Se llevaron a cabo estudios de optimización de los parámetros del cálculo donde se obtuvieron los valores para la energía cinética de corte de las ondas planas de $E_{cut\_LDA}$ =1360.5 eV y $E_{cut\_GGA}$= 2176.8 eV. El muestreo de la zona de Brillouin se basó en el método establecido por Monkhorst y Pack [50], el cual se encuentra implementado en ABINIT. Para dicho muestreo una red de tamaño de $8 \times 8 \times 8$ ostró mejores resultados.

La relación de la energía total con el parámetro de red se muestran en las figuras 5.5 y 5.6 para LDA y GGA respectivamente. Estas curvas fueron ajustadas a un polinomio cúbico para determinar el parámetro de red correspondiente a la mínima energía. Los parámetros de red que resultaron del ajuste son $a_{0\_LDA}$=4.414 Å y $a_{0\_GGA}$=4.527 Å. Además, se minimizó la energía del sistema usando ABINIT, donde los valores obtenidos fueron $a_{0\_LDA}$= 4.413 Å y $a_{0\_GGA}$= 4.526 Å. Estos últimos valores del parámetro de red del TaC fueron los utilizados en los cálculos de las propiedades elásticas. Las figuras 5.7 y 5.8 muestran la relación presión-volumen para el TaC. Estos valores fueron ajustados a la ecuación de estado de Birch-Murnaghan a tercer orden. Para LDA, el parámetro de red a cero presión es $a_{0\_LDA}$=4.406(2) Å y el volumen $v_{0\_LDA}$=85.65(2) Å$^3$. El módulo de volumen resultó ser de $B_{LDA}$=365(4) GPa con un valor de su primera derivada de $B'_{LDA}$=3.6(1). Para GGA, el parámetro de red a cero presión fue $a_{0\_GGA}$=4.52(2) Å con un volumen de $v_{0\_GGA}$=92.79(2) Å$^3$. El módulo de volumen tuvo un valor de $B_{GGA}$=316(2) GPa y $B'_{GGA}$=3.99(8). Por otra parte, en los cálculos realizados con CASTEP se utilizó la aproximación del gradiente generalizado y pseudopotenciales ultrasuaves. La energía de corte fue de 380 eV y para el muestreo de la zona de Brillouin se usó una malla de tipo Monkhorst-Pack de $16 \times 16 \times 16$ puntos $k$. La relajación de la estructura del TaC (con parámetros de la celda fijos) dió como parámetro de red el valor de $a_0$=4.525 Å.

Dada la simetría cúbica de los cristales de TaC, solamente es posible tener tres coeficientes elásticos de rigidez: $c_{11}$, $c_{12}$ y $c_{44}$. Debido a la cercana relación de los coeficientes elásticos

y los módulos de volumen y de Young, y de la razón de Poisson, es posible determinar estas propiedades si los coeficientes son conocidos y viceversa. Los coeficientes de rigidez obtenidos en estos cálculos son $c_{11}$=621(3), $c_{12}$=155.3(2) y $c_{44}$=166.8(3) GPa, mientras que los módulos de volumen y de Young obtenidos de estos coeficientes son $B$=318(4) y $E$=550 GPa, respectivamente. La razón de Poisson calculada tiene un valor de $\nu$=0.21.

Se midieron los coeficientes de rigidez $c_{11}$ y $c_{44}$ y la densidad de masa de un monocristal de TaC con una técnica de ultrasonido. El monocristal tenía la forma de un disco de 5 mm de diámetro y 1.4 mm de espesor. Las caras del disco estaban orientadas de manera paralela al plano (100). La técnica consiste en excitar y medir las frecuencias resonantes en la muestra provocadas con un transductor de cuarzo y, de éstas, determinar los coeficientes elásticos de rigidez. Los valores obtenidos de la medición son $c_{11}$=595(2) y $c_{44}$=153(2)GPa, y $\rho$=14.64(5) g/cm$^3$.

La tabla 5.3 presenta los valores de parámetro de red y de densidad de masa del TaC, teóricos y experimentales, determinados en este trabajo y los reportados en la literatura. El parametro de red del TaC esta bien establecido como $a_0$=4.4547 Å y su densidad como $\rho$=14.5 g/cm$^3$ [8], por lo que el valor de la densidad reportada por Brown *et al.* [16] es inconsistente. Todos los demás valores experimentales, incluyendo el nuestro, están dentro del 1%. En lo que respecta al parámetro de red, los valores obtenidos de los cálculos que utilizaron GGA con ambos códigos se encuentran dentro del 2% respecto al valor experimental mencionado anteriormente, mientras que la densidad de masa esta dentro del 5%. Esta sobreestimación en los valores es característica de GGA. Por otro lado, los parámetros de red calculados usando LDA están dentro del 2% y la densidad de masa dentro de un 4%, comparados con los valores establecidos. De manera contraria a GGA, LDA tiende a subestimar el valor del parámetro de red. Estas diferencias también se observan en los valores reportados por Sahnoun *et al.* [51, 52].

No existen muchos valores reportados en la literatura de los coeficientes elásticos de rigidez y de los módulos de volumen y Young, y de la razón de Poisson para el TaC. Aquellos que encontramos, junto con los obtenidos en este estudio, tanto teóricos y experimentales, se encuentran resumidos en la tabla 5.4. En ella es posible notar las grandes discrepancias de hasta un factor de dos en los coeficientes $c_{11}$ y $c_{12}$ que no se justifican por diferencias en la estequiometría de las muestras usadas en las mediciones. Como los valores de $c_{11}$ obtenidos por Brown *et al.* [16], Jun *et al.* [17], Weber [22] y aquí teórica y experimentalmente concuerdan razonablemente, se puede concluir que el valor más problable, obtenido de promediar los valores mencionados, es de $c_{11}$=606 GPa. Haciendo un análisis similar para $c_{12}$ se puede deducir que los valores de Krajewski *et al.* [12], Bartlett y Smith [15] y Sahnoun *et al.* [52] son demasiado bajos por más de 50 GPa. Promediando los valores que concuerdan razonablemente, el mejor valor para $c_{12}$ es de 166 GPa. Previo a este trabajo sólo se había reportado una medición de $c_{44}$ = 79 GPa hecha por Bartlett y Smith. En su estudio los otros dos coeficientes también muestran valores muy pequeños, por lo que probablemente también lo es $c_{44}$. Además, los valores teóricos reportados por Sahnoun *et al.* utilizando LDA y GGA muestran serias discrepancias al compararlos con los demás valores. El valor de $c_{44}$=190 GPa determinado por Weber [22], el de $c_{44}$= 176 GPa calculado con LDA por Wu *et al.* [53] y aquellos obtenidos aquí por la teoría y el experimento, 153(2) y 166.8(3) GPa, concuerdan de manera aceptable. Esto sugiere que el mejor valor para $c_{44}$ es de 170 GPa.

La tabla 5.5 muestra algunos valores de los módulos de volumen y de Young y la razón de Poisson para el TaC encontrados en la literatura y los obtenidos aquí. La buena concordancia de los coeficientes $c_{ij}$ obtenidos por Brown *et al.* [16] y Jun *et al.* respecto a los valores calculados aquí implica que también los módulos de volumen y de Young presentan buena concordancia. Además, los valores reportados por Dodd *et al.* [54] también están en buena concordancia con los anteriores mencionados. Por lo tanto, se puede determinar un valor de $B$=335 GPa de las mediciones. Los valores de $B$=369.83 y $B$=397.3 GPa obtenidos de los cálculos con LDA hechos por Sahnoun *et al.*, concuerdan en un 9% con el valor de $B$=365(4) GPa obtenido aquí usando la misma aproximación. De forma similar los valores calculados con GGA por Sahnoun de $B$=318.98 y los calculados en este estudio con ambos códigos, de $B$=318(4) y $B$=316(2) GPa, muestran una concordancia de un 1%. Al realizar un análisis de los valores de las propiedades elásticas, se encontraron como los mejores valores el de $B$=335 GPa para el módulo de volumen y el de $B'$=4 para su primera derivada, y para el módulo de Young de $E$=550 GPa y $\nu \approx 0.22$ para la razón de Poisson.

Las curvas de dispersión de fonones para el TaC, calculadas usando ABINIT, en las direcciones de alta simetría se muestran en la figura 5.14. En esta figura se puede observar la gran brecha que separa las frecuencias acústicas de las ópticas. Las curvas de alta frecuencia se originan principalmente en los átomos de carbono, por su bajo peso molecular. Las curvas de dispersión obtenidas del cálculo reproducen las características principales de las curvas medidas por Smith y Gläser [18].

### $Ta_2C$

El estudio del $Ta_2C$ se realizó mediante cálculos con el código ABINIT usando LDA y pseudopotenciales del tipo Hartwigsen-Goedecker-Hutter para el C (4 e$^-$) y para el Ta (13 e$^-$). La energía de corte fue de $E_{cut}$ =1632.6 eV y para el muestreo en el espacio recíproco se usó una malla de puntos $k$ de $8 \times 8 \times 4$. La optimización geométrica de la estructura dió como parámetros de red los valores de $a_0$=3.089 Å y $c_0$=4.837 Å. Con el código CASTEP se calcularon las propiedades elásticas utilizando GGA, pseudopotenciales ultrasuaves, una energía de corte de 330 eV y una malla de puntos $k$ de $10 \times 10 \times 6$. La minimización de la energía realizada con el código dió como parámetros de red los valores de $a_0$=3.152 Åy $c_0$=4.99 Å.

La simetría hexagonal del $Ta_2C$ sólamente presenta cinco coeficientes elásticos de rigidez. Los valores obtenidos para estos coeficientes son $c_{11}$=445(4), $c_{12}$=172.6(1), $c_{13}$=143.8(1), $c_{33}$=492(4) y $c_{44}$=135.6(1) GPa. El módulo de volumen obtenido de estos coeficientes es de $B$=256(5) GPa y el módulo de Young para cada dirección es $E_x$=$E_y$=360.5 y $E_z$=425.1 GPa. También debido a su simetría, el $Ta_2C$ muestra seis valores de la razón de Poisson correspondientes a tensiones y esfuerzos en las direcciones $x$, $y$ y $z$, donde $x$ y $y$ son equivalentes. Esto da como resultado sólo tres valores, los cuales son $\nu_{xy}$=$\nu_{yx}$=0.32, $\nu_{zx}$=$\nu_{zy}$=0.23 y $\nu_{xz}$=$\nu_{yz}$=0.197. Hasta el momento no se han reportado valores de las propiedades elásticas del $Ta_2C$ para comparar con los valores que se obtuvieron aquí. La tabla 5.6 resume los datos calculados con ABINIT (LDA) y CASTEP (GGA) de los parámetros de red. De esta tabla se observa una sobreestimación de los valores calculados con GGA del 2% para $a_0$ y del 1% para $c_0$ en comparación con los valores experimentales de la base de datos ICDD [32]. Por otra parte, la subestimación de los valores obtenidos con LDA está dentro del 1% para $a_0$ y

del 2% para $c_0$. Como no hay valores experimentales disponibles de las propiedades elásticas del $Ta_2C$, los valores obtenidos del cálculo podrían considerarse como predicciones.

Las relaciones de dispersión de fonones en las direcciones de alta simetría se calcularon con el código ABINIT. Estas curvas se presentan en la figura 5.16. Debido a que el $Ta_2C$ tiene asociados tres átomos, sus curvas de dispersión presentan 9 ramas: 3 acústicas y 6 ópticas. De forma similar al TaC, una gran brecha, de 12 THz, separa a las frecuencias acústicas de las ópticas. Al tiempo de escribir esta tesis no han sido publicadas las relaciones de dispersión de fonones del $Ta_2C$, ni experimental ni teóricamente, por lo tanto las curvas obtenidas en este trabajo pueden considerarse como una predicción en futuras mediciones.

### $\delta$-TaN

Los cálculos para $\delta$-TaN realizados con el código ABINIT estuvieron basados en LDA. Se usaron pseudopotenciales del tipo Hartwigsen-Goedecker-Hutter para el N (5 $e^-$) y para el Ta (13 $e^-$). La energía de corte fue de $E_{cut}$ =1632.6 eV y la malla de puntos $k$ de $8 \times 8 \times 8$. La relación del parámetro de red y la energía total se muestra en la figura 5.17. El parámetro de red que minimiza la energía tiene un valor de $a_0$= 4.329 Å. De la optimización geométrica hecha con ABINIT se encontró un parámetro de red de $a_0$=4.3307 Å. La figura 5.18 muestra la relación presión-volumen para $\delta$-TaN. Estos datos fueron ajustados a la ecuación de estado de Birch-Murnaghan a tercer orden y los valores obtenidos del ajuste fueron de $a_0$=4.339(6) Å para el parámetro de red y de $v_0$=81.730(6) Å$^3$ para el volumen. El módulo de volumen fue de $B_0$=373(6) GPa, mientras que su primera derivada fue de $B'$=4(1). Las propiedades elásticas del $\delta$-TaN se obtuvieron con el código CASTEP usando GGA y pseudopotenciales ultrasuaves para Ta y N. La energía de corte fue de $E_{cut}$=380 eV, mientras que la malla de puntos $k$ del tipo Monkhorst-Pack fue de $16 \times 16 \times 16$. De la minimización de la energía se encontró como parámetro de red el valor de $a_0$=4.4905 Å. Los coeficientes elásticos obtenidos de este cálculo son $c_{11}$=700(5), $c_{12}$=128.8(7) y $c_{44}$=34.7(4) GPa. Los módulos de volumen y de Young obtenidos a partir de estos coeficientes son $B$=319(2) y $E$=659.7 GPa, respectivamente. El valor calculado de la razón de Poisson es de $\nu$=0.155.

La tabla 5.7 muestra los valores del parámetro de red $a_0$ y de la densidad de masa $\rho$ para $\delta$-TaN. Todos los parámetros de red obtenidos teóricamente se encuentran en buen concordancia con el valor experimental de $a_0$=4.339 Å reportados por la *National Bureau of Standards* [32]. Sin embargo, los valores obtenidos de los cálculos con LDA en este estudio y por Sahnoun *et al.* [52] muestran una subestimación de un 1%, mientras que los cálculos con GGA están sobreestimados por $\approx$ 3.5 y 2%, respectivamente. A consecuencia de estos valores la densidad de masa calculada presenta una sobreestimación del 1%, usando LDA, al comparar con el valor experimental de 15.842 $g/cm^3$, y una subestimación del 10% cuando se usó GGA. Los valores de los coeficientes elásticos de rigidez para $\delta$-TaN reportados en la literatura y aquellos obtenidos en este estudio se muestran en la tabla 5.8. Para $c_{11}$, el valor calculado de 700(5) GPa concuerda dentro del 3.5% en comparación del valor de 675.95 GPa calculado por Sahnoun *et al.* [52] usando la misma aproximación (GGA).

Por otro lado, los valores obtenidos por Sahnoun (886.9 GPa), y Wu *et al.* [53] (783 GPa), usando LDA muestran una concordancia del 26.7% y del 11.85%, respectivamente. Sin embargo, el valor reportado por Sahnoun es cerca de 100 GPa mayor en comparación con

el valor reportado por Wu. Dado que los valores de Sahnoun *et al.* (usando GGA), Wu *et al.* y los obtenidos aquí muestran una concordancia rasonable, un promedio de estos valores nos indican que el valor más probable es $c_{11}$=720 GPa. Para el caso de $c_{12}$, todos los valores muestran una concordancia razonable, por lo que de manera similar a $c_{11}$, el valor de $c_{12}$=150 GPa es una buena predicción. Aunque todos los valores de la tabla 5.8 fueron obtenidos teóricamente usando DFT, se pueden observar serias discrepancias en los valores de $c_{44}$. Los valores determinados por Sahnoun *et al.* se encuentran algunos cientos de GPa arriba de los valores determinados por Wu *et al.* y de los calculados en este estudio. Como no se ha reportado un valor experimental para $c_{44}$ con el cual comparar, tomamos en consideración la concordancia que mostraron los resultados de los cálculos para TaC y determinamos como mejor valor a $c_{44}$=27 GPa. Sin embargo, es necesario determinar experimentalmente el valor de $c_{44}$ para corroborar la propuesta de este valor. Las propiedades elásticas como el módulo de volumen y su primera derivada, el módulo de Young y la razón de Poisson para $\delta$-TaN se encuentran en la tabla 5.9. Ya que todos los valores del módulo de volumen muestran una buena concordancia entre ellos, el promedio de estos valores de $B$=350 GPa puede considerarse como una predición a esta propiedad. Para el módulo de Young, el valor de Sahnoun *et al.* [52] obtenido de los cálculos usando LDA es mucho mayor en comparación con los valores calculados con GGA, por lo que el valor de $E$=640 GPa sería el mejor valor. Haciendo un análisis similar para la razón de Poisson, el mejor valor para $\nu$ sería el de 0.165.

## $\epsilon$-TaN

Los cálculos realizados utilizando ABINIT para $\epsilon$-TaN se basaron en la aproximación LDA y se emplearon pseudopotenciales del tipo Hartwigsen-Goedecker-Hutter [38] para el N (5 e$^-$) y para el Ta (13 e$^-$). La energía de corte fue de $E_{cut}$ =1632.6 eV y el muestreo de la zona de Brillouin se hizo con una malla de puntos $k$ de $4 \times 4 \times 8$. La optimización de la geometría de la estructura hecha con el código dió como parámetros de red los valores de $a_0$=5.343 Å y $c_0$=3.001 Å.

Las propiedades elásticas del $\epsilon$-TaN se determinaron por medio del programa CASTEP empleando GGA y pseudopotenciales ultrasuaves para el Ta y el N. La energía de corte fue de 330 eV y para el muestreo del espacio recíproco se usó una malla del tipo Monkhorst-Pack de $10 \times 10 \times 6$ puntos $k$. La relajación de la estructura dió como parámetros de red en el equilibrio los valores de $a_0$=5.4404 Å y $c_0$=3.1614 Å. De manera similar al Ta$_2$C, la estructura hexagonal del $\epsilon$-TaN muestra cinco coeficientes elásticos de rigidez independientes cuyos valores obtenidos del cálculo son $c_{11}$=294(4), $c_{12}$=239(4), $c_{13}$=170.1(1), $c_{33}$=374(4) y $c_{44}$=95.5(1) GPa. El módulo de volumen obtenido a partir de estos coeficientes es $B$=236(2) GPa y el módulo de volumen para cada dirección son $E_x$=$E_y$=97.16 y $E_z$=266.17 GPa. Los valores para la razón de Poisson son $\nu_{xy}$=$\nu_{yx}$=0.74, $\nu_{zx}$=$\nu_{zy}$=0.32 y $\nu_{xz}$=$\nu_{yz}$=0.12.

La tabla 5.10 muestra los valores calculados con ABINIT (LDA) y CASTEP (GGA) de los parámetros de red $a_0$ y $c_0$. En comparación con los valores experimentales reportados en el ICDD (International Center for Diffraction Data), los parámetros calculados con LDA muestran una sobreestimación no esperada de un 3% para ambos parámetros. Una razón de esto sería que la descripción de la estructura del $\epsilon$-TaN fue interpretada de manera errónea en el código. Por otra parte, los parámetros de red obtenidos del cículos utilizando GGA

concuerdan dentro del 5% para $a_0$ y del 9% para $c_0$. De la misma manera que Ta$_2$C, como no se encontraron valores reportados de las propiedades elásticas en la literatura para $\epsilon$-TaN, los valores determinados aquí pueden considerarse una predicción para futuras mediciones.

## Capacidad Calorífica

Las curvas de densidad de estados de fonones y de capacidad calorífica para el tantalio, diamante, TaC y Ta$_2$C se determinaron utilizando las relaciones de dispersión de fonones anteriormente calculadas para dichos materiales.

### Tantalio

La figura 6.1 muestra la densidad de estados de fonones del tantalio, normalizada de tal forma que el área bajo la curva sea uno, obtenida de las curvas de dispersión de fonones mostradas en la figura 4.7. Los intervalos de frecuencia utilizados son de 0.15 THz. Esta curva reproduce las principales características de la curva de distribución de frecuencias para Ta calculada por Woods [45] (ver figura 6.2), obtenida al ajustar un modelo general a curvas de frecuencias de fonones medidas por dispersión inélastica de neutrones. La capacidad calorífica a volumen constante $C_v$ del Ta calculada de la densidad de estados de fonones se muestra en la figura 6.3. A temperaturas menores que 25 K, la capacidad calorífica calculada concuerda en $\approx 1$ J K$^{-1}$ mol$^{-1}$ con los valores experimentales de White *et al.* [55]. Sin embargo, a temperaturas mayores que 400 K la capacidad calorífica del Ta se aproxima al valor clásico de $3NK_B$, el cual, para el caso del Ta, es de 25 J K$^{-1}$ mol$^{-1}$.

### Diamante

La densidad de estados de fonones del diamante, obtenida de las relaciones de dispersión (figura 4.14) calculadas con el código ABINIT, se muestra en la figura 6.4. Esta curva se calculó utilizando intervalos de frecuencia de 0.15 THz. La figura 6.5 muestra la densidad de estados de fonones del diamante determinada por Xie y colaboradores [56] mediante cálculos *ab initio*. De esta figura se observa que la curva determinada en este estudio reproduce las principales características de la curva obtenida por Xie. La capacidad calorífica a volumen constante ($C_v$) del diamante, que se muestra en la figura 6.4, se calculó a partir de la densidad de estados en un intervalo de temperatura de 0 a 1100 K. Dado que las mediciones de la capacidad calorífica se realizan a presión constante se le denomina como $C_p$.

Para hacer una comparación directa entre los datos calculados y los medidos, $C_v$ se debe convertir en $C_p$. Esta conversión se lleva a cabo mediante la ecuación (6.14). A temperaturas mayores o igual a 100 K, la concordancia entre los valores calculados aquí y los experimentales publicados por DeSorbo [57], esta dentro de 1.5 J K$^{-1}$ mol$^{-1}$. A altas temperaturas, T $> 700$ K, la concordancia entre valores teóricos y experimentales publicados por Victor [58] es de 1 J K$^{-1}$ mol$^{-1}$ (ver figura 6.7).

*TaC*

A partir de la relación de dispersión calculada para el TaC (ver figura 5.14), se calculó la densidad de estados de fonones $g(\omega)$. Esta densidad se obtuvo calculando un histograma de frecuencias utilizando un intervalo de frecuencia de 0.3 THz y normalizada de tal forma que $\int_0^{w_{\max}} g(w)dw = 1$ (se muestra en la figura 6.8).

La figura 6.9 muestra la capacidad calorífica a volumen constante ($C_v$) del TaC calculada, así como los valores experimentales obtenidos en este estudio utilizando un calorímetro de barrido diferencial tipo Netzsch DSC F1 Phoenix 204. Los valores calculados de $C_v$ concuerdan en 3 J K$^{-1}$ mol$^{-1}$ o menos, con los valores experimentales publicados de C$_p$ por Kelley [59], y en 2.4 J K$^{-1}$ mol$^{-1}$ con los valores experimentales obtenidos en este estudio. En la figura 6.9 se observa que la capacidad calorífica calculada presenta valores notablemente más grandes que los experimentales. Esto puede deberse a que las muestras utilizadas en las mediciones no presentaban una estequiometía Ta$_1$C$_1$, como sucede en los cálculos. Además, en los cálculos se considera al cristal sin imperfecciones y a una temperatura de 0 K.

*Ta$_2$C*

La densidad de estados de fonones para el Ta$_2$C normalizada se muestra en la figura 6.10, donde se utilizó un intervalo de frecuencia de 0.5 THz. La capacidad calorífica del Ta$_2$C se muestra en la figura 6.11. De esta figura se observa que la curva alcanza el valor clásico de 74.7 J K$^{-1}$ mol$^{-1}$ después de una temperatura de 800 K. Debido a que no se encontraron valores experimentales de la capacidad calorífica para este compuesto, los valores teóricos obtenidos en este estudio se pueden considerar como una predicción para futuras mediciones.

## Conclusiones

En ésta tésis se describió el uso de la teoría del funcional de densidad (DFT) en la predicción de las propiedades macroscópicas de carburos y nitruros de tantalio. Estos cálculos muestran una buena concordancia con los valores experimentales reportados en la literatura y, además, proveen valores confiables de las propiedades para las cuales aún no se han hecho mediciones.

*Propiedades Mecánicas*

Se calcularon las propiedades estructurales y las relaciones de presión-volumen (excepto para Ta$_2$C y $\epsilon$-TaN) para tantalio, diamante, TaC, Ta$_2$C, $\delta$-TaN y $\epsilon$-TaN, con el código ABINIT utilizando DFT, pseudopotenciales que conservan la norma y bases de ondas planas. Se utilizó la aproximación de la densidad local (LDA) en los cálculos de todos los compuestos y sólo se usó la aproximación del gradiente generalizado (GGA) en cálculos para el TaC.

También se determinaron los parámetros de red, los coeficientes elásticos de rigidez, los módulos de volumen y de Young y la razón de Poisson para TaC, Ta$_2$C, $\delta$-TaN y $\epsilon$-TaN, mediante cálculos basados en DFT y GGA, usando pseudopoteciales ultrasuaves y bases de ondas planas. Estos cálculos se llevaron a cabo utilizando el código CASTEP. Los resultados obtenidos fueron comparados con valores reportados en la literatura y se sugirieren valores de

cada propiedad para cada compuesto. En el caso del TaC, se midieron los coeficientes elásticos de rigidez $c_{11}$ y $c_{44}$ utilizando un monocristal de TaC en forma de disco mediante una técnica de ultrasonido. Estos valores tienen una concordancia del 8% respecto a los valores teóricos obtenidos aquí.

### Dinámica de la red

Se calcularon las relaciones de dispersión para tantalio, diamante, TaC y $Ta_2C$ en las direcciones de alta simetría. En los casos del tantalio, diamante y TaC, las frecuencias obtenidas de los fonones concuerdan dentro de un pequeño porcentaje respecto a los valores experimetales publicados. Sin embargo, para el $Ta_2C$ no se han reportado valores experimentales, por lo que los resultados teóricos obtenidos en este estudio pueden considerarse una predicción.

### Capacidad Calorífica

Las curvas de la densidad de estados de fonones y de la capacidad calorífica fueron obtenidas a partir de las relaciones de dispersión para el tantalio, diamante, TaC y $Ta_2C$. Para el tantalio la capacidad calorífica calculada concuerda en $\approx 1$ J K$^{-1}$ mol$^{-1}$ con los valores experimentales a temperaturas menores a 25 K. A altas temperaturas la curva tiende a mostrar un comportamiento clásico. Los valores obtenidos de la capacidad calorífica del diamante concuerdan en 1.5 J K$^{-1}$ mol$^{-1}$ a temperaturas menores a 100 K, y en 1 J K$^{-1}$ mol$^{-1}$ a temperaturas mayores a 700 K, en comparación a los valores experimentales publicados. Se midió la capacidad calorífica de un monocristal de TaC en un intervalo de temperaturas de 150 a 600 K. Los valores teóricos concuerdan en 2.4 J K$^{-1}$ mol$^{-1}$ respecto a los valores experimentales medidos aquí, y en 3 J K$^{-1}$ mol$^{-1}$ respecto a los valores experimentales publicados.

*A Ph.D. is more a matter of*
*tenacity than cleverness.*

# Aknowledgements

I thank my unforgettable friends in México, Eric who gave a piece of his office all this years, Débora and Sharon, who always were close to give me their support and nice talks, as well as my good friends in Germany, Ute, Andreas, Antuané and Carlos, who showed me the way to survive in Frankfurt, and also for all the good times we spent together. My mother and sisters, Claudia and Mayra, who always give me their support and love. Finally, I especially thank Pedro, my husband, for his love, support and encouragement in the most difficult moments of this thesis, his patience to all my traveling and for having a Ph.D. student instead of a wife. Also, I thank him for his invaluable help with latex and Matlab. This work was possible also because of you.

# Contents

# List of Figures /*Lista de Figuras*

# List of Tables /*Lista de Tablas*

# Chapter 1

# INTRODUCTION

The properties of materials determine their usefulness. However, for a given application, a combination of properties is usually required. Mechanical properties such as tensile strength, yield strength, elongation (ductility), toughness and hardness are frequently the properties of greatest concern. But also optical, thermal, electrical and magnetic properties are useful properties.

The physical properties of materials depend, in a general sense, on their electronic structure. *Ab initio* calculations, also known as first principles calculations, use quantum theory to determine accurately the electronic structure of materials. Here the atomic numbers of constituent atoms and, usually, some structural information are employed as the only input data.

There are different computational methods to figure out such material properties from first principles calculations, but those based on the density functional theory (DFT)[34] are commonly carried out for solid state systems. In DFT, the complicated many-body interaction of all electrons is replaced by an equivalent but simpler problem of a single electron moving in an effective potential. Although the basic results of such calculations are the electronic structure (eigenvalues, wave functions, etc.) and the total energy of the ground state, many other related physical properties can be deduced from them.

For a given material, the calculated total energy can be used to obtain equilibrium lattice parameters, elastic moduli, relative stabilities of competing crystal structures, energies associated with point and planar defects, etc. [60]. In addition, we also obtain information about electronic density of states and charge density that enables us to attain a deeper insight. The calculations are usually performed at zero temperature (0 K), but the results obtained often constitute the basis for understanding finite-temperature properties.

The advances in *ab initio* electronic structure computation techniques have made possible the calculation of crystal structures and elastic properties for many materials to within 2-5% of experimental results [61]. Such advances in accurate theoretical modeling have created new opportunities for studying hard materials. In addition, the computational modeling

of materials properties is a useful tool that help to determine physical properties when the experimental determination needs expensive apparatus, or special conditions impossible to reproduce such as the temperatures or pressures similar to the Earth's interior.

In the present work, tantalum carbides compounds TaC and $Ta_2C$, as well as tantalum nitrides $\delta$-TaN and $\epsilon$-TaN, were chosen to be studied due to the unusual combination of physical and chemical properties that they exhibit. Although these compounds contain the same elements, Ta and C, and Ta and N, the differences in stoichiometry or crystal structure lead to different mechanical behaviours. The mechanical properties such as bulk and Young moduli, Poisson ratio and the elastic stiffness coefficients, for TaC, $Ta_2C$, $\delta$-TaN and $\epsilon$-TaN, are determined along with phonon dispersion curves for tantalum, diamond, TaC and $Ta_2C$. In addition, the phonon density of states and heat capacity for tantalum, diamond and TaC are obtained. For the TaC case, elastic stiffness coefficients $c_{11}$ and $c_{44}$ as well as the heat capacity curve were obtained experimentally.

## 1.1 Transition Metal Carbides and Nitrides: General Description

Transition metals in groups IV (Ti,Zr and Hf) and V (V, Nb and Ta) forming carbides and nitrides are special compounds. Their physical and chemical properties are of interest for basic research and several technological applications with notorious differences from other common ceramics and metals. Toth [1] explains that, of all compounds formed between transition metal atoms and light elements H, B, C, N, and O, only carbides and nitrides are closely related in crystal structure types, phase relationships, bonding characteristics, and electric and magnetic properties. This close relationship between transition metal carbides and nitrides is easy to understand due to their similarities in electronic structure, size, and the electronegativity of carbon and nitrogen atoms.

These compounds normally exist in substoichiometric phases with a substantial amount of vacancies [15]. The ideal stoichiometry of transition metal carbides and nitrides ($M_1C_1$ and $M_1N_1$, M=metal) is not generally found, and deviations from stoichiometry are far more common. Polymorphs exist in wide composition ranges and vacancies in the nonmetal sites can exist up to a 50% [1]. Normally, it is expected that vacancies reduce the number of chemical bonds and in consequence the strength of materials [62]. However, the hardness of transition metal carbides and nitrides does not behave like this, and the vacancies can act as pinning centers, inhibiting dislocation motion and thus enhancing mechanical strength [2].

The main commercial applications of transition metal carbides are as abrasives, in cutting

tools forming the basis for cemented carbide, and hard coatings, due to their extreme hardness and durability [1, 2, 3]. Many binary carbides have microhardness values between 2000 and 3000 kg/mm$^2$ [1], comparable to that of diamond of 9000 kg/mm$^2$ [4], which is the hardest known material. Their high melting point, excellent high-temperature strength and good corrosion resistance make them useful in heating elements such as filaments and thermal printing heads, used in facsimile and other apparatus [5]. In recent years, transition metal carbides and nitrides have been used as optical coatings, electrical contacts and diffusion barriers in electronics, electrical engineering, and high temperature materials science [6, 7].

**Tantalum Carbides**

Tantalum carbides with a NaCl-type structure are obtained when the carbon atoms fill all the octahedral sites available in the metallic $fcc$ lattice formed by tantalum atoms. There is one octahedral site for every metallic atom. When only one half of the octahedral sites of a hexagonal closest-packed array formed by the tantalum atoms is filled, then carbides like Ta$_2$C are obtained [25].

Carbides rapidly change their properties when the carbon content increases the ratio C/metal to more than 1. The increment of the amount of carbon atoms that fill the octahedral free sites causes a gradual change in the nature of the chemical bond, going from the predominantly metallic to the mixed metallic-covalent bond [12]. In addition, many transition metal carbides posses the NaCl-type structure, like TaC. Therefore, the chemical bond in this kind of compounds is a superposition of covalent, metallic and ionic, which make an interpretation of their electronic structure very difficult [63].

**TaC**

Tantalum carbide, TaC, is a typical representative among transition metal carbides as it has some remarkable properties such as high hardness at room temperature, high melting point (above 3880 °C), resistance to chemical attack and thermal shock [3, 9]. Rowcliffe and Warren [13] mention that the maximum melting point occur at 3983 °C in the TaC$_{0.98}$ phase. Besides, TaC shows excellent electronic conductivity (42.1 $\mu\Omega$ cm at 25 °C), good thermal conductivity (about 22 Wm$^{-1}$C$^{-1}$) and high resistance to oxidation [3, 10, 11].

Because of its high melting temperature, TaC can keep its mechanical properties at temperatures as high as 3200°C [64], and has been used in many special working conditions, for example, as heating element of electric resistance furnaces [7]. In addition, TaC has been pro-

posed as a highly active catalytic material [65] and it is known that its catalytic and adsortive properties are governed by their structure and stoichiometry near the surface [10]. All these notable physical and chemical properties can be attributed to its mixed covalent-metallic bond [12, 13, 14].

A number of authors have investigated TaC elastic stiffness coefficients and elastic properties, such as bulk and Young moduli and Poisson ratio, from diverse methods both experimentally and theoretically since the 1960's [12, 15, 16, 17]. However, the previously reported values for the elastic stiffness coefficients exhibit a large variance of up to 50%. On the other hand, TaC phonon dispersion curves have been obtained experimentally by Smith and Gläser [18] and Smith [19], and reproduced by theoretical methods such as the dielectric-response approach [20], the shell model [21, 22] and the three-body-force shell model [23], all with good agreement. However, there is no reference yet about DFT first principles calculations on TaC determining phonon frequencies.

**Ta$_2$C**

Ta$_2$C has a structure CdI$_2$-type, based on a hexagonal closed-packed lattice formed by the tantalum atoms with the carbon atoms filling one half of the octahedral holes [24, 25]. While the electronic structure and physical properties of tantalum monocarbides, stoichiometric and substoichiometric, has been investigated experimentally and theoretically, the tantalum compound Ta$_2$C has not been explored yet [9].

**Tantalum Nitrides**

Transition metals and nitrogen together make strong and very stable solids. Similar to transition metal carbides, transition metal nitrides are metallic in character with nitrogen occupying interstitial positions of the metal atom arrangement in structures NaCl-type or with a hexagonal closest-packed lattice [66]. Several polymorphs of TaN are known [30]. They show large hardness (1000 kg/mm$^2$ for $\epsilon$-TaN), high melting points near 3000° C, high conductivity, superconductivity and wear resistance [1, 67]. It is known that these properties are due to their strong bonds, and that these properties are the key in applications such as cutting tools, hard coatings, catalysts and diffusion barriers due to their resistance to diffusion of foreign atoms in electronic devices [2, 66, 68, 27]. Also, tantalum nitrides are chemically inert refractory compounds [69].

**$\epsilon$-TaN and $\delta$-TaN**

It is known that the most stable tantalum nitride phase is the $\epsilon$-TaN, with a composition of $Ta_{1.0}N_{1.0}$ and hexagonal symmetry [27]. $\epsilon$-TaN goes through phase transition from hexagonal to face-centered cubic symmetry $\delta$-TaN under high temperature and high pressures [29, 30]. In conventional methods, the synthesis of cubic $\delta$-TaN requires temperatures greater than 1700° C and pressures of minimum 160 bar of nitrogen [70]. However, $\delta$-TaN is more commonly employed than $\epsilon$-TaN.

The $\delta$-TaN phase has a broad composition range and is a typical nonstoichiometric compound with the NaCl-type structure [31]. It is of considerable current interest due to its uses as a diffusion barrier in Cu and Al interconnects on silicon chips, and in manufacturing compact thin film resistors [71]. Also, $\delta$-TaN exhibits superconductivity with a transition temperature of 6.5 K in bulk [33] and 4.8 K as a thin film [29].

## 1.2  Objectives

The present work is about the determination of the macroscopic mechanical properties of tantalum carbides and nitrides, TaC, $Ta_2C$, $\delta$-TaN and $\epsilon$-TaN, from first principles calculations. In addition, structural as well as elastic properties are determined for tantalum and diamond. These are total-energy calculations based on the density functional theory (DFT) within the local density approximation (LDA) and the generalized gradient approximation (GGA). A plane-wave basis set and pseudopotentials are used.

The mechanical properties studied include the elastic stiffness coefficients ($c_{ij}$), bulk modulus and its first derivative, Young modulus and Poisson ratio. Phonon dispersion curves were calculated for tantalum, diamond and the tantalum carbides TaC and $Ta_2C$. Thermodynamic properties such as heat capacity were determined from phonon dispersion curves and phonon density of states for these compounds. Because TaC is the most relevant compound treated here and easier to obtain as single crystal, only its elastic stiffness coefficients and heat capacity were determined experimentally.

## 1.3  Thesis Organization

This thesis is organized as follows: Chapter 2 goes through theories on which the quantum mechanical modeling is based and presents brief descriptions of the two codes used, ABINIT and CASTEP; Chapter 3 contains the fundamental concepts about mechanical properties

concerning this work such as elastic properties and phonons; Chapter 4 contains results on elastic properties and the lattice dynamics calculations for tantalum and diamond. Chapter 5 shows results obtained about mechanical properties calculated for tantalum carbides and nitrides. Chapter 6 contains the phonon density of states (DOS) and heat capacity curves as a function of temperature for diamond, tantalum and TaC determined theoretically, and also experimentally for the latter. Conclusions reached in this work are found in Chapter 7. Finally, some appendices are included in which complementary details are given, as well as some input files of the ABINIT program of the studied compounds.

# Chapter 2

# QUANTUM MECHANICAL MODELING

The need of knowledge about physical properties of materials that are difficult, or in some cases impossible, to measure was the most important reason that physicists had to develop many methods to calculate them [72].

These methods are called *ab initio*, due to the fact that they only require a specification of the ions present by their atomic number. The word *ab initio* means "from first principles", and the main purpose of this kind of methods is to obtain a reasonable approximation to the solution of the Schrödinger equation through quantum mechanics, using only a small number of physical constants. This kind of quantum-mechanical modeling of physical properties relies directly on the capabilities of the computer system used, i.e. the time required for the computational calculation depends on the computer speed and features.

In this chapter, an overview of the most important concepts and theories related with evaluating the ground-state electronic density and total energy using quantum-mechanical *ab initio* calculations is treated. Also, general descriptions of the programs used in this work, ABINIT and CASTEP, are included.

## Total-Energy Pseudopotential Calculations

With most quantum mechanical methods, the total energy of a system of electrons and nuclei, and the subsequent minimization of that energy with respect to the electronic and nuclear coordinates, can be computed. On the other hand, we can say that several physical properties are related to total energies or to differences between total energies. And, if it is possible to calculate total energies from a quantum-mechanical calculation, then any physical property that can be related to a total energy or to a difference of total energies can be determined computationally. Since then, total energy techniques have been successfully used to predict with accuracy properties such as equilibrium lattice constants, bulk moduli, phonons, piezoelectric constants, and phase transition temperatures and pressures [72].

## 2.1 Basic Approximations

A certain number of approximations and simplifications are indispensable to perform total energy calculations. However, there are two fundamental simplifications to take into consideration first.

**Pairwise Additivity**

One of the basic approximations used in total energy calculations is called *pairwise additivity* [73]. The energy of a system of three or more particles can be represented as the sum of interactions between the different pairs. An illustration of this is the following: the energy of a system with two electrons, $e_1$ and $e_2$, and an ion is the sum of the energies between $e_1$-$e_2$, $e_1$-ion and $e_2$-ion.

**Born-Oppenheimer Approximation**

Because electrons move much faster than the atom cores, the electrons are always in an equilibrium configuration when the atom cores are moving [73]. Thus the nuclei can be treated adiabatically, leading to a separation of electronic and nuclear coordinates in the many-body wave function [72]. This approximation is known as the *adiabatic* or *Born-Oppenheimer approximation*. This adiabatic principle reduces the many-body problem to the solution of the dynamics of the electrons in some frozen-in configuration of the nuclei.

Even with these simplifications, the many-body problem still remains difficult. Therefore, further simplifications must be introduced allowing total energy calculations to be performed accurately and efficiently. In a solid, there are two basic interactions that are important to consider: electron-electron interactions and electron-ion interactions.

## 2.2 Electron-Electron Interactions

The most difficult problem in any electronic structure calculation is to take into account the effects of the electron-electron interaction. Due to the Coulumb interaction between their charges, electrons repel each other. The Coulomb energy of a system of electrons can be reduced by keeping the electrons spatially separated, but this has to be balanced against the kinetic energy cost of deforming the electronic wave functions in order to separate the electrons. The effects of the electron-electron interaction is briefly described below.

### 2.2.1 The Many-Body Schrödinger Equation

The electronic and structural properties of a given material can be predicted by solving the Schrödinger equation of a N electrons system,

$$\hat{H}\Psi = E\Psi, \tag{2.1}$$

where $\Psi$ is the many-electrons wave function and is an antisymmetric function of the electron coordinates $\mathbf{r}_i$:$i$=1,...,N. Problems arise in attempting to solve equation (2.1). The Hamiltonian, $\hat{H}$, for a system of electrons and nuclei is given by

$$\hat{H} = -\frac{\hbar^2}{2m_e}\sum_i \nabla^2_{\mathbf{r_i}} + \sum_{i,I}\frac{Z_I e^2}{|\mathbf{r}_i - \mathbf{R}_I|} + \frac{1}{2}\sum_{i\neq j}\frac{e^2}{|\mathbf{r}_i - \mathbf{r}_j|} - \sum_I \frac{\hbar^2}{2M_I}\nabla^2_I + \frac{1}{2}\sum_{I\neq J}\frac{Z_I Z_J e^2}{|\mathbf{R}_I - \mathbf{R}_J|}, \tag{2.2}$$

where electrons coordinates are denoted by $r_{\mathbf{i}}$ and for nuclei, coordinates are $R_{\mathbf{I}}$, charge $Z$ and mass $M$. The first term in the Hamiltonian is the kinetic energy of electrons, followed by the expression for the potential acting on the electrons due to the nuclei and the potential due to the electron-electron interaction, respectively. The last two terms correspond to the kinetic energy of the ions and the classical interaction of nuclei with one another.

Following the Born-Oppenheimar approximation, the nuclei are considered fixed and their kinetic energy can be ignored [74]. In addition, the last term in equation (2.2), corresponding to the classical interaction of nuclei with one another, is included in a fixed potential external to the electrons. Therefore, the three first terms are the key problem for *ab initio* prediction of the properties of materials. Thus the fundamental Hamiltonian can be written as

$$\hat{H} = -\frac{\hbar^2}{2m_e}\sum_i \nabla^2_{\mathbf{r_i}} + V_{ext}(\mathbf{r_i}) + V_{e-e}(\mathbf{r_i}). \tag{2.3}$$

The eigenvalue $E$ in equation (2.1) is the total energy of the system, essentially determined by the external potential $V_{ext}$, which describes the Coulomb interaction between the electrons and a given configuration of nuclei. The term $V_{e-e}$ gives the electron-electron Coulomb interaction, and it is this term which introduces the coupling between the electronic coordinates, avoiding a straightforward separation of the many-body wave function. This coupling is often referred to as *correlation*. When an electron moves, the other electrons feel its Coulomb potential experiencing a force and moving in response. Hence, the motion of electrons is correlated.

**Exchange and Correlation**

As mention above, the wave function of a many-electron system must be antisymmetric under exchange of any two electrons, because electrons satisfy the Fermi statistics. The antisymmetry of the wave function produces a spatial separation between electrons that have the same spin and thus reduces the Coulomb energy of the electronic system. The reduction in the energy of the electronic system due to the antisymmetry of the wave function is called the *exchange energy* [72].

The Coulomb energy of the electronic system can be reduced below its Hartree-Fock value if electrons that have opposite spins are also spatially separated. In this case the Coulomb energy of the electronic system is reduced at the cost of increasing the kinetic energy of the electrons. The difference between the many-body energy of an electronic system and the energy of the system calculated in the Hartree-Fock approximation is called the *correlation energy*.

### 2.2.2 Density Functional Theory (DFT)

In section 2.2.1 it was noted that the term $V_{e-e}$ in equation (2.3) introduces a coupling between the electronic coordinates of the many electrons in the system known as correlation. Although the physics to describe the correlation of electrons is well determined, the mathematics to solve this problem become intractable for all but the simplest systems. Hohenberg and Kohn [34], and Kohn and Sham [35], provided a simple method for describing the effects of exchange and correlation in an electron gas.

Hohenberg and Kohn introduced the concept of electronic density $n(\mathbf{r})$ as a basic variable within the framework of the Density Functional Theory (DFT), showing that the exact total energy $E$, including exchange and correlation, of an electronic gas is a unique functional of the electron density,

$$E[n(\mathbf{r})] = F[n(\mathbf{r})] + \int V_{ext}(\mathbf{r})n(\mathbf{r})d^3\mathbf{r}, \tag{2.4}$$

where $F[n(\mathbf{r})]$ is a universal functional, so that it is $V_{ext}(\mathbf{r})$ which uniquely describes any particular physical system. They also showed that the minimum value of the total energy functional is the ground-state energy of the system, and the density which minimized $E$ in equation (2.4) is the single particle ground-state density. Unfortunately, the functional is not known and as a consequence the theory is not useful in this way.

However, Kohn and Sham [35] showed how it is possible, formally, to replace the many-electron problem by an exactly equivalent set of self-consistent one-electron equations.

### a. Exchange and correlation Functionals

The Hohenberg-Kohn theorem provides some motivation for using approximate methods to describe the exchange-correlation energy as a function of the electron density. The simplest method of describing the exchange-correlation energy of an electronic system is the *local density approximation* (LDA) [35]. However, the *generalized gradient approximation* (GGA) [36] has various theoretical improvements for an electron density that varies in space.

### Local Density Approximation (LDA)

In the local density approximation the exchange-correlation energy of an electronic system is constructed by assuming that the exchange-correlation energy per electron at a point $\mathbf{r}$ in the electron gas, $\varepsilon_{XC}(\mathbf{r})$, is equal to the exchange-correlation energy per electron in a homogeneous electron gas that has the same density as the electron gas at point $\mathbf{r}$ [72]. Thus

$$E_{XC}[n(\mathbf{r})] = \int \varepsilon_{XC}(\mathbf{r})n(\mathbf{r})d^3\mathbf{r} \tag{2.5}$$

and

$$\frac{\partial E_{XC}[n(\mathbf{r})]}{\partial n(\mathbf{r})} = \frac{\partial [n(\mathbf{r})\varepsilon_{XC}(\mathbf{r})]}{\partial n(\mathbf{r})}, \tag{2.6}$$

with

$$\varepsilon_{XC}(\mathbf{r}) = \varepsilon_{XC}^{\text{hom}}[n(\mathbf{r})]. \tag{2.7}$$

LDA assumes that the exchange-correlation energy is purely local. Several parameterizations (Ceperly and Alder [75], Perdew and Zunger [76] and other) exist for the exchange-correlation energy of a homogeneous electron gas, all of which lead to total energy results that are very similar. These parameterizations use interpolation formulas to link exact results for the exchange-correlation energy of high-density electron gases and calculations of the exchange-correlation energy of intermediate and low-density electron gases. LDA, in principle, ignores corrections to the exchange-correlation energy at a point $\mathbf{r}$ due to nearby inhomogeneities in the electron density, i.e., it ignores the fact that the electron density varies from one point to the next. Initially, it was thought that LDA would apply only if the electron

density were a slowly varying functions of position, and that rapid variations in an atom or in the solid would avoid its use, but it worked extraordinarily well even in atoms and solids [77]. However, the failures of LDA are now well established and it is known that has a tendency to favor more homogeneous systems and overbinds molecules and solids [74].

**General Gradient Approximation (GGA)**

The generalized gradient approximation (GGA) [36] for the exchange-correlation energy improves upon the LDA description of atoms, molecules and solids. It has been developed obeying the sum-rule and provides better description of weak molecular bonds than the LDA. GGA treats an electron density that varies in space, i. e. in the GGA approach $\varepsilon_{XC}(n)$ is a function of the density and the gradient of the density at each point [78].

There are many GGA's because the approximation is not universal. However, the effect of all these approximations is: (i) to increase the magnitude of the exchange energy, i. e. lower the total energy; and (ii) to decrease the magnitude of the correlation energy, i. e. raise the total energy. But this last is a smaller effect than that of the exchange. The term *generalized*-gradient (GGA) denotes a variety of ways proposed for functions that modify the behavior at large gradients in such a way as to preserve the desired properties. Thus, the functional in a generalized form is defined as

$$
\begin{aligned}
E_{XC}^{GGA}[n^{\uparrow}, n^{\downarrow}] &= \int d^3 r n(\mathbf{r}) \varepsilon_{XC}(n^{\uparrow}, n^{\downarrow}, \left|\nabla n^{\uparrow}\right|, \left|\nabla n^{\downarrow}\right|, ...) \\
&\equiv^3 r n(\mathbf{r}) \varepsilon_X^{\text{hom}}(n) F_{XC}(n^{\uparrow}, n^{\downarrow}, \left|\nabla n^{\uparrow}\right|, \left|\nabla n^{\downarrow}\right|, ...),
\end{aligned}
\tag{2.8}
$$

where $F_{XC}$ is dimensionless and $\varepsilon_X^{\text{hom}}(n)$ is the exchange energy of the unpolarized gas [74]. GGA expands and softens bonds, an effect that sometimes corrects and sometimes overcorrects the LDA prediction. Typically, GGA favors density inhomogeneity more than LDA and, in comparison, GGA tends to improve total energies, atomization energies, energy barriers and structural energy differences [36].

In this study, a functional type Perdew-Burke-Ernzerhof (PBE) [36] was used in calculations where the GGA approach was employed. A detailed description of the general gradient approximation is found in the reference [74], and for the PBE functional in the reference [36].

### b. The Kohn-Sham energy Functional

The Kohn-Sham approach consists in replacing the difficult interacting many-body system obeying the Hamiltonian in equation (2.2) with a different auxiliary system that can be solved more easily. Kohn and Sham assumed that the ground-state density of the original interacting system is equal to that of some chosen non-interacting system. This leads to independent particle equations for the non-interacting system that can be considered exactly soluble with all the difficult many-body terms incorporated into an *exchange-correlation functional of the density.* By solving the equations one finds the ground-state density and energy of the original interacting system with the accuracy limited only by the approximations in the exchange-correlation functional [74].

Explicitly, Kohn and Sham chose to write the density in terms of a set of orthonormal functions, one for each of the N electrons in the system

$$n(\mathbf{r}) = \sum_{i=1}^{N} |\psi_i(\mathbf{r})|^2 . \tag{2.9}$$

$F[n(\mathbf{r})]$ from equation (2.4) is separated into three terms:

$$F[n(\mathbf{r})] = T_s[n(\mathbf{r})] + E_H[n(\mathbf{r})] + E_{XC}[n(\mathbf{r})], \tag{2.10}$$

where $T_s$ is the kinetic energy term,

$$T_s = \sum_{i} \frac{\hbar^2}{2m} \int \psi_i^* \nabla^2 \psi_i d^3\mathbf{r}. \tag{2.11}$$

This is not equal to the true electronic kinetic energy for the system, but it is of similar magnitude and most important it can be computed exactly. This term is known as the non-interacting kinetic energy. The term $E_H$ describes the Coulomb energy of the electron density $n(\mathbf{r})$, which is the same as the electron-electron energy in the Hartree approximation

$$E_H = \frac{1}{2} \int \int \frac{n(\mathbf{r}')n(\mathbf{r})}{|\mathbf{r}' - \mathbf{r}|} d^3\mathbf{r} d^3\mathbf{r}'. \tag{2.12}$$

Thus far, the terms in the total energy have been defined to be exact. $E_{XC}$ describes the rest of the contributions to the total energy, making up the difference between $T_s + E_H$ and

the true functional $F$. It is known as the *exchange-correlation* energy, and is the only quantity that is approximated in the Kohn-Sham approach.

Only the minimum value of the Kohn-Sham energy functional has a physical meaning. At the minimum, the Kohn-Sham energy functional is equal to the ground-state energy of the system of electrons with the ions in positions $\mathbf{R}_I$.

**Kohn-Sham Equations**

It is necessary to determine the set of wave functions $\psi_i$ that minimize the Kohn-Sham energy functional. These are given by the self-consistent solutions to the Kohn-Sham equations [35]:

$$\left[\frac{-\hbar^2}{2m}\nabla^2 + V_H(\mathbf{r}) + V_{ext}(\mathbf{r}) + V_{XC}(\mathbf{r})\right]\psi_i(\mathbf{r}) = \varepsilon_i\psi_i(\mathbf{r}), \tag{2.13}$$

where $\psi_i$ is the wavefunction of the electronic state $i$, $\varepsilon_i$ is the Kohn-Sham eigenvalue, and $V_H$ is the Hartree potential of the electrons

$$V_H(\mathbf{r}) = \frac{\partial E_H[n(\mathbf{r})]}{\partial n(\mathbf{r})}. \tag{2.14}$$

The exchange-correlation potential, $V_{XC}$, is given formally by the functional derivative

$$V_{XC}(\mathbf{r}) = \frac{\partial E_{XC}[n(\mathbf{r})]}{\partial n(\mathbf{r})}. \tag{2.15}$$

These equations are known as the Kohn-Sham equations, and resemble the non-interacting particle Schrödinger equations where $\psi_i$ are the eigenstates and $\varepsilon_i$ the corresponding eigenvalues. The Kohn-Sham equations represent a mapping of the interacting many-electron system onto a system of non-interacting electrons moving in an effective potential due to all the other electrons. The potentials $V_H$ and $V_{XC}$ depend on the charge density which, through equation (2.9), depends of the Kohn-Sham eigenstates. Therefore, the Kohn-Sham equations must be solved self-consistently so that the occupied electronic states generate a charge density that produces the electronic potential that was used to construct the equations.

The bulk of the work involved in a total energy pseudopotential calculation is related to the solution of this eigenvalue problem once an approximate expression for the exchange-correlation energy is given.

## 2.3   Periodicity

In spite of the fact that the many-body problem can be mapped into equivalent observables in an effective single-particle problem, still remains the difficult task of handling an infinite number of noninteracting electrons, moving in the static potential of an infinite number of nuclei or ions. A wave function must be calculated for each of the infinite number of electrons in the system, and since each electronic wave function extends over the entire solid, the basis set required to expand each wave function is infinite. The use of periodic boundary conditions through Bloch's theorem allow the treatment of very large number of electrons in a crystal using highly desirable plane-wave basis [72].

**Bloch's Theorem**

Bloch's theorem states that in a periodic solid each electronic wave function can be written as the product of a cell-periodic part and a wavelike part. For example, in the one-electron Hamiltonian in equation (2.13), if the potential has a lattice periodicity $U(\mathbf{r}) = U(\mathbf{r} + \mathbf{R})$ for all $\mathbf{R}$, where $\mathbf{R}$ is a lattice vector, the eigenstates of the Hamiltonian can be chosen to have the form of a plane-wave times a cell-periodic function written as

$$\psi_k^n(\mathbf{r}) = e^{ik\cdot\mathbf{r}} u_k^n(\mathbf{r}), \tag{2.16}$$

where $u_k^n(\mathbf{r})$ is the cell-periodic function such that $u_k^n(\mathbf{r}) = u_k^n(\mathbf{r} + \mathbf{R})$ for all lattice vectors $\mathbf{R}$. This implies that

$$\psi_k^n(\mathbf{r} + \mathbf{R}) = e^{ik\cdot\mathbf{R}} \psi_k^n(\mathbf{r}). \tag{2.17}$$

When $\psi_k^n(\mathbf{r})$ is substituted in equation (2.13) a new set of eigenequations for $u_k^n(\mathbf{r})$ is found, one for each continuous variable $\mathbf{k}$ [79].

### 2.3.1   Plane-wave Basis Set and their Representation in Kohn-Sham Equations

Bloch's theorem states that the electronic wave functions at each $\mathbf{k}$ point can be expanded in terms of a discrete plane-wave basis set. However, an infinite plane-wave basis set is required to expand the electronic wave functions. The Kohn-Sham eigenstates when plane-waves are used as a basis set are expressed as

$$\psi_{\mathbf{k}}^n(\mathbf{r}) = \sum_{\mathbf{G}} c_{\mathbf{k}}^n(\mathbf{G}) e^{i(\mathbf{k}+\mathbf{G})\cdot\mathbf{r}}, \tag{2.18}$$

where the sum is over all reciprocal lattice vectors $\mathbf{G}$. The plane-wave basis set can be truncated to include only plane waves that have kinetic energies less than some particular cutoff energy. The sum in the basis set is limited to a set of reciprocal lattice vectors contained within a sphere with a radius defined by the cutoff energy, $E_{cut}$, such that

$$\frac{\hbar^2 |\mathbf{k} + \mathbf{G}|^2}{2m} \leq E_{cut}. \tag{2.19}$$

The introduction of an energy cutoff to the discrete plane-wave basis set produces a finite basis set. In total energy calculations, the cutoff energy should be increased until the calculated energy has converged, but it is possible to perform calculations at lower cutoff energies [72].

### 2.3.2 Brillouin Zone Integration: $k$-point Sampling

The boundary conditions applied to a bulk solid determine the set of $\mathbf{k}$ points at which electronic states are only allowed. The density of allowed $\mathbf{k}$ points is proportional to the volume of the solid. The infinite number of electrons in the solid are accounted for by an infinite number of $\mathbf{k}$ points, and only a finite number of electronic states are occupied at each $\mathbf{k}$ point.

The Bloch theorem changes the problem of calculating an infinite number of electronic wave functions to one of calculating a finite number of electronic wave functions at an infinite number of $\mathbf{k}$ points. The occupied states at each $\mathbf{k}$ point contribute to the electronic potential in the bulk solid so that, in principle, an infinite number of calculations are needed to compute this potential. However, the electronic wave functions at $\mathbf{k}$ points that are very close together will be almost identical. Hence it is possible to represent the electronic wave functions over a region of $\mathbf{k}$ space by the wave functions at a single $\mathbf{k}$ point. In this case the electronic space at only a finite number of $\mathbf{k}$ points is required to calculate the electronic potential and hence determine the total energy of the solid [72]. This suggests that the DFT expressions that contain a sum over $\mathbf{k}$ points, or equivalently an integral over the Brillouin zone, can be efficiently evaluated using a numerical scheme that performs a summation over a small number of special points in the Brillouin zone. In addition, symmetry considerations suggest

that only **k** points within the irreducible segment of the Brilloiun zone should be taken into account.

Many methods have been developed for generating such points and corresponding weights to be used in the summation. Using these methods one can obtain an accurate approximation of the electronic potential and the total energy of an insulator by calculating electronic states at a very small number of **k** points. The calculations for metallic systems require a more dense set of **k** points to determine the Fermi level accurately.

**Monkhorst-Pack Scheme**

Here, the method used for generating **k** points is the one developed by Monkhorst and Pack [50]. This scheme produces a uniform grid of **k** point along the three axes in reciprocal space. The Monkhorst-Pack grid is defined by three integers, $q_i$ where $i = 1, 2, 3$, which specify the number of divisions along each of the axes. These integers generate a sequence of numbers according to the following:

$$u_r = \frac{(2r - q_i - 1)}{2q_i}, \tag{2.20}$$

where $r$ varies from 1 to $q_i$. The Monkhorst-Pack grid is obtained from these sequences by

$$\mathbf{k}_{prs} = u_p \mathbf{b}_1 + u_r \mathbf{b}_2 + u_s \mathbf{b}_3. \tag{2.21}$$

This set of $q_1 q_2 q_3$ distinct points is further symmetrized and weights are assigned according to the number of symmetry images of a given point in the symmetrized set.

## 2.4   Electron-Ion Interactions

It is well known that the chemical bond between atoms is essentially determined by the valence electrons, i.e. the outer shells electrons. The core electrons are in fully occupied shells, and in principle do not contribute to the chemical bond. But this does not mean that core electrons are unimportant. These electrons determine the actual states and energies of the valence electrons, and due to this, core electrons must be included in the Hamiltonian of quantum mechanical descriptions of the electronic structure of atoms, molecules or solids. However, the pseudopotential theory allows one to replace the strong Coulomb potential of the nucleus

and the effects of the tightly bound core electrons by an effective ionic potential acting on the valence electrons [74].

Besides, in order to solve the Schrödinger equation of atoms with more than three electrons, one has to rely on numerical techniques. The pseudopotential approximation is a tool that substantially increases the range of problems in solids that can be treated within computational reach [80].

### 2.4.1   Pseudopotential Approximation

The description of the potential produced by the atom core needs a very large number of plane waves to expand the tightly bound core orbitals and to follow the rapid oscillations of the wave functions of the valence electrons in the core region. Hence, a plane-wave basis set is usually poorly suited to expanding electronic wave functions. In the pseudopotential approach ion cores are considered to be *frozen*. This means that properties of molecules or solids are calculated on the assumption that the ion cores are not involved in chemical bonding and do not change as a result of structural modifications.

The pseudopotential approximation is about to replace the strong electron-ion potential with a much weaker potential, a pseudopotential. In this approach, only the valence electrons are explicitly considered, the effects of the core electrons are integrated within a new ionic potential. Thus the original solid is now replaced by pseudo valence electrons and pseudo ion cores [72]. The valence wave functions need no longer be orthogonal to the core states, and so the orthogonality oscillations disappear, hence far fewer plane waves are required to describe the valence wave functions. These new pseudo electrons experience exactly the same potential outside the core area as the original electrons, but have a much weaker potential inside the core area [39]. A pseudopotential allows to have a simpler solution of the Schrödinger equation by the expansion of the wave functions in a small set of plane-waves.

A pseudopotential is constructed in the following way. An all electron DFT calculation is performed for an isolated atom. A core radius $r_c$ is chosen so that the core regions of neighboring atoms in future studies will not overlap. The smaller the core radius the greater the transferability of the pseudopotential, i.e. the more chemical environments it will be valid in [39]. The all electron valence wave functions are altered within $r_c$ to remove the nodal structrure. These new functions are the pseudowave functions. The Schrödinger equation is then inverted to find the potential that would produce these wave functions, and this is the pseudopotential. Figure 2.1 illustrates schematically an ionic potential, the valence wave

function and the corresponding pseudopotential and pseudo wave function [72]. In the region occupied by the core electrons, the valence wave functions oscillate rapidly due to the strong ionic potential. Outside the core region the two potentials are identical, and the scattering from the two potentials is indistinguishable.

Most pseudopotentials are constructed such that they satisfied four general conditions:(i) the valence pseudowave functions generated from the pseudopotential should contain no nodes; (ii) the normalized atomic radial pseudowave function is equal to the normalized radial all-electron wave function beyond a chosen cutoff radius; (iii) the charge enclosed within the cutoff radius for the two wave functions must be equal; and (iv) the valence all-electron and the pseudopotential eigenvalues must be equal. Pseudopotentials that meet these conditions are known as *norm conserving* pseudopotentials, and simplifies many aspects of their implementation [81]. Constructing a pseudowave function that fulfills these requirements can be accomplished using different schemes.

In this study we used norm-conserving pseudopotentials type Hartwigsen-Goedecker-Hutter (HGH) [38] for LDA calculations, and type Fritz-Haber-Institute based on the Troullier-
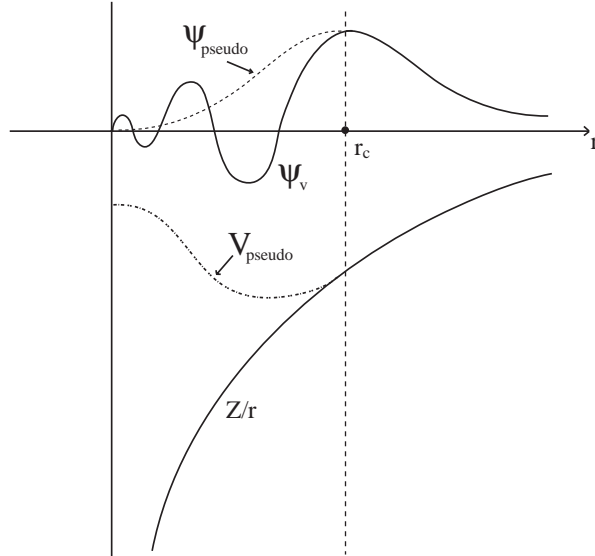


Figure 2.1: Schematic illustration of all-electron (solid lines) and pseudoelectron (dashed lines) potentials and their corresponding wavefunctions [72].

Figura 2.1: *Ilustración esquemática donde se muestra el potencial debido a todos los electrones (línea sólida) y el potencial de los pseudoelectrones (línea punteada), y sus correspondientes funciones de onda [72].*

Martins scheme [39] for GGA calculations performed with ABINIT. The pseudopotentials type HGH are dual-space Gaussian pseudopotentials constructed from a generalization of the norm-conservation property to the relativistic case, in which the parameters are given in the context of the local density approximation [38]. In both real and Fourier space, the projectors which describe the pseudopotentials have the form of a Gaussian multiplied by a polynomial. Due to this property dual-space Gaussian pseudopotentials are the optimal compromise between convergence properties in real and Fourier space [38]. In addition, these type of pseudopotentials take into account the explicit inclusion of semicore electrons into the pseudopotentials of several elements. Particularly, the semicore pseudopotentials for transition metals (groups IIIb-VIIIb) treat the $(n\text{-}1)s$ and the $(n\text{-}1)p$ electrons as semicore electrons. Hence, the semicore pseudopotential for tantalum used in this study treats 13 electrons: $6s^2$ and $5d^3$ as valence electrons, and $5s^2$ and $5p^6$ as semicore electrons.

On the other hand, the pseudopotentials generated under the Troullier-Martins scheme [39] are pseudopotentials that show as main characteristic to be *smoother*. A *smooth* pseudopotential is one in which there is a rapid convergence in the calculated total energy of a system, and therefore a rapid convergence of the properties of the system with respect to an increase in the plane-wave basis set. The smoothness can be achieved by increasing the cutoff radius at which the pseudopotential is generated [39]. Besides, this method improves the transferability of pseudopotentials. Pseudopotentials type Trouillier-Martins can be used to study crystals containing elements from any region of the periodic table [39].

In general, pseudopotentials should have the following characteristics: accuracy, softness and transferability. The *accuracy* and *transferability* of a pseudopotential are the conditions that the pseudoatom must fulfill in order to reproduce the behavior of the all-electron atom in a wide variety of chemical environments. This is essentially the reason why a pseudopotential constructed in one environment, usually an atom, can faithfully describe the valence properties in different environments including atoms, ions, molecules, and condensed matter [74]. An important concept in pseudopotential applications is the degree of *softness* or *hardness* of a pseudopotential. Soft pseudopotentials are those that converge fairly rapidly with respect to the number of plane-waves and require a small number of Fourier components for their accurate representation. Otherwise, they are hard pseudopotentials. Vanderbilt [41] introduced the ultrasoft pseudopotential scheme in which the pseudowave functions are allowed to be as soft as possible within the core region, so that the cutoff energy can be reduced dramatically. Also, these pseudopotentials show the advantage of being much softer than

the norm-conserving potentials. Ultrasoft pseudopotentials are employed on calculations with CASTEP. These pseudopotentials were taken from the CASTEP database.

## 2.5 Iterative Solution of Kohn-Sham Equations

A pseudopotential total energy calculation requires a sequence of steps in which the solutions are found self-consistently. A flow chart representing this procedure is shown in figure 2.2.

The procedure begins with an initial guess on the electronic charge density, from which the Hartree potential and exchange-correlation potential can be calculated. The Kohn-Sham equations are Schrödinger-like independent-particle equations which must be solved subject to the condition that the effective potential $V_{eff}(\mathbf{r})$ and the density $n(\mathbf{r})$ are consistent. This is, the Hamiltonian matrices for each of the $\mathbf{k}$ points included in the calculation must be constructed and diagonalized to obtain the Kohn-Sham eigenstates. Normally, these eigenstates generate a different charge density from the one originally used to construct the electronic potentials, and hence a new set of Hamiltonian matrices must be constructed using the new electronic potentials. The eigenstates of the new Hamiltonian are obtained, and the process is repeated until the solutions probe to be self-consistent. To speed the convergence to self-consistency, the new electronic potential is constructed as a combination of the electronic potentials generated by the old and the new eigenstates.

## 2.6 The ABINIT Program

In the last two decades, the development of faster and more sophisticated computers have allowed the implementation of diverse codes to perform a widely kind of physical calculations. In materials science, first principles or *ab initio* calculations have been used for the determination of electronic and structural properties of materials through electromagnetic and quantum mechanical procedures. To reach the goals of the present work, an *ab initio* computational code named ABINIT was used.

The ABINIT code is a computer software package specialized in *ab initio* calculations and it is comprised of a main code and some utilities programs. It comes from the effort and collaboration of a group of computer scientists from different countries, interested in an advanced and useful tool to perform calculations of physical properties. The ABINIT program is under the GNU General Public License and is available in a public web site [37]. The ABINIT program has different density-functional based calculations covering a wide spectrum of properties such as the computation of equilibrium cell parameters and atomic positions,

Construct $V_{ion}$ given atomic numbers
and positions of ions

Pick a cutoff for the plane-wave basis set

$E_{cut}$

Initial guess

$n(\mathbf{r})$

Calculate effective potential

$V_{eff}(\mathbf{r})=V_{ion}(\mathbf{r})+V_{Hartree}[n]+V_{xc}[n]$

Solve Kohn-Sham equation

$\left[-\frac{1}{2}\nabla^2 + V_{eff}(\mathbf{r})\right]\psi(\mathbf{r}) = \varepsilon\,\psi(\mathbf{r})$

Calculate electron density

$n(\mathbf{r})=\Sigma_i\,f_i\,|\psi(\mathbf{r})|^2$

No

Self consistent?

Yes

Output quantities

Energy, forces, stresses, eigenvalues, ...
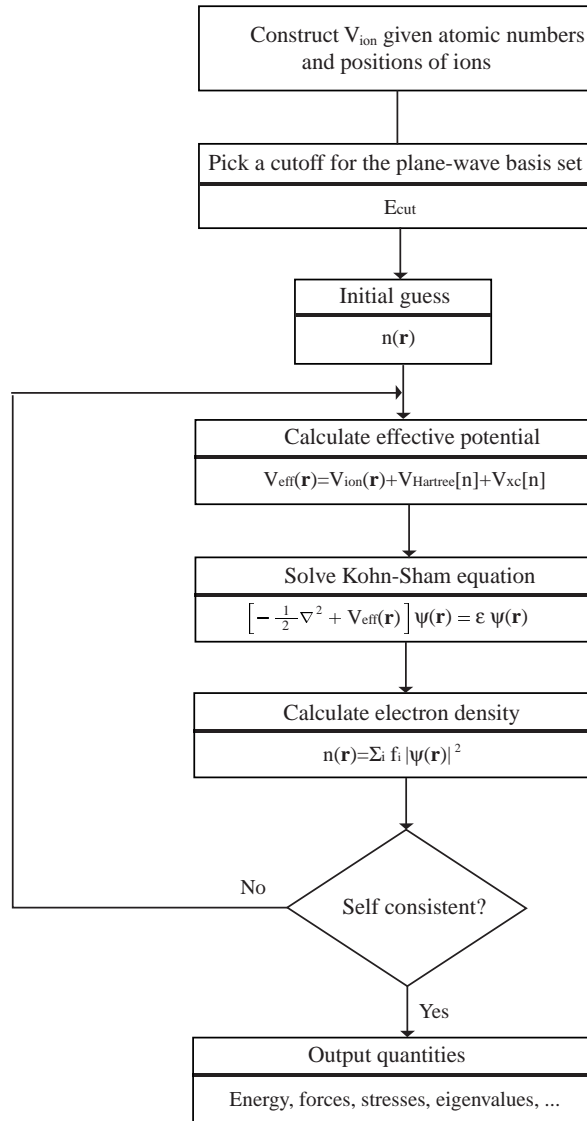
Figure 2.2: Schematic flow chart describing the self-consistent loop for the solution of the Kohn-Sham equations on DFT total energy calculations [74, 72].

Figura 2.2: *Esquema del diagrama de flujo donde se describe el ciclo de auto-consistencia para la solución de las ecuaciones de Kohn-Sham en cálculos de la energía total basados en la teoría del funcional de densidad (DFT) [72, 74].*

vibrational properties, prediction of phase (meta)stability or instability, elastic properties, dielectric and piezoelectric properties, non-linear optical properties, thermodynamic behavior (entropy, free energy, specific heat), electronic properties (metal/insulator characterization),

magnetic properties, space group analysis and many more.

Some of the most relevant calculations perform with ABINIT are the following: (i) the electronic ground-state calculations that allow to find the total energy, charge density and electronic structure of systems made of electrons and nuclei, molecules and solids, within density functional theory (DFT) using pseudopotentials and a plane-wave basis; (ii) the structure-related calculations allow, according to the DFT forces and stresses, to optimize the geometry or to perform molecular dynamics simulation using these forces. Finally, (iii) the response function calculations like vibrations and dielectric or piezoelectric properties are calculated using the Density Functional Perturbation Theory (DFPT)[82] implemented in the program. This kind of calculation allows to consider the responses to atomic displacements and static homogeneous electric fields, producing the generation of dynamical matrices at selected wavevectors, the Born effective charges and the dielectric constant. Another couple of important ABINIT capabilities are the spin-orbit coupling treatment and the adiabatic-connection fluctuation dissipation theorem [83, 84]. With ABINIT it is possible to manage different approximations to the exchange-correlation energy functional such as several versions of the Local Density Approximation and the Generalized Gradient Approximation. In addition, there is a extensive library of norm-conserving pseudopotentials for the whole periodic table.

In the case of the self-consistent cycle, ABINIT uses an iterative minimization algorithm which is a combination of a fixed potential preconditioned conjugated gradient optimization of the wavefunction and a choice of different algorithms for updating the potential, one of which is a potential-based conjugate gradient algorithm. The ABINIT code has two basic versions, sequential and parallel. The sequential version is designed to work on single computers, PC's or workstations. The parallel version allows the use of different processors at the same time distributing the computational work between them. The code has shown to be very portable and can be installed in many different computer platforms including several varieties of Unix (or Linux) and also Windows. A more detailed description of ABINIT and its documentation can be found in the references [37, 83, 84].

One disadvantage the user could find working with ABINIT is the indispensable knowledge of each command needed on every calculation. ABINIT performs a calculation through an input file designed by the user, which consists of a group of commands that most of the times are not as user friendly as one would wish. The user must clearly understand the function and its characteristics in order to write a correct input file.

## 2.7   The CASTEP Program

The CASTEP program (CAmbridge Serial Total Energy Package), similar to ABINIT, is a quantum mechanics based program that performs first-principles calculations employing the DFT plane-wave pseudopotential method [40]. Diverse materials such as ceramics, metals, semiconductors, zeolites and minerals (as crystals or surfaces) can be studied employing this code. Some other studies are about surface chemistry, structural properties, band structure, density of states and optical properties. It is also possible to calculate the full tensor of second order elastic constants and related mechanical properties of a crystal, such as bulk modulus, Poisson ratio and Lamé constants. In addition, the vibrational properties of solids such as phonon dispersion, total and projected density of phonon states and thermodynamic properties, using the linear response methodology, can be calculated for some materials. Properties of point defects such as vacancies, interstitials and substitutional impurities, and extended defects (grain boundaries and dislocations) of semiconductors and other materials, can be calculated with CASTEP.

A CASTEP calculation allows one to select input options such as the basis set, the exchange correlation potential and convergence criteria, and to specify the required properties to study: structural, electronic or vibrational. After a calculation is performed, the analysis of results is possible through volumetric visualizations, as well as plot of band structure, density of states, optical, vibrational and thermodynamic properties. The CASTEP program provides an implementation of DFT which is based on the following concepts: (i) pseudopotencial description of the electron-ion interaction; (ii) supercell approach with periodic boundary conditions; (iii) plane-wave basis set; (iv) extensive use of fast Fourier transform (FFT) for evaluation of the Hamiltonian terms; (v) iterative schemes for the self-consistent electronic minimization and, (vi) implementation of the most popular DFT expressions for the exchange-correlation functional. CASTEP can be used in a PC as well as workstation computers with the ability to control the current calculation and some running parameters from the program itself. It is a user friendly program with a very detailed and useful help file.

# Chapter 3

# MECHANICAL PROPERTIES: FUNDAMENTAL CONCEPTS

In many cases, mechanical properties are the most important factor in determining potential applications. The stiffness, tensile strength, and elastic coefficients of materials are considered important in applications as seemingly diverse as the sound production from piano strings, to the strength of dental porcelain to the protective use of a bulletproof vest and many more [85].

Elastic properties such as elastic stiffness coefficients $c_{ij}$, bulk and Young moduli, Poisson ratio, the fit of the Birch-Murnaghan equation of state, and the determination of phonon dispersion relations, are studied here for some tantalum carbides and nitrides.

## 3.1   Hooke's Law and Elastic Coefficients $c_{ij}$

When a solid body is subjected to stress, its shape changes. If the applied stress is below a certain limit value called the *elastic limit*, the strain is recoverable, that is, when the stress is removed the body returns to its original shape. It has been observed that for sufficiently small stresses the amount of strain is proportional to the magnitude of the applied stress. This relation is known as Hooke's Law.

For example, suppose a bar of an isotropic solid is loaded in pure tension so that the tensile stress is $\sigma$. The longitudinal strain $\epsilon$ equals $\Delta l/l$, where $\Delta l$ is the increase in length and $l$ is the original length. Hooke's law states that

$$\epsilon = s\sigma, \tag{3.1}$$

where $s$ is called the *elastic compliance coefficient* or simply the *compliance*, for this particular arrangement of stress and strain directions. As an alternative we could write

$$\sigma = c\epsilon, \tag{3.2}$$

25
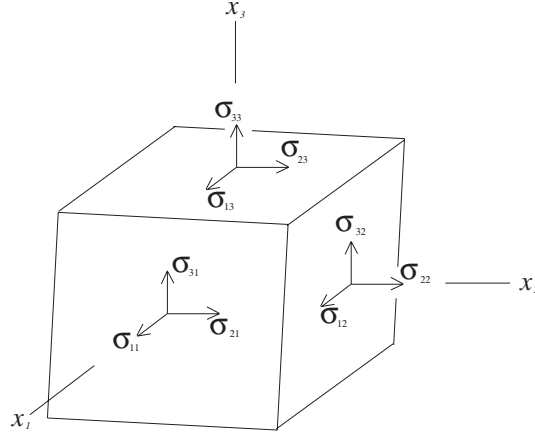
Figure 3.1: The forces on the faces of a unit cube in a homogeneously stressed body [86].

Figura 3.1: *Esquema de las fuerzas en las caras de un cubo debidas a la tensión aplicada homogéneamente a un cuerpo [86].*

and

$$c = \frac{1}{s}, \tag{3.3}$$

where $c$ is the *elastic stiffness coefficient*, also known as the Young modulus or modulus of elasticity [86].

As a general example consider a crystal to be under an homogeneous stress, where all the crystal parts are in statical equilibrium, and there are no body-forces or body-torques. Figure 3.1 shows a unit cube within a crystal under homogeneous stress. The edges of the cube are parallel to the axes $x_1$, $x_2$, and $x_3$. A force will be transmitted across each face of the cube, exerted by the material outside the cube upon the material inside the cube. The force transmitted across each face may be resolved into three components.

We will consider first the three faces over the three positive ends of the axes. $\sigma_{ij}$ denotes the force component in the $+x_i$ direction transmitted across that face of the cube which is perpendicular to $x_j$. Here, the sign convention indicates that $\sigma_{ij}$ is the force exerted in the $x_i$ direction on the face normal to $x_j$. Since the applied stress is homogeneous, the forces exerted on the cube across the three opposite faces must be equal in magnitude but opposite in direction to the three ones shown in figure 3.1. $\sigma_{11}$, $\sigma_{22}$, and $\sigma_{33}$ are known as the *normal components* of stress and $\sigma_{12}$, $\sigma_{21}$, $\sigma_{23}$, etc. are the *shear components*. A positive value of $\sigma_{11}$, $\sigma_{22}$, $\sigma_{33}$ implies a corresponding tensile stress, while a negative value implies a compressive

stress [86].

The assumption that the unit cube should be in statical equilibrium imposes the condition

$$\sigma_{ij} = \sigma_{ji}. \tag{3.4}$$

This condition continues valid even when the stress is inhomogeneous, when the body is not in statical equilibrium, and when body-forces are present.

In a general case, the stiffness and compliance coefficients are defined as follows. If a general homogeneous stress $\sigma_{ij}$, as in the latter example, is applied to a crystal, the resulting homogeneous strain $\epsilon_{ij}$ is such that each component is linearly related to all the components of the stress. For example, $\epsilon_{11}$ can be written as

$$\begin{aligned}
\epsilon_{11} = s_{1111}\sigma_{11} + s_{1112}\sigma_{12} + s_{1111}\sigma_{13} + \\
s_{1121}\sigma_{21} + s_{1122}\sigma_{22} + s_{1131}\sigma_{31} + \\
s_{1131}\sigma_{31} + s_{1132}\sigma_{32} + s_{1133}\sigma_{33},
\end{aligned}$$

as well as eight other similar equations for the rest of the eight components $\epsilon_{ij}$, where the $s$'s represent constants. The Hooke's law in a generalized form may therefore be written as

$$\epsilon_{ij} = s_{ijkl}\sigma_{kl}, \tag{3.5}$$

where $s_{ijkl}$ are the compliances of the crystal. Here, the Einstein's summation convention is used, and when a letter suffix occurs twice in the same term, summation with respect to that suffix is to be automatically understood. Equation (3.5) stands for nine equations, each with nine terms on the right-hand side. There are 81 $s_{ijkl}$ coefficients. If one component of stress is applied, for example $\sigma_{11}$, equation (3.5) indicates that all the strain components $\epsilon_{ij}$ would be different from zero. Alternatively, the stresses in equation (3.5) can be expressed in terms of the equations

$$\sigma_{ij} = c_{ijkl}\epsilon_{kl} \tag{3.6}$$

where the $c_{ijkl}$ are the 81 stiffness coefficients of the crystal. The solution of the simultaneous equations formed with equation (3.5) for the $\sigma_{ij}$ would give a set of solutions of the form of equation (3.6), where the coefficients $c_{ijkl}$ are functions of the $s_{ijkl}$.

The physical meaning of the $s_{ijkl}$ may be appreciated by imagining the crystal to be subjected to various simple stress conditions. $\sigma_{ij}$ may always be taken as symmetrical. Hence, if a shear stress is applied about the $x_3$ direction, both $\sigma_{12}$ and $\sigma_{21}$ would be present and we obtain

$$\epsilon_{11} = s_{1112}\sigma_{12} + s_{1121}\sigma_{21} = (s_{1112} + s_{1121})\sigma_{12}. \tag{3.7}$$

where the coefficients $s_{1112}$ and $s_{1121}$ always occur together. It is in principle impossible to devise an experiment by which $s_{ijkl}$ can be separated from $s_{ijlk}$. Therefore, to avoid an arbitrary constant, the two components can be set equal

$$s_{ijkl} = s_{ijlk}. \tag{3.8}$$

If, on the other hand, a uniaxial tension is applied parallel to $x_3$, the components of the stress would be given by

$$\epsilon_{11} = s_{1133}\sigma_{33}, \ \ \epsilon_{22} = s_{2233}\sigma_{33}, etc. \tag{3.9}$$

In particular,

$$\epsilon_{12} = s_{1233}\sigma_{33} \ and \ \epsilon_{21} = s_{2133}\sigma_{33}. \tag{3.10}$$

But, from the definition of the components of the strain tensor, $\epsilon_{12} = \epsilon_{21}$. Hence, $s_{1233} = s_{2133}$ and, in general, it is possible to state that

$$s_{ijkl} = s_{jikl}. \tag{3.11}$$

Relations (3.8) and (3.11) show that only 36 components of the 81 are independent. On the other hand, the physical meaning of $c_{ijkl}$ on equation (3.6) can be understood if we imagine a set of stress components applied to the crystal, and chosen in such a way that all the components of strain, except for one normal component or a pair of shear components, vanish. Thus the required stresses to produce the tensor shear strain components $\epsilon_{12}$, $\epsilon_{21}$ are

$$\sigma_{ij} = c_{ij12}\epsilon_{12} + c_{ij21}\epsilon_{21} = (c_{ij12} + c_{ij21})\epsilon_{12}. \qquad (3.12)$$

In this relation, the pair of coefficients that always occur together are equal to one another, and in general

$$c_{ijkl} = c_{ijlk}. \qquad (3.13)$$

In a similar way that with the $s_{ijkl}$, if special cases are considered, one can find that

$$c_{ijkl} = c_{jikl}. \qquad (3.14)$$

These equations, (3.13) and (3.14), reduce the number of independent $c_{ijkl}$ from 81 to 36 as it happened with the $s_{ijkl}$ in the most general case. The 81 compliances $s_{ijkl}$, as well as the 81 elastic stiffness coefficients $c_{ijkl}$, form a fourth-rank tensor [86]. However, the number of independent elastic coefficients will be further reduced by the symmetry operations of the respective crystal classes. For example, there are only 9 independent constants for the orthorhombic classes, 5 for the hexagonal classes, and 3 for the cubic classes.

It its possible to introduce matrix notation to manage the compliance and stiffness coefficients, $s_{ijkl}$ and $c_{ijkl}$, due to its symmetry in the first two and the last two suffixes. The two first suffixes of the $s_{ijkl}$ and $c_{ijkl}$ coefficients are abbreviated into a single one running from 1 to 6, and the last two in a similar way but with some factors introduced only in the case of $s_{ijkl}$. Then, equation (3.5) takes the shortest form

$$\epsilon_i = s_{ij}\sigma_j \, (i, j = 1, 2, ..., 6). \qquad (3.15)$$

For $c_{ijkl}$ if it is simply written as

$$c_{ijkl} = c_{mn} \, (i, j, k, l = 1, 2, 3; m, n = 1, ..., 6), \qquad (3.16)$$

it may be shown by writing out some typical members that equations (3.6) take the form

$$\sigma_i = c_{ij}\epsilon_j \, (i, j = 1, 2, ..., 6). \qquad (3.17)$$

## 3.2   Elastic properties: Bulk and Young Moduli and Poisson Ratio

Mechanical properties such as tensile strength, elongation or ductility, toughness and hardness are frequently the properties of greatest concern in metals. The elastic properties under study are the bulk and Young moduli, and Poisson ratio. A description of these properties is given in this section.

**Bulk modulus**

The variation of the volume of a solid with pressure is characterized by the *bulk modulus* [87], defined as

$$B = -V \frac{\partial P}{\partial V},$$

(3.18)

where the negative sign indicates that the volume decreases as pressure increases. The bulk modulus has units of pressure that normally are GPa ($N/m^2$) and indicates the compressibility or incompressibility of materials [88]. For an isotropic material with cubic symmetry subjected to hydrostatic pressure, the bulk modulus written as function of the stiffness coefficients is [86]

$$B = \frac{(c_{11} + 2c_{12})}{3}.$$

(3.19)

The determination of the bulk modulus on different materials has become more important in the last decades. There are many studies in which the bulk modulus is obtained in relation with other physical properties. As an example, He and Yan [89] determined the temperature dependence of bulk modulus and the interatomic separation on sixteen ionic solids with the NaCl-type structure, from room temperature to the melting temperature. A similar study was performed by Makino and Miyake [90] where they empirically determined relations between bulk modulus and interatomic distance for five groups of elemental substances. In a theoretical work performed by Raju *et al.* [91], they attempted to develop certain simple thermodynamic relations connecting thermal and elastic properties such as bulk modulus. Also, Ledbetter [92] studied the relationship between the bulk modulus temperature dependence and the thermal expansivity.

**Young modulus**

The modulus for tensile and compressive stresses, i.e. the ratio of the stress to the strain, is called *Young modulus* and is represented by the symbol $E$ writen, from equation (3.2) as

$$E = \frac{\sigma}{\epsilon}. \tag{3.20}$$

This modulus can be written also as a function of the compliance coefficient,

$$E = \frac{1}{s_{11}}. \tag{3.21}$$

Although the Young modulus may be almost the same for both tension and compression, the strength could be different for the two cases. For example, concrete is very strong in compression but is so weak in tension that is almost never used in this way [88]. Young modulus can be used to predict the elongation or compression of an object as long as the stress is less than the yield strength of the material.

Most materials are strongly anisotropic in their elastic constants. Therefore, a polycrystal such as a ceramic can vary its Young modulus depending on the preferred orientation texture. In addition, the electronic structure is an important factor in determining the Young modulus of elements. This was clearly seen by Krajewski *et al.* [12] on pure materials where the periodicity of the modulus change with the atomic number. Transition elements seem to have particularly high Young modulus values. This can probably be attributed to the strong binding of atoms from electrons in the $d$ shell [12].

**Poisson ratio**

When a metal is subjected to an axial tensile stress, it expands in the direction of the stress and contracts laterally. The Poisson ratio is the ratio of transverse contraction strain to longitudinal extension strain in the direction of the stretching force [88]. Tensile deformation is considered positive and compressive deformation is considered negative. The Poisson ratio is represented by the symbol $\nu$, and is defined as

$$\nu = \frac{-\epsilon_y}{\epsilon_z}, \tag{3.22}$$

where $-\epsilon_y$ is the lateral contraction and $\epsilon_z$ is the axial elongation.

The Poisson ratio as a function of elastic properties is determined by

$$\nu = -s_{12}E. \tag{3.23}$$

The definition of Poisson ratio contains a minus sign so that normal materials have a positive ratio. Poisson ratio values can vary for initially 0 to about 0.5, assuming that the material volume do not change after loading. Generally, stiffer materials will have lower Poisson ratios than softer materials. In addition, the brittle behavior of metals and metallic compounds can be measured using the Poisson ratio. For ductile materials, the Poisson ratio is 1/3. On the other hand, for brittle materials such as ceramics, the Poisson ratio is less than 1/3 [93].

## 3.3 Birch-Murnaghan Equation of State

An equation of state (EoS) gives a relationship between pressure, volume and temperature, and it can take several different forms depending of the situation being modeled. In diffraction experiments at high pressures, it is determined the variation of the sample unit cell parameters as a function of pressure, and thereby the variation of its volume (or equivalently, its density) with pressure and sometimes temperature. This variation of volume with pressure is known as the 'equation of state' of the material [87].

To derive an EoS for solids, it is sufficient to note that there is no absolute thermodynamic basis for specifying the correct form of the EoS of solids. Therefore, all EoS that have been developed and are in use are based on a number of assumptions. The validity of such assumptions can only be judged in terms of whether the derived EoS reproduces experimental data for the volume or elasticity.

In the previous section, the bulk modulus of a solid was defined as the variation of volume with pressure. When the equations of state are measured, they are usually parameterized in terms of values of bulk modulus and its pressure derivatives $B'$ and $B"$ defined as,

$$B' = \frac{\partial B}{\partial P} \tag{3.24}$$

and

$$B" = \frac{\partial^2 B}{\partial P^2}, \tag{3.25}$$

evaluated at zero pressure and symbolized as $B'_0$ and $B"_0$, respectively.

**Birch-Murnaghan Equation of State at 3rd Order**

The Birch-Murnaghan EoS is an isothermal equation of state derived in the assumption that the bulk modulus varies linearly with pressure and treats finite strain. Finite strain are based upon the assumption that the strain energy of a solid undergoing compression can be expressed as a Taylor series in the finite strain $f$. Thus, the Birch-Murnaghan EoS is based upon the Eulerian strain,

$$f_E = \frac{1}{2}\left[\left(\frac{V_0}{V}\right)^{\frac{2}{3}} - 1\right]. \tag{3.26}$$

An expansion to fourth order in the strain yields an EoS:

$$P = 3B_0 f_E (1 + 2f_E)^{\frac{5}{2}}\left(1 + \frac{3}{2}(B' - 4)f_E + \frac{3}{2}(B_0 B" + (B' - 4)(B' - 3) + \frac{35}{9})f_E^2\right). \tag{3.27}$$

If equation (3.27) is truncated at second order, then the coefficient of $f_E$ must be zero, and this requires that B' has the fixed value of 4. The third order truncation, in which the coefficient of $f_E{}^2$ is set to zero yields a three parameter EoS ($V_0$, $B_0$ and B') [87]

$$P = 3B_0 f_E (1 + 2f_E)^{\frac{5}{2}}\left(1 + \frac{3}{2}(B' - 4)f_E\right), \tag{3.28}$$

where $f_E$ is defined in equation (3.26) and an implied value of B" is given by

$$B" = \frac{-1}{B_0}\left((3 - B')(4 - B') + \frac{35}{9}\right). \tag{3.29}$$

In practice, data about the variation of volume with respect to pressure obtained experimentally or theoretically is fitted with an EoS. The values of volume, bulk modulus and the first derivative of bulk modulus are determined at zero pressure.

## 3.4   Lattice Dynamics

Lattice dynamics is about the vibrations of atoms inside a crystal. The static lattice model, which is only concerned with the average positions of atoms and neglects their motions, can explain a large number of materials features. However, there are some properties that are not possible to be described by the static model. These include properties such as thermal

expansion, phase transitions, transport properties, certain electrical properties, and many other. Is then when the study of motion of atoms gives the expected answers through the theory of lattice dynamics [73]. Calculations of vibrational frequencies provide useful tests for any proposed model of interatomic interaction. Thus, given a working microscopy model, lattice dynamics calculations enable the calculation of macroscopic thermodynamic properties [94].

### 3.4.1 Dynamics of diatomic crystals: general principles

Lattice dynamics extends the concept of crystal lattice to an array of atoms with finite masses that are capable of motion. This motion is not random, but is the superposition of vibrations of atoms around their equilibrium sites due to the interaction with neighbor atoms. A collective vibration of atoms in the crystal forms a wave of allowed wavelength and amplitude, and the problem of lattice dynamics is to find the normal modes of vibration of the crystal [79].

In a similar way as photons are the energy quantized of light, phonons are the quantum of vibrational energy. A phonon dispersion relation associates the frequency of the elastic wave in terms of the wave vector that describes the wave. There are two possible modes of vibrations of atoms in the crystal: longitudinal and transverse. In case of a longitudinal mode, the displacement of atoms from their equilibrium position coincides with the propagation direction of the wave, whereas for a transverse mode, atoms move perpendicular to the propagation wave [94]. For one atom per unit cell, the phonon dispersion curves are represented only by the so called acoustical branches. However, if there are two atoms or more in the primitive cell, for each polarization mode in a given propagation direction the dispersion relation $\omega$ versus $k$ develops two branches, known as acoustical and optical branches. Generally, for $p$ atoms in the primitive cell there will be $3p$ branches to the dispersion relation: 3 acoustical branches, one longitudinal and two transverse, and $3p-3$ optical branches, $p-1$ longitudinal and $2p-2$ transverse [94].

The classical theory of lattice dynamics relies on the Newton equation, and considers the solid as an arrangement of atoms joined by springs representing the interactions between atoms. The simple model shown in figure 3.2 represents a harmonic chain with two different atom types in the unit cell. From this figure, each atom is characterized by force constants $G$ and $g$, and masses $M$ and $m$ separated by $a/2$ when at rest. The displacements of atoms $U$ and $u$ correspond to atoms $M$ and $m$ respectively. Each atom only feels the force of its immediate neighbor, which is known as nearest-neighbor interaction [73] .
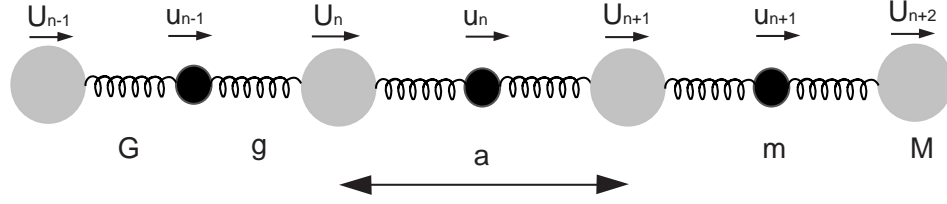
Figure 3.2: Diatomic linear harmonic chain with masses $M$ and $m$ separated by $a/2$ and connected by force constants $G$ and $g$. The displacements of atoms $M$ are denoted by $U_{n-1}$, $U_n$, $U_{n+1}$,..., and of atoms $m$ by $u_{n-1}$, $u_n$, $u_{n+1}$ [73].

*Figura 3.2: Cadena lineal diatómica en el modelo armónico con masas $M$ y $m$, separadas una distancia $a/2$ y conectadas por las constantes de fuerza $G$ y $g$. Los desplazamientos de los átomos de masa $M$ se denotan por $U_{n-1}$, $U_n$, $U_{n+1}$,..., y los desplazamientos de los átomos de masas $m$ por $u_{n-1}$, $u_n$, $u_{n+1}$ [73].*

The energy of the lattice is the same as the energy of a set of harmonic oscillators, so this approximation is called the *harmonic approximation*. Hence, the energy of this diatomic model is given as

$$E = \frac{1}{2} \sum_n \left[ G(U_n - u_n)^2 + g(u_{n-1} - U_n)^2 \right]. \tag{3.30}$$

The equations describing the motion for atoms of masses $m$ and $M$ are

$$\begin{aligned} \frac{M \partial^2 U_n}{\partial t^2} &= -\frac{\partial E}{\partial U_n} \\ &= -G(U_n - u_n) - g(U_n - u_{n-1}) \\ &= -(G+g)U_n + g u_{n-1} + G u_n \end{aligned} \tag{3.31}$$

and

$$\begin{aligned} \frac{m \partial^2 u_n}{\partial t^2} &= -\frac{\partial E}{\partial u_n} \\ &= -g(u_n - U_{n+1}) - G(u_n - U_n) \\ &= -(G+g)u_n + g U_{n+1} + G U_n. \end{aligned} \tag{3.32}$$

The motion of the whole system will correspond to a set of traveling waves with form

$$U_n = \sum_k \widetilde{U}_k e^{i(kna - \omega_k t)} \tag{3.33}$$

$$u_n = \sum_k \widetilde{u}_k e^{i(kna - \omega_k t)}, \tag{3.34}$$

where $k$ is any wave vector, $\omega_k$ is the corresponding angular frequency of a given mode, and $\widetilde{U}_k$ and $\widetilde{u}_k$ are the two amplitudes for a single given mode. In general, the amplitudes are complex and contain the information about the relative phases of the two atoms motions.

The wave equations for the two atoms are defined so that they have the same origins, by which it means that the exponents give the position of the origins of the unit cells rather than the mean positions of the individual atoms. On substitution of the two solutions (3.33) and (3.34) for an individual wave vector into the equations of motion (3.31) and (3.32), and after cancelling the factors common to both sides of the resultant equations, the following simultaneous equations are obtained,

$$-M\omega_k^2 \widetilde{U}_k = -(G+g)\widetilde{U}_k + (G+ge^{-ika})\widetilde{u}_k \tag{3.35}$$

$$-m\omega_k^2 \widetilde{u}_k = -(G+g)\widetilde{u}_k + (G+ge^{ika})\widetilde{U}_k. \tag{3.36}$$

These linear equations can be written on the matrix form

$$\begin{pmatrix} M\omega_k^2 - (G+g) & G+ge^{-ika} \\ G+ge^{ika} & m\omega_k^2 - (G+g) \end{pmatrix} \begin{pmatrix} \widetilde{U}_k \\ \widetilde{u}_k \end{pmatrix} = 0. \tag{3.37}$$

This equation have a solution only if the determinant is equal to zero,

$$[M\omega_k^2 - (G+g)][m\omega_k^2 - (G+g)][G+ge^{ika}][G+ge^{-ika}] = 0. \tag{3.38}$$

Thus this gives a quadratic equation for $\omega_k^2$:

$$Mm\omega_k^4 - (M+m)(G+g)\omega_k^2 + 4Gg\sin^2(ka/2) = 0. \tag{3.39}$$
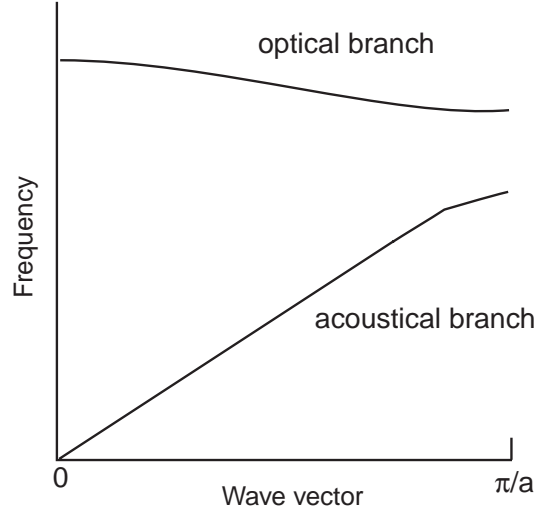
Figure 3.3: Dispersion curves for the one-dimensional diatomic chain [73].

Figura 3.3: *Curvas de dispersión para una cadena diatómica unidimensional [73].*

The solution of equation (3.39) is found with the help of the known quadratic equation solution, which gives

$$\omega_k^2 = \frac{(M + m)(G + g)}{2Mm} \pm \frac{\left((M + m)^2 (G + g)^2 - 16MmGg\sin^2(\frac{ka}{2})\right)^{\frac{1}{2}}}{2Mm}. \qquad (3.40)$$

This equation is known as the *dispersion relation* because it relates the angular frequency $\omega$ with the wave vector $k$. It contains two solutions that produce two branches, acoustical and optical, in the dispersion diagram due to that the two atoms involve two motion equations. Figure 3.3 represents a complete solution to equation (3.40) for all wave vectors [73]. There is a band of frequencies between the two branches that can not propagate. The width of this forbidden band depends on the difference of the masses. If three-dimensional motion were considered, then one would have six equations of motion and six branches in the dispersion diagram. Therefore, the number of branches in a three-dimensional crystal with $z$ atoms in the unit cell is $3z$.

One important feature of the dispersion curve is the periodicity of the function. For a unit cell length $a$, the repeat period is $2\pi/a$, which is equal to the unit cell length in the reciprocal lattice. Therefore the useful information is contained in the waves with wave vectors lying between the limits $-\pi/a < k < \pi/a$. This range of wave vectors is called the *first Brillouin*

*zone* [94]. At the Brillouin zone boundaries the nearest atoms of the chain vibrate in the opposite directions and the wave becomes a standing wave.

**Solution in the long-wavelength limit**

For $k$ small or long wavelengths, equation (3.40) can be solved by taking the linear limit of the sine:

$$Mm\omega_k^4 - (M + m)(G + g)\omega_k^2 + 4Gga^2 = 0. \tag{3.41}$$

Solving the quadratic equation for $\omega_k^2$,

$$\begin{aligned}
\omega_k^2 &= \frac{(M + m)(G + g)}{2Mm} \pm \frac{1}{2Mm} \left[ (M + m)^2 (G + g)^2 - 4MmGgk^2a^2 \right]^{\frac{1}{2}} \\
&= \frac{(M + m)(G + g)}{2Mm} \left[ 1 \pm \left( 1 - \frac{2MmGgk^2a^2}{(M + m)^2 (G + g)^2} \right) \right].
\end{aligned} \tag{3.42}$$

Note that a series expansion of the square root for the limit $k \to 0$ is taken, and only the lowest order term is retained. Then equation (3.42) has the two roots for the frequency:

$$\omega_k^2 = \frac{(M + m)(G + g)}{Mm} - O(k^2) \; ; \; \frac{Ggk^2a^2}{(M + m)(G + g)}. \tag{3.43}$$

Clearly the first frequency is large and varies weakly with $k$. The first branch, flat at $k = 0$, is called the *optic mode* because its frequencies are near the optical region of the electromagnetic spectrum. On the other hand, the second branch is directly proportional to $k$ and is called the *acoustical mode*, because the frequencies are similar to those in long wavelength acoustical vibrations. In more complex crystal with $z$ atoms in the unit cell, there will always be 3 acoustic branches, one longitudinal and two transverse, and $3(z - 1)$ optic branches [73].

### 3.4.2 Formal description of lattice dynamics

The lattice dynamics of a diatomic linear chain as was seen in section 3.4.1, is a simple model which have given us a number of results that are of general use. However, the problems with this simple approach are the following: (a) the simple approach only works in high-symmetry cases, where any mode will contain only one direction of motion. Generally, there is a mixing

of different motions in each vibrational mode, and different modes may correspond to different mixtures of the same atomic motions. (b) The equations of motion are difficult to solve when there are many (i.e. more than two) atoms in the unit cell. (c) The equations get cumbersome when forces from distant neighbors are included. And finally, it is not explicitly considered how to treat atoms in general positions in the unit cell.

Hence, it is necessary to define a general theoretical framework of the basic lattice dynamics problem. To do this, the one-dimensional diatomic model discussed above will be of use to develop the basic ideas of a formal description. The first step is to re-write the basic equations of motion by making a change of variables

$$E = M^{\frac{1}{2}}\widetilde{U}_k; e = m^{\frac{1}{2}}\widetilde{u}_k, \tag{3.44}$$

so that equations will be now solve for $(E, e)$ instead of $(U, u)$. The equations of motion in matrix form are now

$$\begin{pmatrix} E \\ e \end{pmatrix}\omega_k^2 = \mathbf{D}(\mathbf{k})\begin{pmatrix} E \\ e \end{pmatrix}, \tag{3.45}$$

where the matrix $\mathbf{D}(\mathbf{k})$, which is known as the *dynamical matrix*, is given by

$$\mathbf{D}(\mathbf{k}) = \begin{pmatrix} \frac{(G+g)}{M} & -\frac{(G+ge^{(-ika)})}{(Mm)^{\frac{1}{2}}} \\ -\frac{(G+ge^{(ika)})}{(Mm)^{\frac{1}{2}}} & \frac{(G+g)}{M} \end{pmatrix}. \tag{3.46}$$

This matrix has two symmetry properties that are apparent, that $\mathbf{D(-k)}=\mathbf{D}^*(\mathbf{k})$, and that the matrix is *Hermitian*, i. e. $\mathbf{D}^T(\mathbf{k})=\mathbf{D}^*(\mathbf{k})$. This latter property gives the condition that the eigenvalues of $\mathbf{D}(\mathbf{k})$ are real, that is that the squares of the frequencies of the lattice vibrations are necessarily real. Equation (3.46) can be compared with equation (3.37). Equations (3.45) and (3.46) have two general solutions,

$$\begin{aligned} solution\ 1: \ & \omega_1^2, (E_1, e_1), \\ solution\ 2: \ & \omega_2^2, (E_2, e_2). \end{aligned} \tag{3.47}$$

If both solutions are included in the matrix equation of motion (3.45), we obtain

$$\mathbf{e} \cdot \Omega = \mathbf{D}(\mathbf{k}) \cdot \mathbf{e}, \tag{3.48}$$

where the *frequency* and *displacement* matrices are, respectively, equal to

$$\Omega = \begin{pmatrix} \omega_1^2 & 0 \\ 0 & \omega_2^2 \end{pmatrix} ; \mathbf{e} = \begin{pmatrix} E_1 & E_2 \\ e_1 & e_2 \end{pmatrix}. \tag{3.49}$$

The frequency matrix $\Omega$ can be obtained from the dynamical matrix $\mathbf{D}$ by a simple procedure. Equation (3.48) can be simply rearranged to give

$$\Omega = \mathbf{e}^{-1} \cdot \mathbf{D} \cdot \mathbf{e}. \tag{3.50}$$

As the frequency matrix $\Omega$ is diagonal by definition, all we have done is to diagonalize the dynamical matrix $\mathbf{D}$. The elements of the diagonal matrix are the eigenvalues of the diagonalized matrix, and the elements of the diagonalizing matrix (the displacement matrix $e$) are the eigenvectors of the matrix being diagonalized (the dynamical matrix $\mathbf{D}$). Thus, we refer to the squares of the frequencies as the *eigenvalues* of the dynamical matrix, and the displacements produced by the corresponding modes of vibration as the *mode eigenvectors*. The solution to equation (3.50) contains an arbitrary scale factor on the eigenvectors, which are therefore defined to be normalized such that

$$E_1^2 + e_1^2 = E_2^2 + e_2^2 = 1. \tag{3.51}$$

The eigenvectors give the relative atomic displacements rather than their absolute values. Also, they are orthogonal, which is described by the condition,

$$E_1 E_2 + e_1 e_2 = 0. \tag{3.52}$$

The physical meaning is that different modes are independent, and can therefore be added linearly without interacting. All the information that determines both the frequencies and displacements associated with the sets of vibrations of a system is contained in the dynamical matrix, and the task of calculating the dispersion curves resolves itself as the task of setting

up the dynamical matrix. The hermitian character of the dynamical matrix is the condition that the eigenvalues are real, although they may be negative. Negative eigenvalues imply unphysical imaginary frequencies, and imaginary mode frequencies implies that the crystal is unstable with respect to the distortion described by the corresponding eigenvector. In general, calculations of dispersion curves are performed by evaluating the dynamical matrix, and obtaining the eigenvalues and eigenvectors [73].

**The equations of motion and the dynamical matrix**

The lattice energy $W$ as as sum over all atom-atom interactions is defined as:

$$W = \frac{1}{2} \sum_{jj',ll'} \varphi\binom{jj'}{ll'}, \tag{3.53}$$

where $j$ denotes an atom in the $l-$th unit cell, and the interaction energy $\phi$ is for the pair of atoms $(jl)$ and $(j'l')$. The harmonic displacement energy is expressed in matrix form as

$$E^{harm} = \frac{1}{2} \sum_{jj',ll'} \mathbf{u}^T(jl) \cdot \Phi \cdot \mathbf{u}(j'l') = \frac{1}{2} \sum_{jj',ll'} \sum_{\alpha\beta} u_\alpha(jl)\Phi_{\alpha\beta} u_\beta(j'l'), \tag{3.54}$$

where we define the $3 \times 1$ displacement matrix, $u(jl)$, as

$$u(jl) = \begin{pmatrix} u_x(jl) \\ u_y(jl) \\ u_z(jl) \end{pmatrix} \tag{3.55}$$

and $u^T$ is the transpose of $u$.

The force constant matrix $\Phi$ is a $3 \times 3$ matrix, with elements

$$\Phi_{\alpha\beta}\binom{jj'}{ll'} = \frac{\partial^2 W}{\partial u_\alpha(jl)\partial u_\beta(j'l')}. \tag{3.56}$$

The subscripts $\alpha$ and $\beta$ denote the cartesian vector components $x$, $y$ and $z$. Thus, the harmonic energy has the form

$$E^{harm} = \frac{1}{4} \sum_{jj',ll'} [\mathbf{u}(jl) - \mathbf{u}(j'l')]^T \cdot \phi\binom{jj'}{ll'} \cdot [\mathbf{u}(jl) - \mathbf{u}(j'l')], \tag{3.57}$$

where the matrix $\Phi$ has elements

$$\phi_{\alpha\beta}\begin{pmatrix} jj' \\ ll' \end{pmatrix} = \frac{\partial^2 \varphi\begin{pmatrix} jj' \\ ll' \end{pmatrix}}{\partial u_\alpha(jl)\partial u_\beta(j'l')}. \tag{3.58}$$

Equation (3.57) contains an extra factor $1/2$ because of double counting backwards and forwards. By expanding all the terms it is straightforward to show that equation (3.57) is consistent with equation (3.54), with

$$\Phi_{\alpha\beta}\begin{pmatrix} jj' \\ ll' \end{pmatrix} = -\phi_{\alpha\beta}\begin{pmatrix} jj' \\ ll' \end{pmatrix} + \delta_{jj'}\delta_{ll'} \sum_{j''l''} \phi_{\alpha\beta}\begin{pmatrix} jj'' \\ ll'' \end{pmatrix}. \tag{3.59}$$

The second term in equation (3.59) arises from the interaction of any atom $(jl)$ with the rest of the crystal, and it is known as the *self term*.

In the general case, therefore, the equation of motion of the $j$-th atom in the $l$-unit cell is given by

$$m_j \ddot{\mathbf{u}}(jl,t) = -\sum_{j'l'} \Phi\begin{pmatrix} jj' \\ ll' \end{pmatrix} \cdot \mathbf{u}(j'l',t), \tag{3.60}$$

where $m_j$ is the mass of the $j$-th atom. We have now included the time dependence in the displacement vector $u(jl,t)$. The solution for $u(jl,t)$ will be a linear superposition of travelling harmonic waves of different wave vector $k$ and mode label $\nu$

$$\mathbf{u}(jl,t) = \sum_{\mathbf{k},\nu} \mathbf{U}(j,\mathbf{k},\nu)e^{(i[\mathbf{k}\cdot\mathbf{r}(jl)-\omega(\mathbf{k},\nu)t])}, \tag{3.61}$$

where $\mathbf{r}(jl)$ can be taken as either of two quantities. It can be taken as the equilibrium (or mean) position of the atom $(jl)$, or else it can be taken as the origin of the unit cell $(l)$. When we substitute the wave equation (3.61) into the equation of motion (3.60) we obtained the standard equation of motion,

$$m_j \boldsymbol{\omega^2}(\mathbf{k},\nu)\mathbf{U}(j,\mathbf{k},\nu) = \sum_{j'l'} \Phi\begin{pmatrix} jj' \\ 0l' \end{pmatrix} \cdot \mathbf{U}(j',\mathbf{k},t)e^{(i\mathbf{k}\cdot[\mathbf{r}(jl)-\mathbf{r}(\mathbf{j}0)])} \tag{3.62}$$

where the reference atom is in the unit cell $l=0$.

The equations of motion for a single solution (labelled $\nu$) can now be expressed in vector form, where the following final result can be compared with equation (3.45)

$$\omega^2(\mathbf{k}, \nu)\mathbf{e}(\mathbf{k}, \nu) = \mathbf{D}(\mathbf{k}) \cdot \mathbf{e}(\mathbf{k}, \nu). \tag{3.63}$$

The column vector $e(\mathbf{k}, \nu)$ is composed of the displacement vector weighted by the square root of the atomic mass, so that it has $3n$ elements ($n$ is the number of atoms per unit cell)

$$\mathbf{e}(\mathbf{k}, \nu) = \begin{pmatrix} \sqrt{m_1}U_x(1, \mathbf{k}, \nu) \\ \sqrt{m_1}U_y(1, \mathbf{k}, \nu) \\ \sqrt{m_1}U_z(1, \mathbf{k}, \nu) \\ \sqrt{m2}U_x(2, \mathbf{k}, \nu) \\ . \\ . \\ . \\ \sqrt{m_n}U_z(n, \mathbf{k}, \nu) \end{pmatrix}. \tag{3.64}$$

This is the generalization of equation (3.44). $\mathbf{D}(\mathbf{K})$ is the $3n \times 3n$ dynamical matrix. We write $\mathbf{D}(\mathbf{k})$ in terms of blocks of $3 \times 3$ matrices. Each block corresponds to pairs of atoms labels $j$ and $j'$, and the elements of each block have labels $\alpha, \beta= 1,2,3$, representing $x, y, z$ respectively. The full matrix $\mathbf{D}(\mathbf{k})$ is composed of an $n \times n$ array of these smaller $3 \times 3$ matrices. The elements of the small $3 \times 3$ blocks of the dynamical matrix are given as

$$D_{\alpha\beta}(jj', \mathbf{k}) = \frac{1}{(m_j m_{j'})^{\frac{1}{2}}} \sum_{l'} \Phi_{\alpha\beta}\begin{pmatrix} jj' \\ 0l' \end{pmatrix} e^{(i\mathbf{k}\cdot[\mathbf{r}(j'l') - \mathbf{r}(\mathbf{j0})])}, \tag{3.65}$$

where $l=0$ refers to the reference unit cell.

As equation (3.63) has $3n$ components, there will be $3n$ solutions corresponding to the $3n$ branches in the dispersion diagram. We can compact the equations making the $3n \times 3n$ matrix $\mathbf{e}(\mathbf{k})$, by joining together the column vectors $\mathbf{e}(\mathbf{k}, \nu)$, and defining the frequency matrix $\Omega(k)$ as the diagonal matrix of the squares of the angular frequencies;

$$\Omega(\mathbf{k}) = \begin{pmatrix} \omega^2(\mathbf{k},1) & & & & & \\ & \omega^2(\mathbf{k},2) & & & & \\ & & \omega^2(\mathbf{k},3) & & & \\ & & & \cdot & & \\ & & & & \cdot & \\ & & & & & \cdot \\ & & & & & & \omega^2(\mathbf{k},3n) \end{pmatrix} \qquad (3.66)$$

$$\mathbf{e}(\mathbf{k}) \cdot \Omega(\mathbf{k}) = \mathbf{D}(\mathbf{k}) \cdot \mathbf{e}(\mathbf{k}). \qquad (3.67)$$

This formalism always gives real values for the solutions of $\omega^2$. Moreover, it generates the complete set of atomic motions associated with each wave. These motions are linearly independent (orthogonal), in that the motions associated with one wave do not generate the motions for any other. This can be expressed as

$$(\mathbf{e}(\mathbf{k},\nu))^T \cdot \mathbf{e}(-\mathbf{k},\nu') = \delta_{\nu\nu'}. \qquad (3.68)$$

These are called *normal modes*, and are the fundamental vibrational motions [73].

### 3.4.3  Lattice dynamics of Transition Metal Carbides with NaCl-Type Structure

The lattice dynamics of transition metal carbides has been studied in the last sixty years. Particularly, transition metal carbides with structure NaCl-type such as TiC, ZrC, HfC, VC, NbC and TaC, are crystals with ionic, covalent and metallic characters. These compounds have phonon dispersion curves with acoustical and optical branches. Usually, the phonon dispersion curves are measured and calculated in the high-symmetry directions. In addition, it is well known that these dispersion relations show a degeneracy of the optical vibrations frequencies at the $\Gamma$ point, and show a gap between the acoustical and optical branches [73].

The interest in these kind of materials is related with they extremely high melting points and hardness, and to the fact that some of them are superconductors with temperatures higher than the pure metals [95, 18]. In fact, TaC and NbC show superconductivity with transition temperatures about 10 K. Their superconducting properties are closely related to the formal valence of the metal and non-metal, while TiC, HfC and ZrC, have eight valence electrons and are non-superconductors [96, 97].

Many authors have studied the lattice dynamics of diverse transition metal carbides with structure NaCl-type experimentally and theoretically. Phonon dispersion curves were measured by inelastic neutron scattering in the high symmetry directions and at room temperature, for TaC and HfC by Smith and Gläser [18], and for $TiC_{0.95}$ and $TiC_{0.89}$ by Pinschovius and coworkers [97], who also reproduced the phonon dispersion curves using a shell model with free electron screening. Several theoretical models have been applied to reproduce and predict the dispersion curves of carbides. Mostoller [20] applied the dielectric-response approach using pseudopotentials and free-electron screening to approximately reproduced the phonon dispersion curves for HfC, NbC and TaC. The model failed in reproduce some details, or anomalies, in the curves. Weber and coworkers [21] described the anomalies in the phonon spectra of TaC and HfC as resonances in the electronic polarization using an extension of the shell model. In addition, their model predicts an anomaly in the transverse acoustic mode in the [110] direction for TaC. In another study, Weber [22] used a double shell model to calculated the dispersion relations for TaC ad NbC, and a shell model with a free-screening term for HfC and ZrC. Verma and Gupta [23] used a three-body-force shell model to reproduce the phonon dispersion curves for TaC and HfC. They concluded that this model presents a good agreement with experimental values as do the different modified versions of the shell model also applied to these crystals. Upadhyaya *et al.* [96] determined the phonon dispersion curves and Debye temperature variations for TiC, ZrC and HfC, using the rigid shell model by including effects of free-carrier doping and three-body interactions.

In the last years, *ab initio* calculations have been used to calculate phonon dispersion curves which reproduce in good agreement the experimental curves and predict their anomalies. Works by Jochym *et al.* for TiC [98] and ZrC [99], and Savrasov [100] for NbC using density functional theory (DFT), reproduce the major anomalies found experimentally in phonon dispersions.

## 3.5  *Ab initio* Calculations of Mechanical Properties

### 3.5.1  Calculation of elastic properties with the CASTEP code

It is well established that first principles studies based on density-functional theory (DFT) can be used to obtain reliable elastic properties of inorganic compounds [93, 101, 102, 103, 104]. The elastic properties $c_{ij}$, bulk and Young moduli, and Poisson ratio, were calculated with the CASTEP code. Several methods are available for the computation of elastic stiffness coefficients, but currently the 'stress-strain' method seems to be most commonly used. With

this approach, the ground-state structure is strained according to symmetry-dependent strain patterns with varying amplitudes. A subsequent computing of the stress tensor after a re-optimization of the internal structural parameters, i.e. after a geometry optimization with fixed cell parameters, is then carried out. The elastic stiffness coefficients are then the proportionality coefficients relating the applied stress to the computed strain. The computational cost of this procedure is reasonable compared to other approaches, as ultrasoft pseudopotentials can be employed. The stress-strain method can be applied regardless whether the material under investigation is an insulator or a metal. For high symmetry compounds it is reasonable to expect deviations within a few percent from the experimentally observed values.

### 3.5.2 Calculation of phonon dispersion curves with the ABINIT code

The phonon frequencies of normal modes corresponding to wave vectors in the high symmetry directions were calculated with the ABINIT code based in the harmonic approximation. Linear responses of the crystal, such as vibrations and other, were determined using the Density Functional Perturbation Theory (DFPT) [82, 84] implemented in the code. First, a ground-state calculation is performed in order to get the ground-state wave functions. Then, the individual atomic displacement perturbations are performed at a given $q$ point to obtain the dynamical matrix. As seen in section 3.4.2, the squares of the phonon frequencies $\omega^2$ at $q$ are obtained as eigenvalues of the dynamical matrix $\mathbf{D}(\mathbf{q})$. The second derivative of the total energy with respect to collective atomic displacements is related with the interatomic force constants through equation (3.56). The total energy is made from a contribution of the electron system and from a contribution from the electrostatic energy between ions. In this way, the dispersion relations of a material can be determined from first principles calculations.

# Chapter 4

# TANTALUM AND DIAMOND

In order to determine the essential parameters and the accuracy of the planned total energy calculations of the carbides, convergence studies as well as the pressure-volume relation and phonon dispersion curves were determined on crystalline tantalum and diamond, using the ABINIT program.

## 4.1 Tantalum

The tantalum crystal study was performed using the ABINIT program and a pseudopotential for tantalum from the ABINIT database. This pseudopotential is a Hartwigsen-Goedecker-Hutter (HGH) pseudopotential and includes semi-core states, so that a total of 13 electrons are explicitly included. Also, the local density approximation (LDA) was used in these calculations.
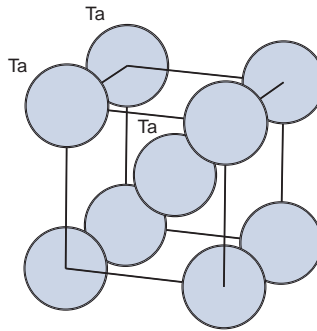


Figure 4.1: Conventional unit cell of tantalum. Tantalum crystallizes in a *bcc* structure with lattice parameter $a$=3.305 Å (6.247 Bohr) [42].

Figura 4.1: *Celda convencional del tantalio. El tantalio cristaliza en una estructura bcc con un parámetro de red a=3.305 Å (6.247 Bohr) [42].*

**Tantalum: General Description**

Tantalum is a transition metal that crystallizes in a structure with a body-centered cubic (*bcc*) lattice (see figure 4.1), with a lattice parameter of $a$=3.305 Å(6.247 Bohr) [42]. The primitive cell has a basis with one atom in position (0, 0, 0) and one in (1/2,1/2,1/2), in a simple cubic lattice. It belongs to the space group $Im\bar{3}m$ (International Tables No. 229). Tantalum shows a high hardness, high ductility and high melting temperature of 3269 K at ambient pressure [43]. These properties make tantalum an outstanding material for tools and high stress components. It has been an important high technology material due to its high thermal, mechanical and chemical stability and is used in jet engines and electronic devices. In addition, the incomplete $d$-shell of electrons defines, to a significant extent, its thermal and vibrational properties [105].

**Convergence Studies**

The convergence studies for crystalline tantalum calculations have as a purpose the determination of the optimal amount of the kinetic energy cutoff of plane-waves ($E_{cut}$), the number of $k$-points necessary to sample the Brillouin zone and the equilibrium lattice parameter, all this for a determined pseudopotential. In this particular case, a pseudopotential type HGH for tantalum is used. All determined values from this study are used in the subsequent calculations in order to improve its convergence and speed and, as consequence, the accuracy of the results. Because tantalum is a metal, it is necessary to consider as well the temperature of smearing of electrons. Here, we used the Fermi-Dirac smearing with a value suggested by the ABINIT documentation for $d$-band metals of 2.72 eV or 0.01 Hartree (1 Hartree=27.2 eV).

Figure 4.2, shows the dependence of $E_{cut}$ as a function of the total energy using the tantalum experimental lattice parameter and a $k$-point grid of $2 \times 2 \times 2$. In the case of tantalum, the value of $E_{cut}$ converges at 1360.5 eV (50.0 Hartree), which could be considered computationally expensive, indicating that the pseudopotential used is a little hard.

The sampling of the Brillouin zone is performed by the ABINIT code using the Monkhorst-Pack scheme [50]. The convergence study associated to this sampling needs to test different $k$-point grids. Figure 4.3 shows the relation of total energy with respect to the number of $k$-points in the Brillouin zone and grids tested. Similar to the $E_{cut}$ convergence calculation, the time for calculation will increase as the value of the $k$-point grid increases. For tantalum, a k-point grid of $6 \times 6 \times 6$ or greater gives good convergence. The found value of $E_{cut}$=1360.5 eV was used in this calculation.
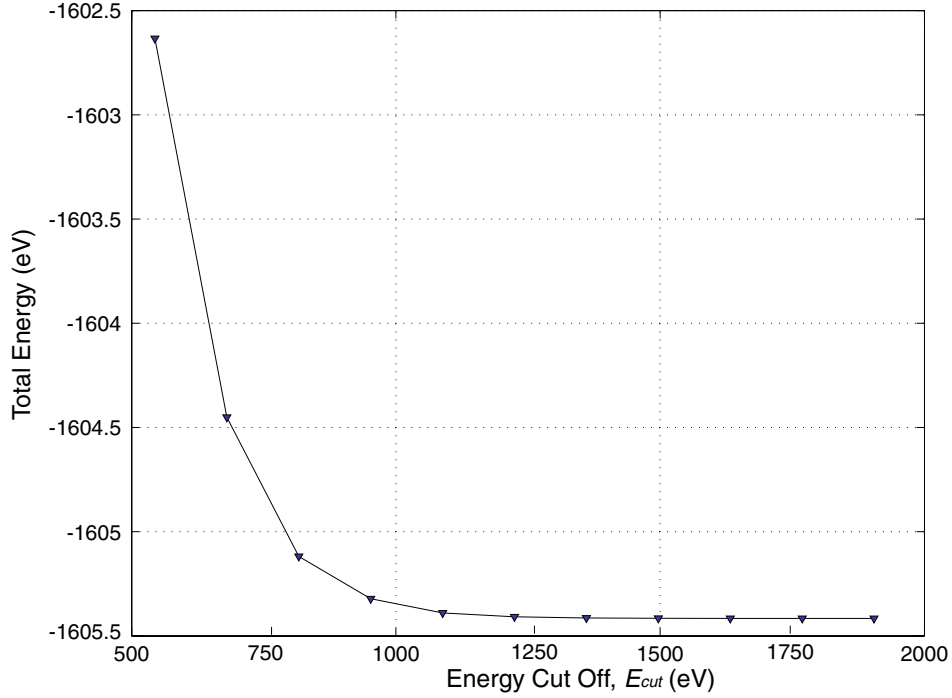
Figure 4.2: Relation of the kinetic energy cutoff of plane waves, $E_{cut}$, with respect to total energy for Ta.

Figura 4.2: *Relación de la energía cinética de corte de las ondas planas, $E_{cut}$, con respecto a la energía total para Ta.*

Figure 4.4, shows the relation between the tantalum lattice parameter and the total energy of the system, calculated using a $E_{cut}$=1360.5 eV and a $k$-point grid of $10 \times 10 \times 10$ to sample the Brillouin zone. The optimal value for the lattice parameter is that in which the total energy is minimum. The data obtained were fitted with a cubic polynomial equation finding the minimum energy at a lattice parameter of $a_0$=3.255 Å (6.154 Bohr). Also, using the automatic geometry optimization feature in the ABINIT program, the minimum energy for the crystalline tantalum was found at a lattice parameter of $a_0$=3.251 Å (6.146 Bohr), with a remaining pressure of $5.74 \times 10^{-4}$ GPa. This latter lattice parameter value was used in the following calculations.

**Birch-Murnaghan equation of state for tantalum**

The volume at zero pressure, bulk modulus and the first derivative of bulk modulus with respect to pressure were obtained fitting a 3rd order Birch-Murnaghan equation of state (EoS).
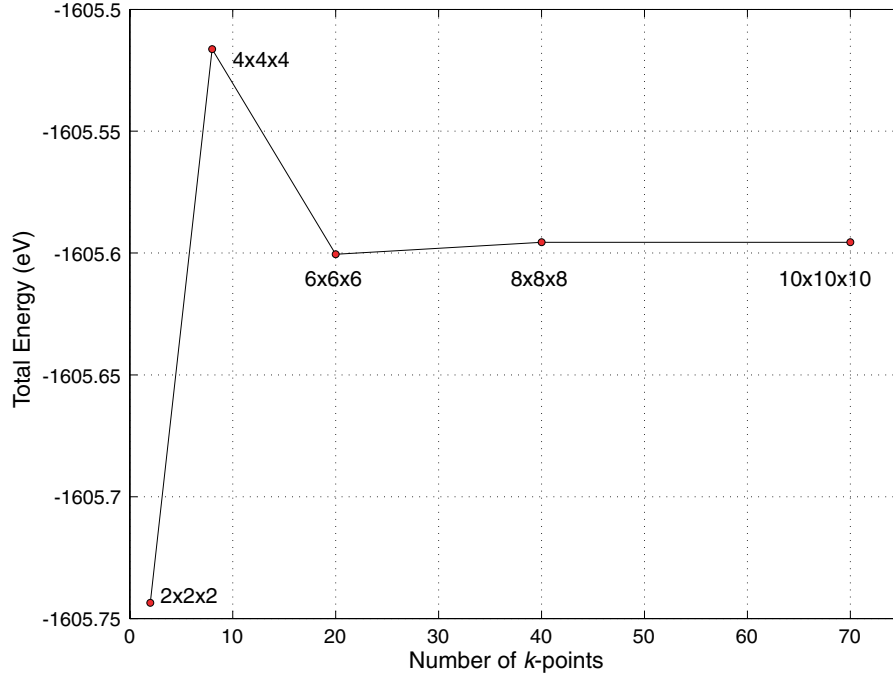
Figure 4.3: Relation of $k$-point number with respect to total energy for Ta.

Figura 4.3: *Relación del número de puntos k con respecto a la energía total para Ta.*

The data of volume and pressure used in this fitting were calculated from the convergence study of lattice parameter and total energy mentioned above. The curve relating volume and pressure for crystalline tantalum is shown in figure 4.5. Values at zero pressure found are $v_0$=34.39(2) Å$^3$ for volume, $B$=221(9) GPa for the bulk modulus and $B'$=4(1) for the first derivative of $B$, where the values in brackets correspond to the variation in the values. The lattice parameter associated with these values is $a_0$=3.25(2) Å (6.143 Bohr).

Table 4.1 shows values of lattice parameter, bulk modulus and first derivative of bulk modulus for tantalum, both published and those obtained here from calculation. The lattice parameter determined from the geometry optimization calculation $a_0$=3.251 Å (6.146 Bohr), agrees within 2% with the reported value by the Inorganic Crystal Structure Database (ICSD) of $a_0$=3.305 Å (6.247 Bohr)[42]. A similar agreement apply to the lattice parameter obtained from fitting a 3rd order Birch-Murnaghan equation.

Values of the bulk modulus and its first derivative, $B$=221(9) GPa and $B'$=4(1), determined here from fitting a Birch-Murnaghan EOS, show a reasonable agreement with published values by Cynn and Yoo [43] of $B$=194.7(4.8) GPa and $B'$=3.4(0.1), obtained by fitting their
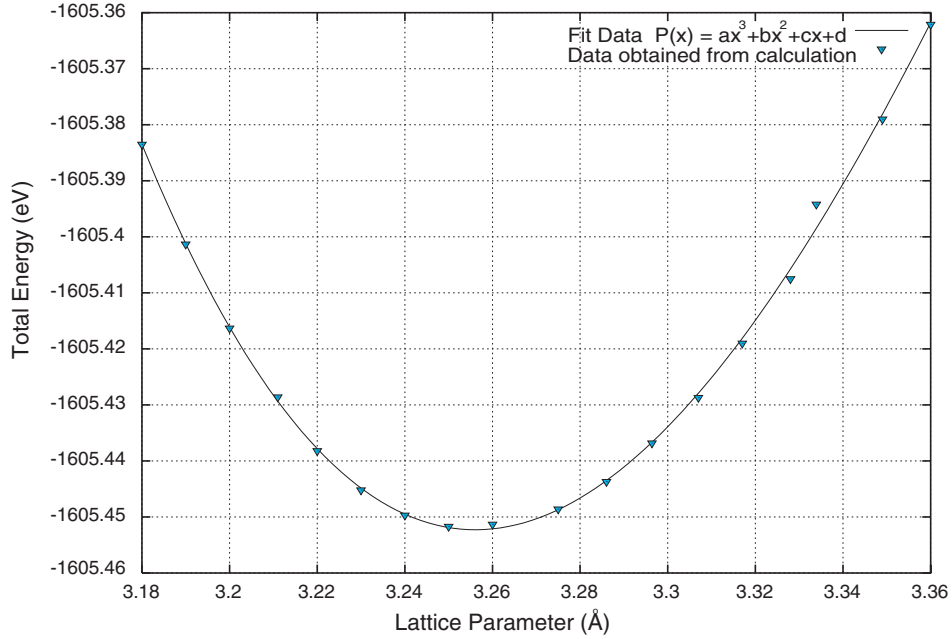
Figure 4.4: Relation of lattice parameter with respect to total energy for Ta.

Figura 4.4: *Relación del parámetro de red con respecto a la energía total para Ta.*

measured compression data to an equation of state. A similar agreement can be observe from values $B$=196 GPa and $B'$=3.79 by Katahara *et al.* [44], obtained from ultrasonic measurements .

**Lattice dynamics of Tantalum**

Table 4.2 shows a comparative study of phonon frequencies calculations of tantalum for a wave vector $q$=[0.3 0.3 0.3]. Different values of parameters such as shift of $k$-point grid, number of $k$-point grids and number of electronic bands are used. As expected, the use of a large $k$-point grid has a strong dependence with the time of computation. However, total energy and pressure vary with little significance. In the case of different shifts of $k$-point grid and number of bands, there is no relevant difference in results and time of calculation.

The phonon dispersion curves at high symmetry directions $[00x]$, $[0xx]$ and $[xxx]$ (see figure 4.6) for tantalum, at zero pressure and 0 K, are shown in figure 4.7. These curves were calculated using the ABINIT program, with $E_{cut}$=1360.5 eV (50 Hartree) and a $k$-point grid of $10 \times 10 \times 10$. Transformations of wave vectors from coordinates in the conventional cell to coordinates in the primitive cell were done as indicate in appendix A. Calculated phonon
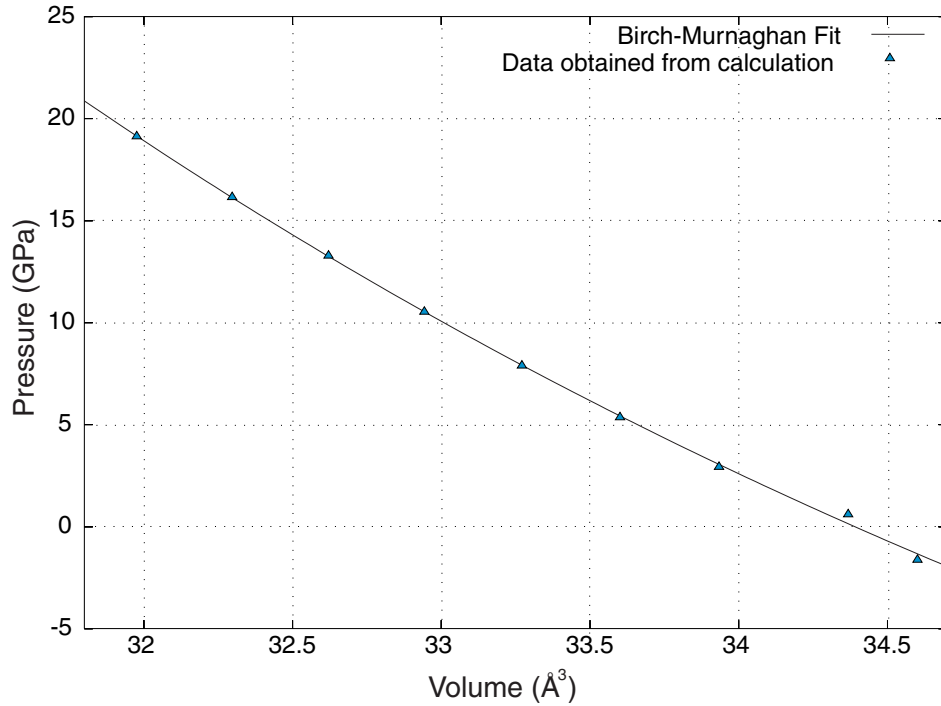
Figure 4.5: Pressure-volume relation for tantalum. Triangles show data points obtained from the ABINIT calculation and the line is a fit with a 3rd order Birch-Murnaghan equation of state.

Figura 4.5: *Relación presión-volumen para Ta. Los triángulos muestran los valores obtenidos en el cálculo con ABINIT y la línea representa el ajuste a la ecuación de estado de Birch-Murnhagan a tercer orden.*

frequencies are represented with filled circles and lines drawn through the calculated points are a guide to the eye. Triangles (transversal modes) and squares (longitudinal modes) show experimental values by Woods [45] at 296 K obtained by inelastic neutron scattering. The measured frequencies are about 0.5 THz higher than experimental data, particularly at high symmetry points $H$ and $N$. A reason to this could be that the unit cell volume used in these calculations is smaller than the volume considered in experimental measurements. However, all features from experimental curves are well reproduced. $L$ and $T$ branches at $[00x]$ are observed to cross at x $\approx$ 0.7, and the tendency for the $[00x]$ and $[xx0]$ transverse branches to avoid normal dispersive behavior is apparent.

Calculations on tantalum were performed using the ABINIT code versions 4.0.4 and 4.4.3, for a windows platform on a personal computer with processor type Intel Pentium 4.
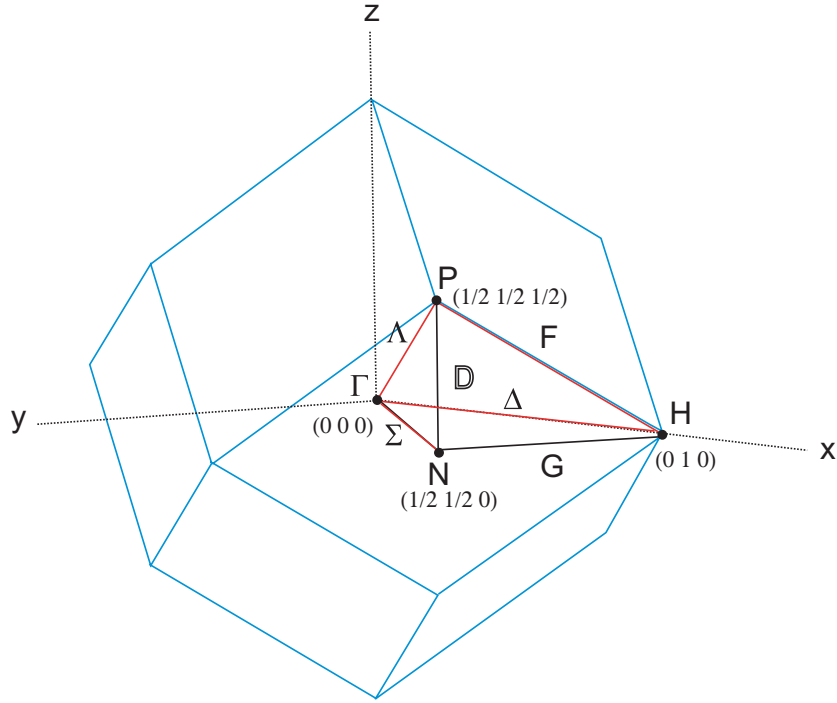
Figure 4.6: First Brillouin zone of the *bcc* lattice showing high symmetry directions.

Figura 4.6: *Esquema de la primera zona de Brillouin corresponediente a la red tipo bcc mostrando las direcciones de alta simetría.*

Table 4.1: Lattice parameter $a_0$, bulk modulus and first derivative of bulk modulus for tantalum. Experimental values are at room temperature.

Tabla 4.1: *Parámetro de red $a_0$, módulo de volumen y la primera derivada del módulo de volumen para el tantalio. Los valores experimentales son a temperatura ambiente.*

| Reference | $a_0$ (Å) | B (GPa) | B' |
|---|---|---|---|
| National Bureau of Standards [42] | 3.305 | ... | ... |
| Cynn & Yoo [43] | ... | 194.7(4.8) | 3.4(0.1) |
| Katahara *et al.* [44] | ... | 196 | 3.79 |
| Present work ABINIT (DFT-LDA) from cubic fit | 3.255 | ... | ... |
| Present work ABINIT (DFT-LDA) from geometry optimization | 3.251 | ... | ... |
| Present work ABINIT (DFT-LDA)from EOS | 3.25(2) | 221(9) | 4(1) |

Table 4.2: Comparative values of some parameters in a DFT-LDA phonon calculation for Ta with wave vector $\mathbf{q}$=[0.3 0.3 0.3] using the ABINIT code.

Tabla 4.2: *Valores comparativos de algunos parámetros en los cálculos de fonones para Ta usando DFT-LDA y un vector de onda $\mathbf{q}$=[0.3 0.3 0.3] con el programa ABINIT.*

| number of shifts | shift of $k$ point grids | Grid of $k$ point grids | number of $k$ points | Pressure (GPa) | Total Energy (Hartree) | Phonon Frequencies (THz) | Time (h) |
|---|---|---|---|---|---|---|---|
| 1 | 0.5 0.5 0.5 | $8 \times 8 \times 8$ | 512 | 0.39516 | -59.004266 | 2.869, 2.87, 4.71 | 16.15 |
| 1 | 0.5 0.5 0.5 | $10 \times 10 \times 10$ | 1000 | -0.4848 | -59.004742 | 2.77, 2.77, 4.68 | 25.12 |
| 1 | 0.5 0.5 0.5 | $8 \times 8 \times 8$ | 512 | 0.39519 | -59.004266 | 2.865, 2.865, 4.71 | 16.52 |
| 1 | 0.5 0.5 0.5 | $8 \times 8 \times 8$ | 512 | 0.39519 | -59.004266 | 2.867, 2.867, 4.71 | 21.11 |
| 2 | 0.25  0.25  0.25 <br> -0.25 -0.25 -0.25 | $8 \times 8 \times 8$ | 512 | -0.1242 | -59.004614 | 2.79, 2.796, 4.74 | 15.89 |
| 2 | 0.25  0.25  0.25 <br> -0.25 -0.25 -0.25 | $10 \times 10 \times 10$ | 1000 | -0.23014 | -59.004610 | 2.836, 2.836, 4.72 | > 24 |
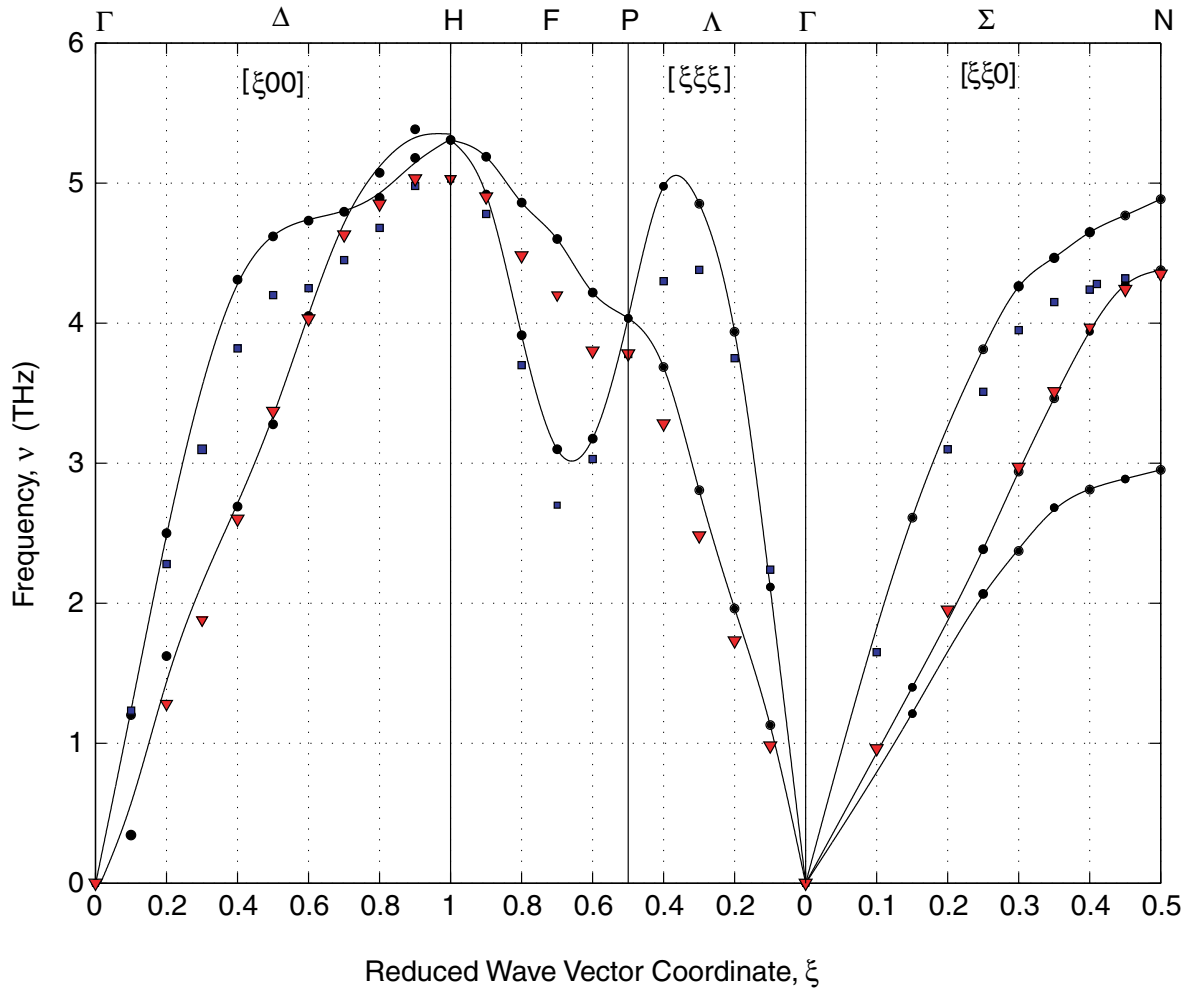
Figure 4.7: Phonon dispersion curves of Ta in the high symmetry directions. Filled circles indicate calculated values and lines are a guide to the eye. Triangles (transversal modes) and squares (longitudinal modes) represent experimental data by Woods [45].

Figura 4.7: *Curvas de dispersión de fonones del Ta en las direcciones de alta simetría. Los círculos indican los valores calculados y las líneas son una guía para la vista. Los triángulos (modos transversales) y cuadrados (modos longitudinales) representan los valores experimentales obtenidos por Woods [45].*

## 4.2   Diamond

Because carbon is an element present in tantalum carbide compounds, a study of carbon in
the diamond structure were performed with the ABINIT program using LDA, at zero pressure
and 0 K, similar to the one described in section 4.1 for tantalum. The diamond structure
was chosen between other carbon structures due to its cubic structure and its remarkable
mechanical properties. The convergence studies necessary for an optimum calculation, as
well as its pressure-volume relation and phonon dispersion curves calculation, are given in
this section. From convergence studies, the optimal values of the cutoff kinetic energy of
plane waves, $E_{cut}$, $k$-point grid and equilibrium lattice parameter were determined. All these
calculations were performed using a Hartwigsen-Goedecker-Hutter (HGH) pseudopotential for
carbon taking into account the valence electrons, i.e. 4 electrons.

### Diamond: General Description

Diamond has a face-centered cubic lattice (see figure 4.8). Its structure has a lattice parameter
$a$=3.5668 Å (6.7425 Bohr) and it belongs to the space group $Fd\bar{3}m$ (227) [46]. The diamond
structure can be viewed as two interpenetrating face-centered cubic lattices shifted along the
body diagonal by (1/4, 1/4, 1/4)$a$. The primitive cell of diamond has a basis of two carbon
atoms in positions (0,0,0) and (1/4, 1/4, 1/4) associated with each point of the $fcc$ lattice
[94]. Diamond most relevant characteristics are its unique high hardness, highest thermal
conductivity at room temperature and several of its mechanical properties, such as bulk
modulus, are also the highest known. The unusual bonding strength of diamond makes it an
extremely low compressible material, which is characterized by a very large bulk modulus [4].

### Convergence Studies

Studies of convergence were done to test the carbon pseudopotential. These tests are used to
determine an optimal $E_{cut}$ and appropriate $k$-point grid to sample the Brillouin zone. They
also indicate the expected accuracy of the equilibrium lattice parameter. Figure 4.9 shows the
relation of $E_{cut}$ with respect to the total energy for diamond using the experimental lattice
parameter and a $k$-point grid of $2 \times 2 \times 2$. The values converged to within 1360.5 eV (50
Hartree). Then, in order to do the calculation as computationally cheaper as possible, an
$E_{cut}$ of 1360.5 eV was used in the following calculations.

Figure 4.10 shows the relation of number of $k$-points used, or the $k$-point grid, to sample
the Brillouin zone with respect to the total energy for diamond. A $4 \times 4 \times 4$ grid shows the

convergence necessary for good calculations. However, a $10 \times 10 \times 10$ grid, corresponding to 110 $k$-points, is used in the following calculations to perform a more detailed sampling, getting more accurate values particularly in the phonon calculation.

The relation of the diamond lattice parameter with respect to the total energy is shown in figure 4.11. Dots indicate the values obtained by calculation and the line is a fit employing a cubic polynomial to find the equilibrium lattice parameter. The energy minima gives a lattice parameter of 3.536 Å (6.686 Bohr). In addition, an equilibrium lattice parameter for diamond was calculated using the automatic geometry optimization feature in the ABINIT program. The value found is 3.531 Å (6.675 Bohr), with a remaining pressure of $2.219 \times 10^{-3}$ GPa. This latter lattice parameter was used in the next calculations.

**Birch-Murnaghan equation of state of diamond**

The variation of the unit cell volume of diamond at different pressures is shown in figure 4.12. The data points were obtained from the previous lattice parameter and total energy calculation above discussed, and the line represents a fit with a 3rd order Birch-Murnaghan equation of state. From the fit, the volume at zero pressure is $v_0 = 43.62(2)$ Å$^3$, the bulk modulus at zero pressure is $B = 471(8)$ GPa, and the first derivative of $B$, $B' = 3.7(2)$. The lattice parameter associated with these values is $a_0 = 3.52(2)$ Å (6.65(2) Bohr).

Table 4.3 shows some earlier published experimental values of lattice parameter and bulk modulus, together with those obtained here from calculation. The lattice parameter $a = 3.531$ Å(6.675 Bohr), obtained from the geometry optimization calculation, is 1% smaller than the
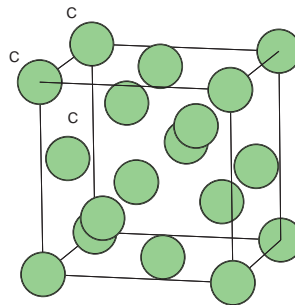


Figure 4.8: Conventional unit cell of diamond. Diamond has a crystal structure with a $fcc$ lattice and a lattice parameter of $a = 3.5668$ Å(6.7425 Bohr).

Figura 4.8: *Celda unitaria convencional del diamante. El diamante tiene una estructura cristalina asociada a una red del tipo fcc, y un parámetro de red a=3.5668 Å(6.7425 Bohr).*
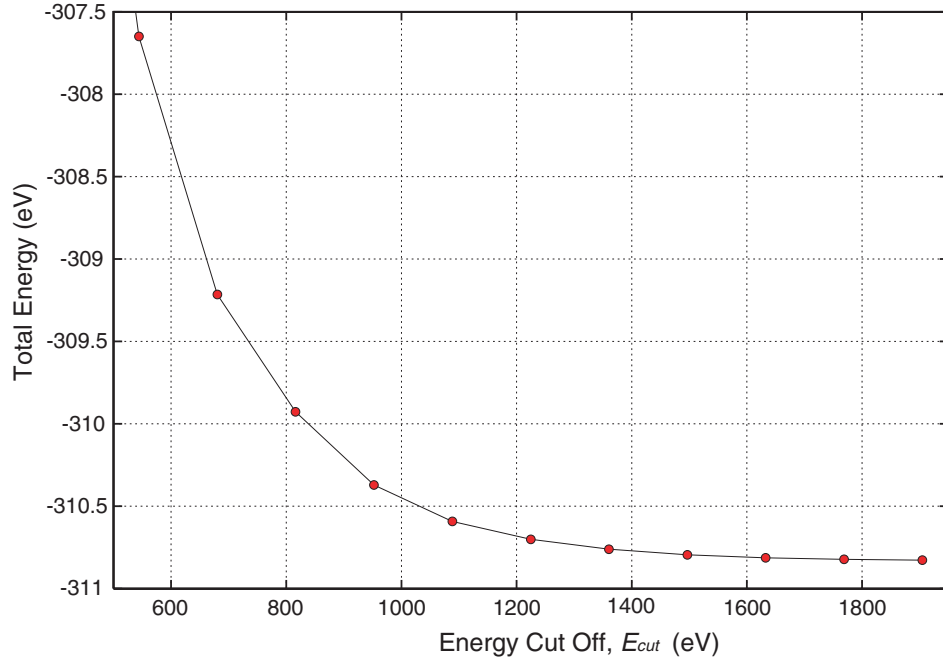
Figure 4.9: Relation of cutoff kinetic energy of plane-waves, $E_{cut}$, with respect to total energy for diamond.

Figura 4.9: *Relación de la energía cinética de corte $E_{cut}$ de las ondas planas con respecto a la energía total para el diamante.*

experimental lattice parameter reported by Straumanis & Aka [46] of $a_0$=3.5668 Å (6.7425 Bohr). In addition, the $a_0$= 3.52(2) Å (6.65(2) Bohr) value obtained from fitting a 3rd order Birch-Murnaghan equation, and the $a_0$=3.536 Å (6.686 Bohr) from a cubic fit, are better within a 2% and a 1%, respectively, in comparison to the experimental value. On the other hand, the bulk modulus $B$=471(4) GPa obtained from fitting a Birch-Murnaghan agrees within a 6.5% with respect to the value of $B$=442 GPa reported by McSkimin *et al.* [47]. These relatively small differences with the reported values are indicative of the reliability of further calculations.

**Lattice dynamics of Diamond**

The dispersion relations curves for the optical and acoustical branches of diamond were calculated with ABINIT. An energy cutoff of $E_{cut}$=1360.5 eV (50 Hartree), a $k$-point grid of $10 \times 10 \times 10$ and a lattice parameter of 3.531 Å(6.675 Bohr) were used. The resulting dispersion curves at high symmetry wave vectors (see figure 4.13) in reduced coordinates are shown
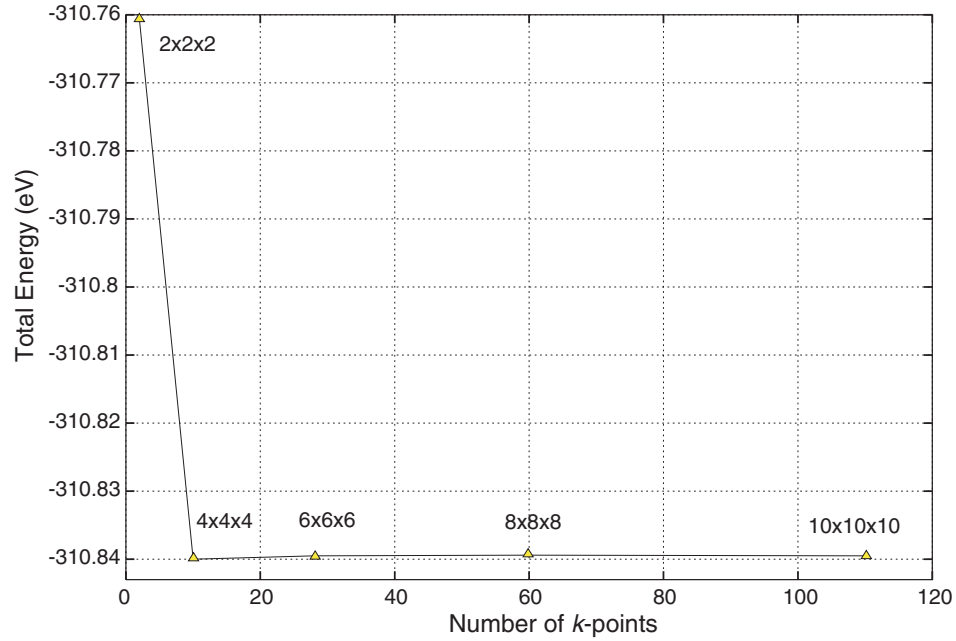
Figure 4.10: Relation of $k$-point number with respect to total energy for diamond.

Figura 4.10: *Relación del número de puntos $k$ con respecto a la energía total para el diamante.*

Table 4.3: Structural properties for diamond.

Tabla 4.3: *Propiedades estructurales del diamante.*

| Reference | $a_0$ (Å) | B (GPa) | B' |
|---|---|---|---|
| Straumanis & Aka [46] | 3.5668 | ... | ... |
| McSkimin *et al.* [47] | 3.5667 | 443(22) | ... |
| Present work ABINIT (DFT-LDA) from cubic fit | 3.536 | ... | ... |
| Present work ABINIT (DFT-LDA) from geometry optimization | 3.531 | ... | ... |
| Present work ABINIT (DFT-LDA) from EOS | 3.52(2) | 471(4) | 3.7(2) |

in figure 4.14. Wave vectors were transformed from coordinates in the conventional cell to coordinates in the primitive cell as indicated in appendix A. The labeling of directions of wave vectors corresponds to the standard convention used in the Brillouin zone high symmetry directions. Filled circles indicate calculated values and lines drawn through the calculated points are a guide to the eye. Squares (transversal modes), triangles (longitudinal modes) and diamonds represent experimental data obtained by inelastic neutron scattering from Warren
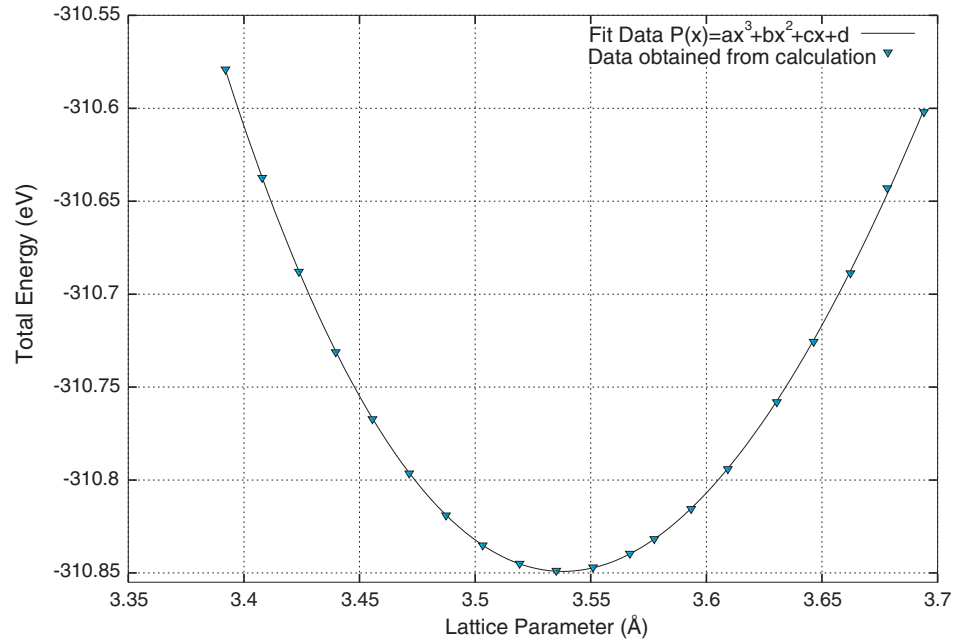
Figure 4.11: Relation of diamond lattice parameter with respect to total energy.

Figura 4.11: *Relación del parámetro de red con respecto a la energía total del diamante.*

*et al.* [48] in directions [$x00$] and [$xxx$], and Warren *et al.* [49] for data in direction [$xx0$]. The calculated frequencies are in excellent agreement in comparison with the experimental values. In addition, all features of the phonon curves are well reproduced.

These calculations were performed using ABINIT version 4.0.4. for a Windows platform on a personal computer with an Intel Pentium 4 processor.
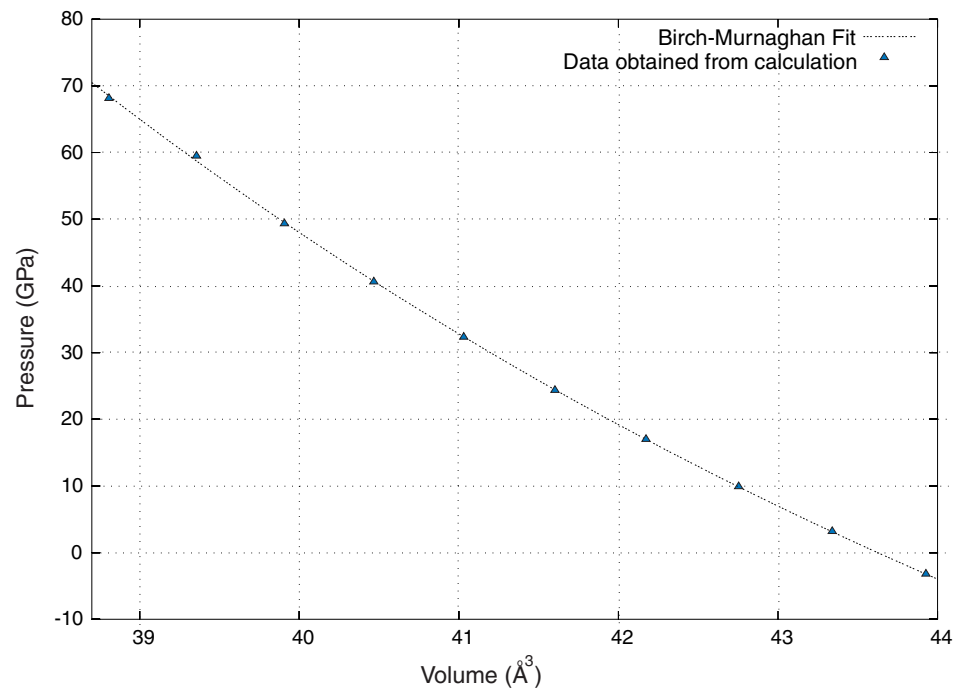
Figure 4.12: Pressure-volume relation for diamond. Triangles show the data points obtained from ABINIT calculation and the line is a fitting with a 3rd order Birch-Murnaghan equation of state.

Figura 4.12: *Relación presión-volumen para el diamante. Los triángulos muestran los valores obtenidos del cálculo con ABINIT y la línea representa el ajuste con la ecuación de estado de Birch-Murnhagan a tercer orden.*
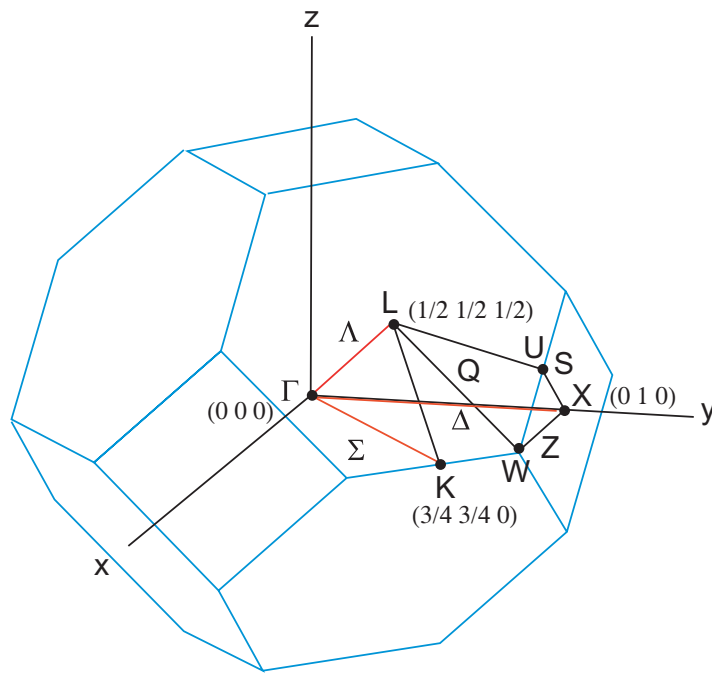
Figure 4.13: First Brillouin zone of the *fcc* lattice showing high symmetry directions.

Figura 4.13: *Esquema de la primera zona de Brillouin de la red tipo fcc mostrando las direcciones de alta simetría.*
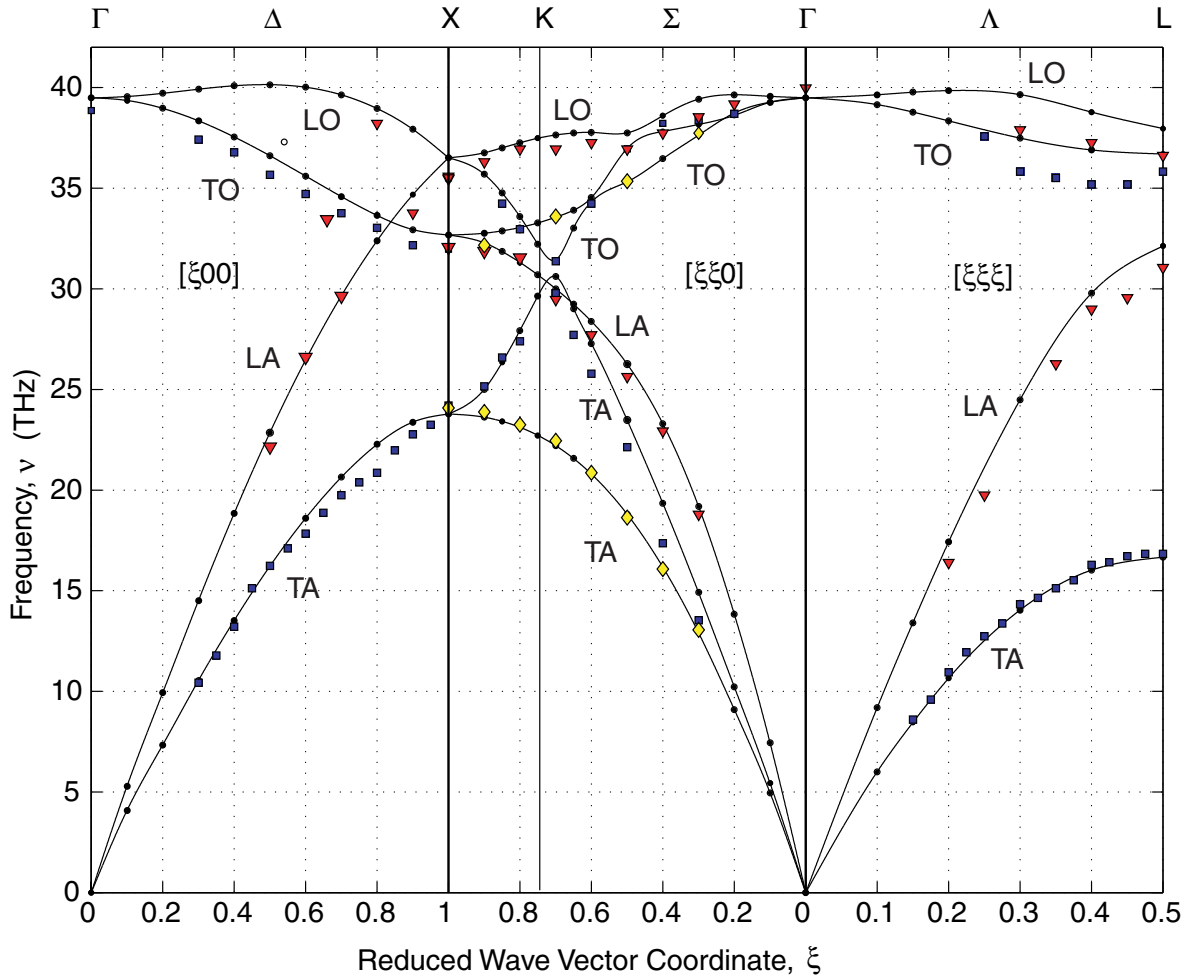
Figure 4.14: Phonon dispersion curves for diamond in the high symmetry directions. Filled circles indicate calculated values and lines are intended to be a guide to the eye. Triangles (longitudinal modes), squares and diamonds (transversal modes both) represent experimental data by Warren *et al.* [49].

Figura 4.14: *Curvas de dispersión de fonones del diamante en las direcciones de alta simetría. Los círculos indican los valores calculados y las líneas son una guía para la vista. Los triángulos (modos longitudinales), cuadrados y diamantes (modos transversales ambos) representan los valores experimentales obtenidos por Warren et al. [49].*

# Chapter 5

# MECHANICAL PROPERTIES OF BINARY TANTALUM CARBIDES AND NITRIDES

In this chapter are described the results of mechanical properties obtained by computationally modeling the compounds TaC, Ta$_2$C, $\epsilon$-TaN and $\delta$-TaN. Some properties experimentally determined for TaC are included. Analysis and discussions about these results are also presented.

## 5.1 Crystalline Structures of the Studied Tantalum Compounds

The tantalum compounds under study, TaC, Ta$_2$C, $\epsilon$ and $\delta$-TaN, show remarkable chemical and physical properties which make them suitable for special mechanical applications. A brief description of their crystalline structures is the following.

TaC crystallizes in the NaCl-type structure, with space group $Fm\bar{3}m$ (225)[8], and exists over a wide range of substoichiometries, i. e. there are diverse compounds with Ta$_1$C$_x$ where usually $0.5 < x \leq 1$ [13]. The primitive cell of TaC has a basis of two atoms, one Ta at (0, 0, 0) and one C at (1/2, 1/2, 1/2), associated with each point of the $fcc$ lattice. Figure 5.1 shows the conventional unit cell with a NaCl-type structure of TaC with lattice parameter $a$=4.454 Å (see table 5.1), and density of 14.498 g/cm$^3$ [8]. The smaller carbon atoms fit in the octahedral interstices of a face-center cubic metal sublattice giving the NaCl-type structure. The chemical bonding is mixed covalent and metallic and large deficiencies in carbon content are tolerated without a change in structure [15]. However, the mechanical properties are correlated with vacancies in the carbon sublattice [62].

Ta$_2$C has a trigonal symmetry corresponding to space group $P\bar{3}m1$ (164), where the C atoms occupy the Wyckoff 1($a$) sites and the Ta atoms occupy the 2($d$) sites [26]. Figure 5.2 shows the conventional unit cell of Ta$_2$C with lattice parameters $a$=3.1059 Å and $c$=4.946 Å, and density of 15.02 g/cm$^3$ [26].

The $\delta$-TaN phase, similar to TaC, shows a NaCl-type structure with lattice parameter of $a$=4.339 Å (see figure 5.3). It belongs to the space group $Fm\bar{3}m$ (225) and has a density of 15.842 g/cm$^3$ [32]. The primitive cell has a basis with two atoms, one Ta at (1/2, 1/2, 1/2)

Table 5.1: Structure characteristics of tantalum carbides and nitrides.

Tabla 5.1: *Características de las estructuras de los carburos y nitruros de tantalio.*

| Compound | Structure | Lattice Parameter(Å) | Space Group | Density (g/cm$^3$) |
|---|---|---|---|---|
| TaC [8] | Cubic | $a$=4.454 | $Fm\bar{3}m$ (225) | 14.498 |
| Ta$_2$C [26] | Hexagonal | $a$=3.1059 | $P\bar{3}m1$ (164) | 15.02 |
| | | $c$=4.946 | | |
| $\epsilon-$TaN [28] | Hexagonal | $a$=5.191 | $P6/mmm$ (191) | 14.306 |
| | | $c$=2.908 | | |
| $\delta-$TaN [32] | Cubic | $a$=4.339 | $Fm\bar{3}m$ (225) | 15.842 |

and one N at (0,0,0) associated with each point of the $fcc$ lattice.

$\epsilon$-TaN has a hexagonal symmetry with lattice parameters $a$=5.1918 Å and $c$=2.9081 Å, and a density of 14.306 g/cm$^3$ [28]. $\epsilon$-TaN belongs to the space group $P6/mmm$ (191) where the N atoms occupy the Wyckoff sites 1($a$) and 2($d$), and the Ta atoms the 3($f$) sites (see appendix C). The crystal structure corresponding to the conventional unit cell of $\epsilon$-TaN phase is shown in figure 5.4.

## 5.2 Elastic properties

The elastic properties of interest in this work are the elastic stiffness coefficients $c_{ij}$, bulk and Young moduli and Poisson ratio. These properties were determined theoretically with *ab initio* calculations for the tantalum compounds TaC, Ta$_2$C, $\epsilon$-TaN and $\delta$-TaN. The stiffness coefficients as well as mass density for TaC were determined also experimentally.

To do this, the two *ab initio* total-energy pseudopotential codes mentioned earlier, CASTEP and ABINIT, were used. The ABINIT code is used to relax the structures, finding the minimum ground-state energy, and to calculate the phonon dispersion curves of TaC and Ta$_2$C. Whereas the CASTEP code is utilized to calculate elastic properties such as stiffness coefficients ($c_{ij}$), bulk and Young moduli and Poisson ratio for all the studied compounds.

All calculations were performed using the ABINIT program versions 4.0.4, 4.4.3 and 4.6.5 for Windows and Linux, and CASTEP version 3.0 for Windows, on a personal computer with a Pentium Intel 4 processor.
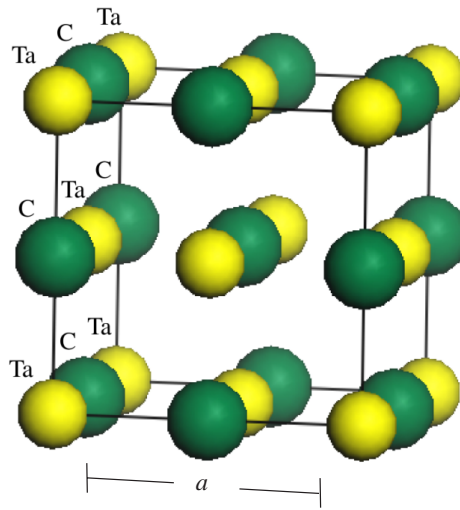
Figure 5.1: Conventional unit cell of TaC ($a$=4.454 Å) which has a NaCl-type structure with space group $Fm\bar{3}m$ (225) [8].

Figura 5.1: *Celda unitaria convencional del TaC ($a$=4.454 Å) la cual muestra una estructura tipo NaCl correspondiente al grupo espacial $Fm\bar{3}m$ (225) [8].*
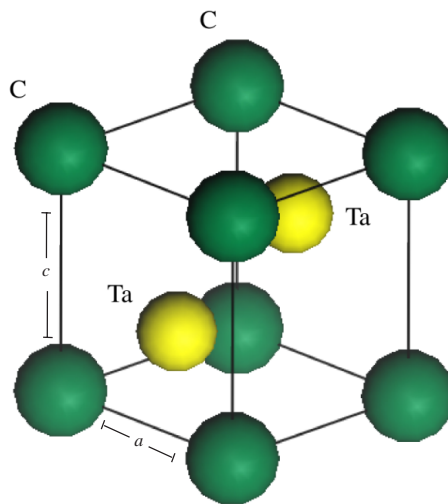


Figure 5.2: Conventional unit cell of Ta$_2$C with lattice parameters $a$=3.1059 Å and $c$=4.946 Å corresponding to the space group of $P\bar{3}m1$ (164) [26].

Figura 5.2: *Celda unitaria convencional del Ta$_2$C con parámetros de red a=3.1059 Å y c=4.946 Å, perteneciente al grupo espacial $P\bar{3}m1$ (164) [26].*
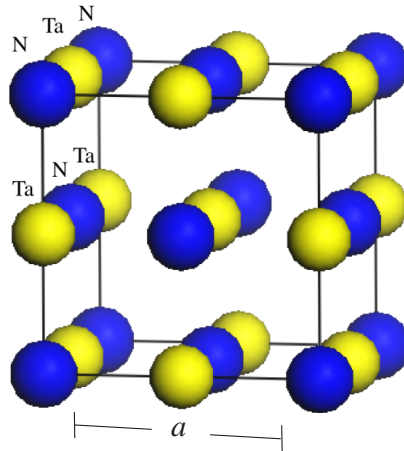
Figure 5.3: Conventional unit cell of $\delta$-TaN showing a NaCl-type structure ($a$=4.339 Å) corresponding to the space group $Fm\bar{3}m$ (225) [32].

Figura 5.3: *Celda unitaria convencional del $\delta$-TaN la cual muestra una estructura tipo NaCl correspondiente al grupo espacial $Fm\bar{3}m$ (225) [32].*
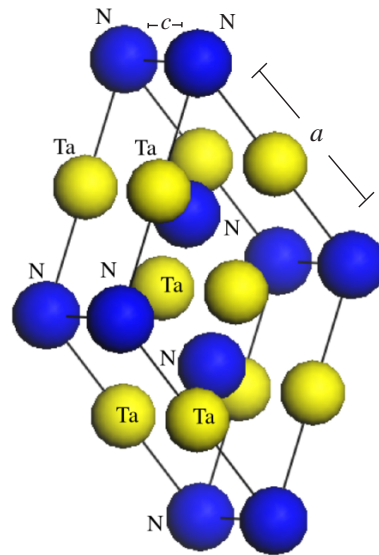


Figure 5.4: Conventional unit cell of $\epsilon$-TaN with lattice parameters $a$=5.1918 Å and $c$=2.9081 Å corresponding to the space group $P6/mmm$ (191) [28].

Figura 5.4: *Celda unitaria convencional del $\epsilon$-TaN con parámetros de red $a$=5.1918 Å y $c$=2.9081 Å correspondiente al grupo espacial $P6/mmm$ (191) [28].*

### 5.2.1   TaC

**Elastic properties from calculation for TaC**

The *ab initio* calculations performed on TaC with the ABINIT code are based on the density functional theory using the Local Density Approximation (LDA) and the General Gradient Approximation(GGA), with a plane-wave basis set. Pseudopotentials type Hartwigsen-Goedecker-Hutter [38] with semi-core states for Ta (13 e$^-$) and C (4 e$^-$) were used in the LDA case. These pseudopotentials were tested for tantalum and diamond in chapter 4. For GGA, Troullier-Martins [39] type pseudopotentials were used taking into account 5 e$^-$ for Ta and 4 e$^-$ for C. All these pseudopotentials were taken from the ABINIT data base. In calculations as those performed here, the influence of temperature is completely neglected.

Studies of convergence of two fundamental parameters, kinetic energy cutoff of plane waves and number of $k$-points, are necessary to obtain accurate results in the less possible computing time.

For TaC, the optimum kinetic energy cutoff value using LDA is $E_{cut\_LDA}$ =1360.5 eV (50 Hartree, 1 Hartree= 27.211 eV), and $E_{cut\_GGA}$= 2176.8 eV (80 Hartree) for GGA. Using the Monkhorst-Pack [50] scheme established and implemented in ABINIT, a grid of $8 \times 8 \times 8$ for the $k$-point sampling of the Brillouin zone was the best for both approximations.

The relation of the total energy of the system with respect to lattice parameter is shown in figure 5.5 for LDA and figure 5.6 for GGA. Dots indicate calculated values and the dashed line is a fit to these data with a cubic function in order to determine the lattice parameter corresponding to the minimum energy in both cases. The lattice parameters related to these fits are $a_{0\_LDA}$=4.414 Å (8.34 Bohr) and $a_{0\_GGA}$=4.527 Å (8.55 Bohr). The structure relaxation optimization performed with the ABINIT code gives a value of $a_{0\_LDA}$= 4.413 Å (8.343 Bohr), with a remaining pressure of $2.096 \times 10^{-4}$ GPa and $a_{0\_GGA}$= 4.526 Å (8.556 Bohr), with a remaining pressure of $1.2\text{x}10^{-4}$ GPa. These lattice parameters were used in the following calculations for TaC using LDA and GGA.

Figures 5.7 and 5.8 show the pressure-volume relation of the TaC structure for LDA and GGA, respectively. The data points were obtained from the previously mentioned lattice parameter calculations, and the dashed line is a fit with a Birch-Murnaghan third order equation of state. For LDA, the lattice parameter at zero pressure is $a_{0\_LDA}$=4.406(2) Å (8.33 Bohr) and the volume $v_{0\_LDA}$=85.65(2) Å$^3$. The bulk modulus is $B_{LDA}$=365(4) GPa with a first derivative of $B'_{LDA}$=3.6(1). For GGA, the lattice parameter at zero pressure is $a_{0\_GGA}$=4.52(2) Å (8.54 Bohr) with a volume $v_{0\_GGA}$=92.79(2) Å$^3$. The bulk modulus is
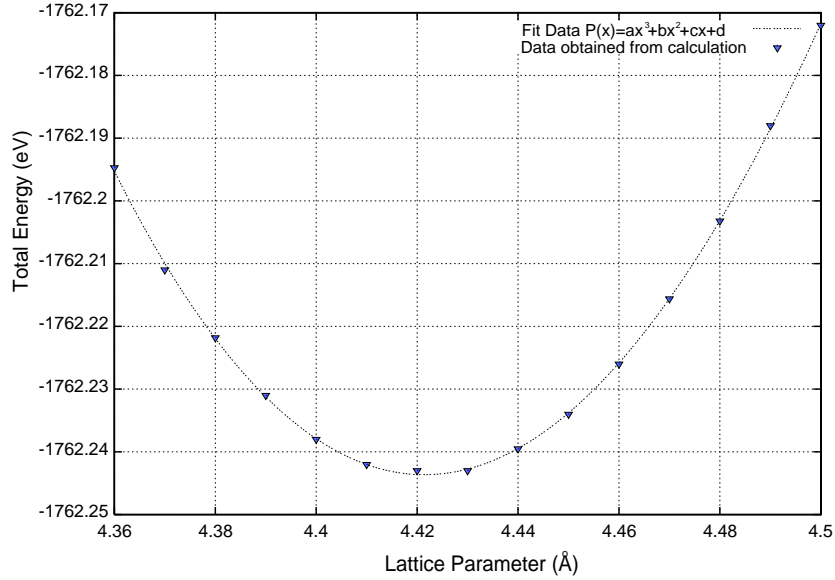
Figure 5.5: Relation of total energy with respect to lattice parameter of TaC using LDA. A kinetic energy cutoff of plane waves of 1360.5 eV (50 Hartree) and a $k$-point grid of $8 \times 8 \times 8$ were used.

Figura 5.5: *Relación de la energía total con respecto al parámetro de red del TaC usando LDA. Se usó una energía de corte de 1360.5 eV (50 Hartree) y una malla de puntos k de $8 \times 8 \times 8$.*

$B_{GGA}$=316(2) GPa and $B'_{GGA}$=3.99(8).

The study of elastic properties of TaC was performed using a standard technique based on the density functional theory implemented in CASTEP [40]. Ultrasoft pseudopotentials were used from the CASTEP/MSI database in conjunction with a plane-wave basis set, and the Generalized Gradient Approximation (GGA). The kinetic energy cutoff employed was 380 eV (13.96 Hartree) and for the sampling of the Brillouin zone a Monkhorst-Pack grid of $16 \times 16 \times 16$ $k$-points was employed. A geometry optimization of the TaC structure with fixed cell parameters gives a lattice parameter of $a_0$=4.525 Å (8.55 Bohr).

Due to their cubic symmetry, TaC crystals have only three elastic constants, $c_{11}$, $c_{12}$ and $c_{44}$, corresponding to a dilation normal to the stress, perpendicular to the stress, and shear [15]. Due to the close relation between the elastic stiffness coefficients and the bulk and Young moduli and Poisson ratio, it is possible to determine these properties if the elastic coefficients are known, and vice versa. The stiffness coefficients obtained in this calculation are $c_{11}$=621(3), $c_{12}$=155.3(2) and $c_{44}$=166.8(3) GPa, and the bulk and Young moduli obtained from these coefficients are $B$=318(4) and $E$=550 GPa, respectively. The calculated Poisson
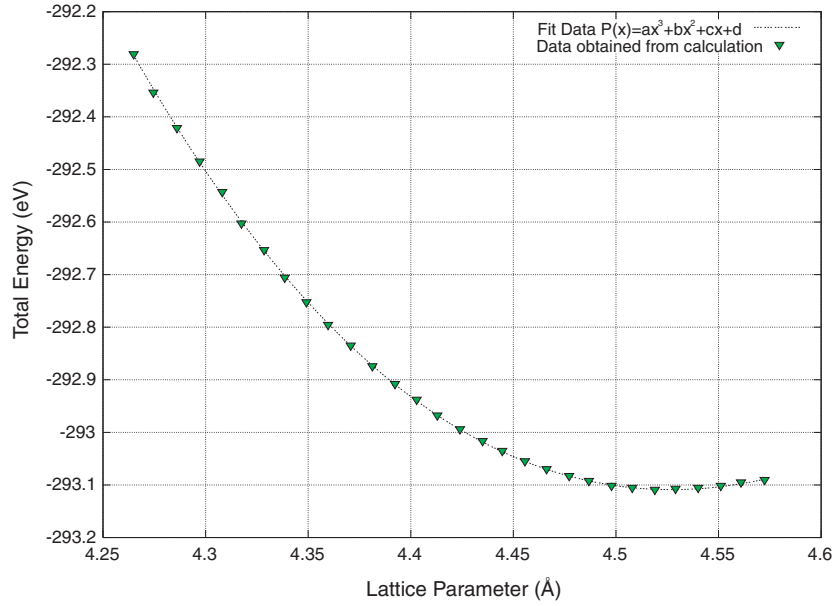
Figure 5.6: Relation of total energy with respect to lattice parameter of TaC using GGA. A kinetic energy cutoff of plane waves of 2176.8 eV (80 Hartree) and a $k$-point grid of $8 \times 8 \times 8$ were used.

Figura 5.6: *Relación de la energía total con respecto al parámetro de red del TaC utilizando GGA. Se usó una energía de corte de 2176.8 eV (80 Hartree) y una malla de puntos k de $8 \times 8 \times 8$.*

ratio has a value of $\nu$=0.21.

**Experimental Determination of TaC Elastic Stiffness Coefficients $c_{ij}$**

Tantalum carbide discs with faces parallel to (100) and dimensions of about 5 mm in diameter and 1.4 mm in thickness were cut from a single crystal rod purchased from Applied Physics Technologies Inc. using a low speed saw with a diamond wafering blade. The faces of the discs were polished to be parallel within $\pm 1 \, \mu$m. The orientation of all samples have been controlled by Laue backscattering and Bragg diffraction methods. Figure 5.9 shows a x-ray diffraction pattern showing the (100) plane obtained by Laue diffraction with a Philips Kristalloflex 710/710H type diffractometer. The mass density, $\rho$, was measured by the buoyancy method on one of the raw crystals in pure water with a value of $\rho$=14.64(4) g/cm$^3$.

The longitudinal and shear stiffness, $c_{11}$ and $c_{44}$, were determined from ultrasonic resonance frequencies using a plate mode technique [106]. The propagation of plane waves traveling along the normal of the plane parallel plates was studied. Modes were excited be-
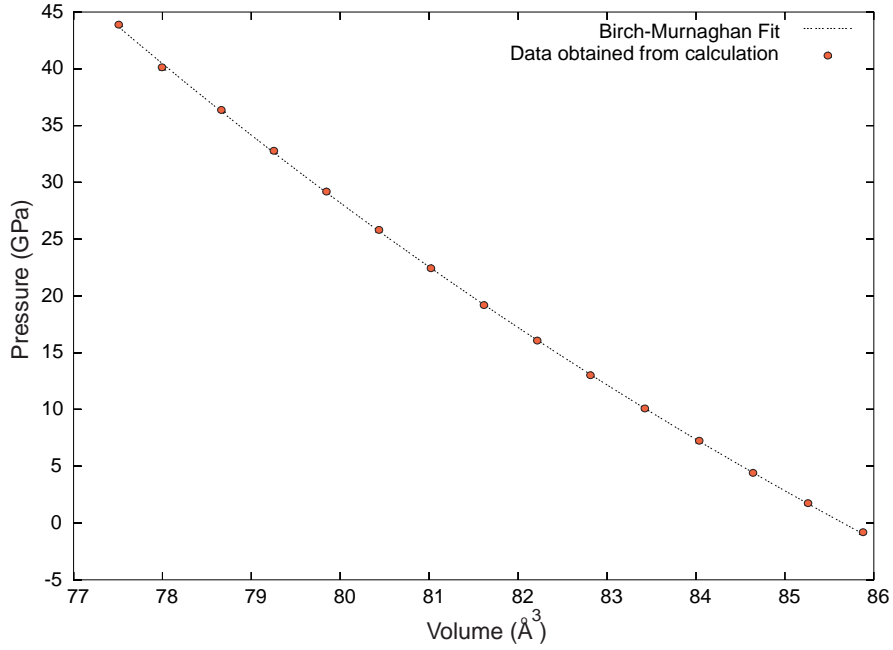
Figure 5.7: Pressure-volume relation for TaC. Circles show the data points obtained from ABINIT calculation using LDA and the dashed line is a fitting to a 3rd order Birch-Murnaghan equation of state.

Figura 5.7: *Relación presión-volumen para el TaC. Los círculos muestran los valores obtenidos de los cálculos con ABINIT usando LDA y la línea punteada muestra el ajuste a la ecuación de estado de Birch-Murnhagan a tercer orden.*

Table 5.2: Resonance number and their frequencies of a TaC single crystal.

Tabla 5.2: *Modos resonantes y sus frecuencias para un monocristal de TaC.*

| Resonance number | Frequency (THz) | | |
|---|---|---|---|
| 11 | 13.035 | 17 | 20.110 |
| 12 | 14.211 | 18 | 21.285 |
| 13 | 15.390 | 19 | 22.455 |
| 14 | 16.572 | 20 | 23.634 |
| 15 | 17.740 | 21 | 24.812 |

tween 4 and 30 MHz with X- and Y-cut $\alpha$-quartz transducers. Resonances were detected by measuring the frequency dependence of the impedance of the generator-sample system. From the $m$th and $n$th resonance frequency (table 5.2), $f_m$ and $f_n$, the corresponding wave velocity
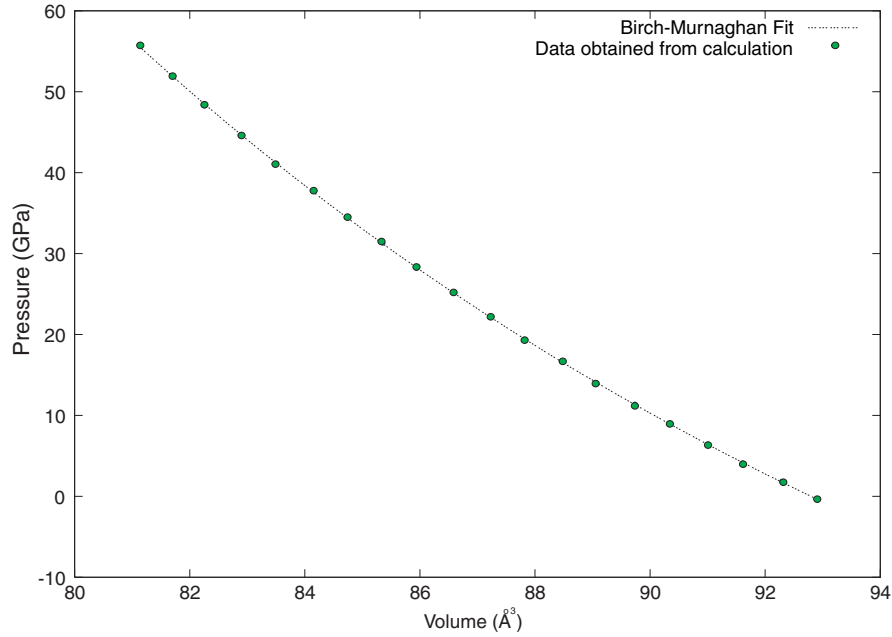
Figure 5.8: Pressure-volume relation for TaC. Circles show the data points obtained from ABINIT calculation using GGA and the dashed line is a fitting to a 3rd order Birch-Murnaghan equation of state.

*Figura 5.8: Relación presión-volumen para el TaC usando GGA. Los círculos indican los valores obtenidos de los cálculos con ABINIT usando GGA y la línea punteada muestra el ajuste a la ecuación de estado de Birch-Murnhagan a tercer orden.*

$v$ of a certain mode is obtained by $v = 2D(f_n - f_m)/(n - m)$, where $D$ is the thickness of the sample. Figure 5.10 shows the frequencies corresponding to the resonances produced in the TaC single crystal. The effective elastic stiffness constant $c$ of a mode is related to its wave velocity and the mass density, $\rho$, by $c = \rho v^2$. Due to the cubic symmetry of TaC, $c_{11}$ and $c_{44}$ correspond directly to the effective stiffness of a longitudinal and transverse ultrasound wave, respectively, traveling along [100].

**TaC Elastic Properties: Results and Discussion**

Table 5.3 presents experimental and theoretical values of mass density and lattice parameter for TaC determined here and in early published works. It is well established that the lattice parameter of stoichiometric TaC is $a_0$=4.4547 Å [8]. The dependence of TaC lattice parameter on the composition is $a_0$=4.3007 + 0.1563$x_C$ for $0.71 \leq x_C < 0.994$ [107], where $x_C$ is the carbon content. The mass density of stoichiometric TaC is $\rho_{x-ray} = 14.54 \, \text{g cm}^{-3}$. Obviously,

the value reported by Brown *et al.* [16], who determined the density of $TaC_{0.994}$ samples by dimension and weight measurements in air and mercury, is inconsistent with the expected value, specially as they reported a near-ideal stoichiometry. All other reported experimentally determined values for the density, including those obtained here, are within 1% of the value derived from lattice parameter determinations.

Sahnoun *et al.* [51] determined the TaC lattice parameter $a_0$=4.42 Å from first principles full-potential linearized augmented plane wave (FP-LAPW) calculations within DFT-LDA. This value is 1% smaller than the experimental value. In addition, using FP-LAPW and DFT-LDA and DFT-GGA, Sahnoun and coworkers [52] found $a_0$=4.39 Å and $a_0$=4.48 Å, respectively. The value from DFT-LDA is within a 2% smaller in comparison with experimental $a_0$. The value of $a_0$ from DFT-GGA is better than 1%.

In this study, the agreement of lattice parameter $a_0$ calculated with DFT-GGA with both codes, ABINIT and CASTEP, in comparison with the experiment is better than 2%
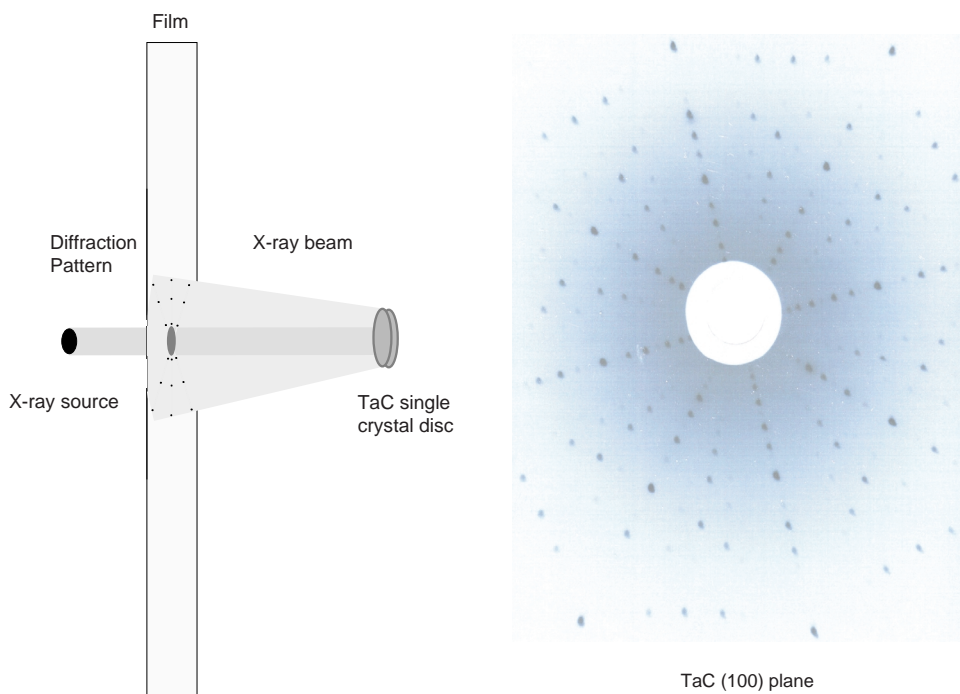


Figure 5.9: X-ray diffraction pattern of TaC showing (100) planes obtained by Laue backscattering with a Philips Kristalloflex 710/710H type diffractometer.

Figura 5.9: *Patrón de difracción del TaC mostrando los planos (100) obtenido por retrodispersión de Laue con un difractómetro tipo Philips Kristalloflex 710/710H.*
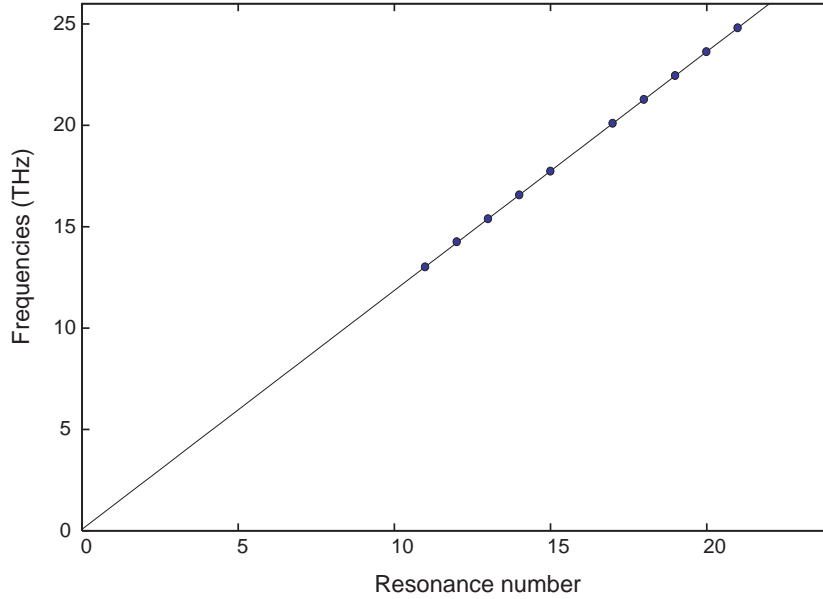
Figure 5.10: Resonances excited in a TaC single crystal to determine stiffness coefficients.

Figura 5.10: *Resonancias producidas en un monocristal de TaC para determinar los coeficientes elásticos.*

for $a_0$ and, consequently, better than 5% for the mass density. The slight overestimation of the lattice parameter, the so-called 'underbinding', is a feature consistently encountered in DFT-GGA calculations such as those presented here. On the other hand, results obtained from calculations performed with DFT-LDA show an $a_0$ value smaller than 2% and a mass density larger than 4% when compared with TaC ideal values. The underestimation of lattice parameter with respect to the ideal value of 4.4547 Å is due to the 'overbinding', which is a general feature of LDA-based DFT calculations. These features are also presented in lattice parameters determined by Sahnoun [51, 52].

There are some values of the elastic stiffness coefficients and moduli (bulk and Young, Poisson ratio) of TaC reported from experimental and theoretical works. The measured elastic stiffness coefficients at room temperature, along with the values obtained here in the athermal limit from the theory and the results published earlier, are summarized in table 5.4. Brown *et al.*[16], Jun *et al.* [17] and Krajewski *et al.* [12] reported measurements of Young modulus $E$ and Poisson ratio $\nu$ that were converted into $c_{ij}$. This was done by computing

Table 5.3: Lattice parameter $a_0$ and mass density $\rho$ for TaC. Experimental values are at room temperature.

Tabla 5.3: *Parámetro de red $a_0$ y densidad de masa $\rho$ del TaC. Los valores experimentales son a temperatura ambiente.*

| Reference | $a_0$ (Å) | $\rho$ (g/cm$^3$) |
|---|---|---|
| Bartlett & Smith[15] (TaC$_{0.90}$) | ... | 14.65 |
| Brown *et al.*[16] (TaC$_{0.994}$) | 4.4551 | 12.29 |
| Jun *et al.*[17] (TaC$_{0.99}$) | 4.454 | 14.5 |
| Krajewski *et al.*[12] | 4.455 | 14.47 |
| McKenna[108] (at 20° C) | 4.445 | 14.48 |
| National Bureau of Standards[8] | 4.454 | 14.498 |
| Sahnoun *et al.*[51] FP-LAPW (DFT-LDA) | 4.42 | ... |
| Sahnoun *et al.*[52] FP-LAPW (DFT-LDA) | 4.39 | ... |
| Sahnoun *et al.*[52] FP-LAPW (DFT-GGA) | 4.48 | ... |
| Present work (experimental) | ... | 14.64(5) |
| Present work from CASTEP (DFT-GGA) | 4.525 | 13.83 |
| Present work from ABINIT (DFT-GGA) from cubic fit | 4.527 | ... |
| Present work from ABINIT (DFT-GGA) from geometry optimization | 4.526 | ... |
| Present work from ABINIT (DFT-GGA) from EOS | 4.52 (2) | 13.88 |
| Present work from ABINIT (DFT-LDA) from cubic fit | 4.414 | ... |
| Present work from ABINIT (DFT-LDA) from geometry optimization | 4.413 | ... |
| Present work from ABINIT (DFT-LDA) from EOS | 4.406(2) | 14.98 |

first the elastic compliances $s_{11}$ and $s_{12}$ through equations

$$E = \frac{1}{s_{11}} \tag{5.1}$$

and

$$\nu = \frac{-s_{12}}{s_{11}}. \tag{5.2}$$

Then, the elastic stiffness coefficients were calculated according to equations [86].

$$c_{11} = \frac{s_{11} + s_{12}}{(s_{11} - s_{12})(s_{11} + 2s_{12})}, \tag{5.3}$$

$$c_{12} = \frac{-s_{12}}{(s_{11} - s_{12})(s_{11} + 2s_{12})}. \tag{5.4}$$

In table 5.4 it is possible to observe the large scatter, about a factor of 2 for $c_{11}$ and $c_{12}$, of the available data which cannot be explained by differences in the stoichiometry. While it

is known that the mechanical properties of carbides, such as their hardness, depend on the stochiometry, variations in excess of a few ten GPa are very unlikely.

As the data of Brown *et al.* [16], Jun *et al.* [17], Weber [22] and the experimental and theoretical values obtained here are in reasonable agreement, it can be conclude that the most likely value for the longitudinal elastic stiffness, obtained by averaging over these values, is $c_{11}$=606 GPa. A comparison with other transition metal carbides with rock salt structure, which is describe below, confirms this finding.

From a similar analysis for $c_{12}$, it can be deduced that values by Krajewski *et al.* [12], Bartlett and Smith [15] and Sahnoun *et al.* [52] for DFT-GGA, seem to be too low by about 50-70 GPa, and that the most likely value for $c_{12}$, obtained from average, is $c_{12}$=166 GPa.

Previously to this work, there had been only one experimental value published for $c_{44} = 79$ GPa by Bartlett and Smith. In their study, the two other elastic stiffness coefficients are systematically too low compared to other results, and this is probably true for the value of $c_{44}$ as well. In addition, values calculated using DFT-LDA and DFT-GGA by Sahnoun *et al.*, 410.44 and 315.47 respectively, show serious discrepancies with respect to all other values.

The values $c_{44}$=190 GPa determined by Weber [22] from extrapolations of neutron data, $c_{44}$= 176 GPa obtained from DFPT-LDA by Wu *et al.* [53], and those obtained here from experiment and calculation, 153(2) and 166.8(3) GPa, are found in acceptable agreement. This suggests a most likely value of $c_{44} = 170$ GPa. This will be discussed below and confirmed by a comparison with data for other carbides.

In table 5.5, further elastic properties, namely the bulk and Young moduli and the Poisson ratio are shown. Although Brown *et al.* [16] measured the density value of TaC$_{0.994}$ samples, they adjusted their elastic property data to theoretical densities obtained from X-ray diffraction and chemical analysis. The Poisson ratio and bulk modulus values were obtained by extrapolation of the reported elastic properties values to 0% porosity, in a study realized by Jun and Shaffer [17] about percentage of volume porosity versus bulk moduli.

The good agreement of $c_{ij}$ obtained by Brown *et al.* [16] and Jun *et al.* with values calculated here implies that the bulk and Young moduli are also in good agreement. In addition, values of elastic properties reported by Dodd *et al.* [54] measured using an ultrasonic technique, are in good agreement with those determined here. Hence, a preferred value of $B$=335 GPa can be deduced from the experiments.

Results of $B$=369.83 and $B$=397.3 GPa from quantum mechanical calculations using DFT-LDA performed by Sahnoun and coworkers, agree within 9% with that of $B$=365(4) GPa

Table 5.4: Elastic stiffness coefficients $c_{ij}$ for TaC. Experimental values are at room temperature.

Tabla 5.4: *Coeficientes de elasticidad $c_{ij}$ del TaC. Los valores experimentales son a temperatura ambiente.*

| Reference | $c_{11}$ (GPa) | $c_{12}$ (GPa) | $c_{44}$ (GPa) |
|---|---|---|---|
| Bartlett & Smith[15] ($TaC_{0.90}$) | 505(10) | 91(22) | 79(6) |
| Brown *et al.*[16] ($TaC_{0.994}$) | 634[a] | 200[a] | ... |
| Jun *et al.*[17] ($TaC_{0.99}$) | 631[b] | 168[b] | ... |
| Krajewski *et al.*[12] | 347[a] | 110[a] | ... |
| Weber [22] | 550 | 150 | 190 |
| Sahnoun *et al.*[52] FP-LAPW (DFT-LDA) | 880.37 | 156.24 | 410.44 |
| Sahnoun *et al.*[52] FP-LAPW (DFT-GGA) | 732.86 | 112.04 | 315.47 |
| Wu *et al.*[53] PW-PP (DFT-LDA) | 740 | 165 | 176 |
| Present work (experimental) | 595(2) | ... | 153(2) |
| Present work from CASTEP (DFT-GGA) | 621(3) | 155.3(2) | 166.8(3) |

[a]Values calculated from the reported Young modulus and Poisson ratio.
[b]Values obtained from elastic properties extrapolated to 0% porosity.

obtained here for the same approximation. In a similar way, results from DFT-GGA calculations by Sahnoun of $B$=318.98, and those determined here using both codes of $B$=318(4) and $B$=316(2) GPa, show an agreement better than 1%. The agreements on these results confirms the reliability of quantum mechanical calculations in the determination of elastic properties. After an analysis, a value of $B$=335 GPa is also in agreement with results from quantum mechanical calculations. For the first derivative of the bulk modulus, a value of $B'$=4 is preferred.

A comparison between values calculated with LDA and GGA shows some tendencies of the approximations. As it has been mentioned above the calculations based on LDA, in contrast to GGA, tends to 'overbind', i.e. give smaller lattice parameters. The 1% deviation in $a_0$ is therefore expected. As consequence of the overbonding an overestimation of the bulk modulus can be expected, and indeed $B_{\mathrm{EOS,LDA}} > B_{c_{ij},\mathrm{GGA}}$.

Young modulus and Poisson ratio were computed from the elastic constants reported by Sahnoun *et al.* [52]. This was done by computing the elastic compliances $s_{11}$ and $s_{12}$ from equations

Table 5.5: Bulk modulus ($B_0$), first derivative of bulk modulus, Young modulus ($E$), and Poisson ratio ($\nu$) for TaC.

Tabla 5.5: *Módulo de volumen ($B_0$), primera derivada del módulo de volumen, módulo de Young ($E$), y razón de Poisson ($\nu$) para TaC.*

| Reference | $B_0$ (GPa) | $B'$ | $E$ (GPa) | $\nu$ |
|---|---|---|---|---|
| Bartlett & Smith[15] (TaC$_{0.90}$) | 229[a] | ... | 477[a] | 0.152[a] |
| Brown *et al.*[16] (TaC$_{0.994}$) | 344(8)[b] | ... | 537(7)[b] | 0.24(0)[b] |
| Dodd *et al.*[54] (TaC$_{0.98}$) | 332(39)[c] | ... | 567(68) | 0.21(2)[c] |
| Jun *et al.*[17](TaC$_{0.99}$) | 329[d] | ... | 560[d] | 0.21 |
| Krajewski *et al.*[12] | 188[a] | ... | 294 | 0.24 |
| Sahnoun *et al.*[51] FP-LAPW (DFT-LDA) from EOS | 369.83 | 4.58 | ... | ... |
| Sahnoun *et al.*[52] FP-LAPW (DFT-LDA) | 397.6 | 3.64 | 833.27[e] | 0.15[e] |
| Sahnoun *et al.*[52] FP-LAPW (DFT-GGA) | 318.98 | 4.34 | 703.23[e] | 0.13[e] |
| Present work from CASTEP(DFT-GGA) from $c_{ij}$ | 318(4) | ... | 550 | 0.21 |
| Present work from ABINIT (DFT-GGA) from EOS | 316(2) | 3.9(8) | ... | ... |
| Present work from ABINIT (DFT-LDA) from EOS | 365(4) | 3.6(2) | ... | ... |

[a]Values calculated from elastic coefficients.

[b]Corrected to theoretical density.

[e]Values corrected to zero porosity.

[d]Values obtained from elastic properties extrapolated to 0% porosity.

[e]Calculated from $c_{ij}$.

$$s_{11} = \frac{c_{11} + c_{12}}{(c_{11} - c_{12})(c_{11} + 2c_{12})}, \tag{5.5}$$

and

$$s_{12} = \frac{-c_{12}}{(c_{11} - c_{12})(c_{11} + 2c_{12})} \tag{5.6}$$

and equations (5.1) and (5.2). Because their $c_{11}$ value from both approximations, LDA and GGA, are large in comparison with experimental values, the Young moduli computed are also large and therefore Poisson ratios are too low.

Thus, the derived values of Young modulus and Poisson ratio for TaC from experimental values and those obtained here from calculation are $E$=550 GPa and $\nu \approx$0.22, respectively.

These data can be compared to data obtained for other cubic carbides crystallizing in the rock salt structure, namely VC, TiC, NbC, HfC, ZrC. The average lattice parameters of these carbides have been obtained from the Inorganic Crystal Structure Database [109],

and from first principles calculations performed with the CASTEP code. The average lattice parameters are 4.689(6) Å for ZrC, 4.468(8) Å for NbC, 4.16(1) Å for VC, 4.640(2) Å for HfC and 4.323(5)Å for TiC, where the values in brackets correspond to the variation in the reported results, which will be mostly due to the non-stoichiometry.

Figure 5.11 demonstrates the linear relation between the lattice parameters and the ionic radii of the metal ions. For the latter, the data published by Shannon [110] was used, for six-fold coordinated cations formally in a 4+ oxidation state. An extrapolation of this graph points towards the structures of carbides with even smaller lattice parameters, such as CoC. This could, in principle, be used to search for very incompressible materials, as for several classes of materials it has been shown that $B \times V_0 = $ const. [111]. As the known carbides are already incompressible, it seems possible to search for structures which are as incompressible as diamond. However, figure 5.12 clearly shows that due to the very large scatter in the data at the moment such an empirical correlation cannot be established. It is unlikely that small changes in the stoichiometry will change the bulk modulus by a factor of two, and hence part of the scatter may be due to the microstructures of the samples.

The scatter in the bulk moduli reflect the significant variations between individual data sets of elastic stiffness coefficients of other rock salt structure transition metal cabides. For example, values for $c_{44}$ for TiC range from 175 - 217 GPa [113]. All these values, however, are a factor of 2 larger than the only previously reported experimental value for TaC, $c_{44} = 79(6)$ GPa [15]. This is also true for values of $c_{44}$ reported for NbC, which range from 153 - 205 GPa [114, 113], and VC (155-192 GPa [113]).

This further supports the conclusion that the value obtained for $c_{44}$ for TaC (170 GPa) is preferable to the one reported earlier. For $c_{12}$ the situation is less clear, as the scatter of data is even larger than for the other elastic stiffness coefficients. This is problematic, as without an accurate knowledge of $c_{12}$ the bulk moduli cannot reliably be obtained from the elastic stiffness coefficients.

As the experimental difficulties are obvious from the analysis of data published earlier, it now has become clear that it would be very desirable if two complementary methods would be employed to improve the quality of the available data. Compression studies with diamond anvil cells could be used to determine bulk moduli, while resonant ultrasound spectroscopic measurements will give all symmetrically independent elastic coefficients of a sample at once with high internal consistency [115]. A combination of these two approaches seems to be the only way to obtain data sufficiently accurate to establish the desired composition-properties
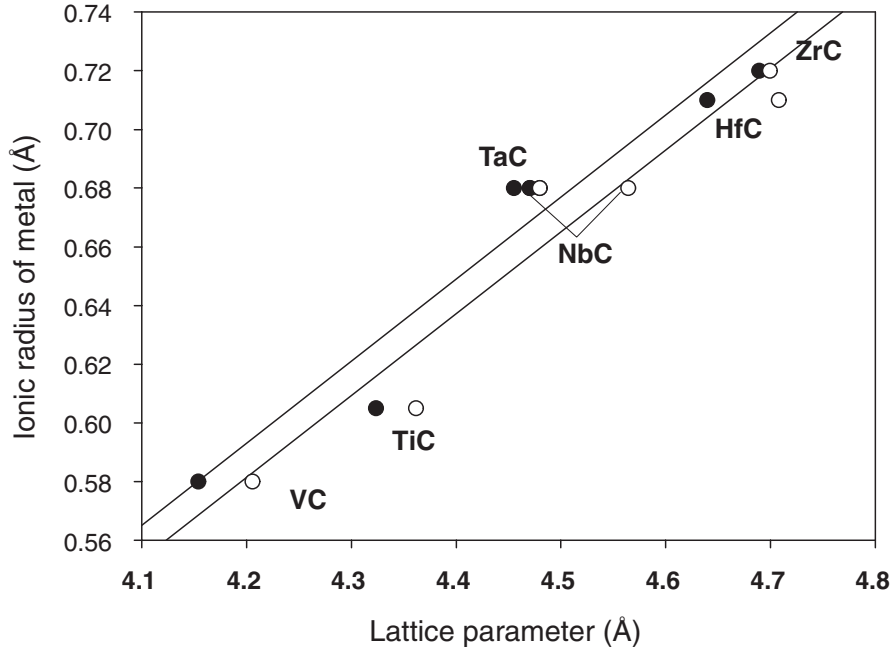
Figure 5.11: The lattice parameters of cubic carbides, crystallizing in the NaCl-type structure, depend linearly on the effective ionic radii of the metal cations. Lattice parameters have been obtained from the ICSD [112], the effective ionic radii are from Shannon [110]. Filled circles are experimental data, open circles are values obtained here from *ab initio* calculations. The two lines are linear regression analysis to the experimental (upper line) and theoretical data (lower line), respectively. The 'underbinding' of the DFT-GGA calculations leads to a systematic shift in the lattice parameters.

Figura 5.11: *Los parámetros de red de carburos cúbicos con estructura tipo NaCl varian linealmente respecto a los radios iónicos efectivos de los cationes metálicos. Los parámetros de red se obtuvieron de la base de datos ICSD [112] y los radios atómicos efectivos de Shannon [110]. Los círculos rellenos muestran los valores experimentales y los círculos vacios indican los valores obtenidos aquí mediante los cálculos ab initio. Las dos líneas muestran una regresión lineal resultado del análisis de los valores experimentales (línea superior) y teóricos (línea inferior), respectivamente. La baja estimación en los valores que producen los cálculos utilizando DFT-GGA conduce a un corrimiento sistemático en los parámetros de red.*

dependencies.

**Lattice Dynamics of TaC**

The dynamics of the TaC lattice was studied through phonon dispersion relations calculated with the ABINIT code, based on GGA and density function perturbation theory (DFPT), in the high symmetry directions $[x00]$, $[xx0]$ and $[xxx]$. Figure 5.13 contains an schematic draw
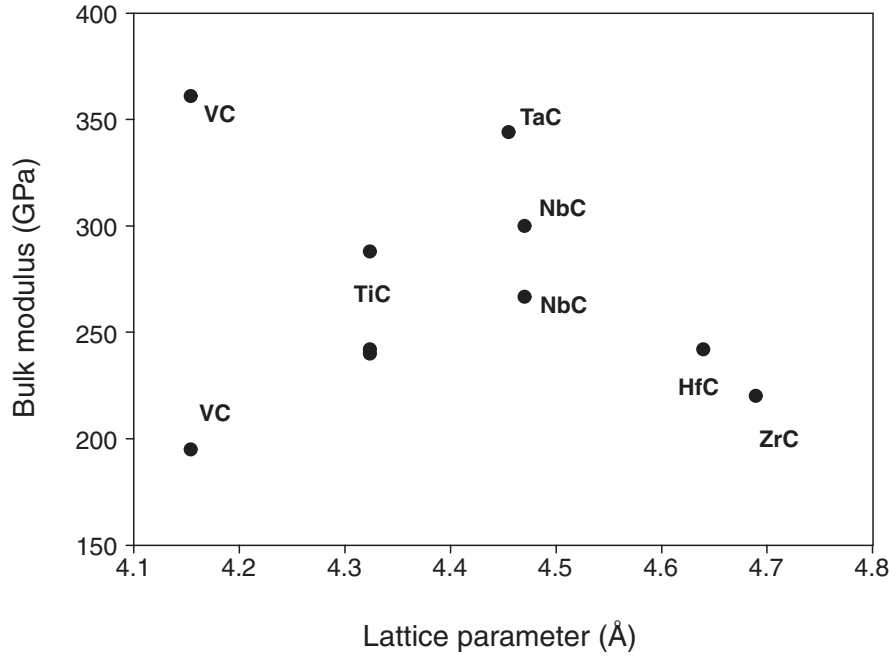
Figure 5.12: Dependence of the bulk modulus as a function of lattice parameter of cubic (NaCl-type structure) carbides. Data are from Kumashiro *et al.* for TiC, VC and NbC [113], from Brown *et al.* for HfC and NbC [16], from Ledbetter *et al.* for NbC [114] and from Toth for ZrC [1]. It is not yet clear whether the large scatter is only due to small differences in the stoichiometry of the samples.

Figura 5.12: *Dependencia del módulo de volumen en función del parámetro de red de carburos cúbicos (estructura tipo NaCl). Los valores para TiC, VC y NbC son tomados de Kumashiro et al. [113], para HfC y NbC de Brown et al. [16], para NbC de Ledbetter et al. [114] y para ZrC de Toth [1]. Todavía no es claro si las diferencias entre los valores se deben solamente a pequeñas diferencias en la estequiometría de las muestras.*

of the Brillouin zone corresponding to the structure of TaC showing the path (dashed line) on high symmetry directions followed in the calculation. The zone center ($k$=0) is designated by $\Gamma$ while the interior lines by Greek letters and points in the zone boundary by Roman letters.

Convergence studies, structure relaxation and phonon dispersion relations were calculated for diamond and tantalum as an initial study to test the accuracy of *ab initio* calculations performed with the ABINIT code. Diamond dispersion curves were reproduced in good agreement with experimental data and tantalum phonon frequencies are about 0.5 THz higher in comparison with experimental values. However, the main dispersion relations features are well reproduced by the calculations. More details about these calculations are found in chapter 4.

(a)



(b)
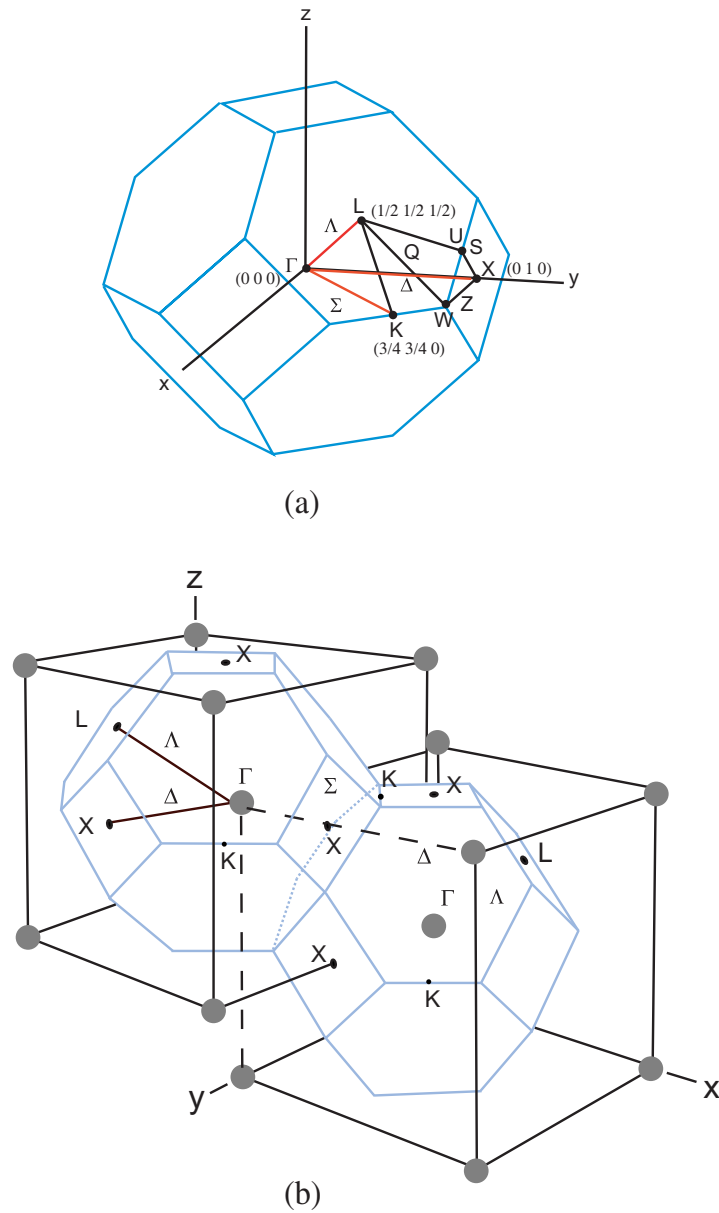
Figure 5.13: (a) Brillouin zone of the *fcc* structure showing the high symmetry points and lines. The dashed line indicates the path follow for calculations of TaC. (b) Brillouin zone in two neighbor cells .

Figura 5.13: *(a) Esquema de la zona de Brillouin de una red fcc donde se muestran los puntos y líneas de alta simetría. La línea punteada indica la trayectoria que se recorrió en los cálculos para TaC. (b) La zona de Brillouin en dos celdas vecinas.*

Phonon dispersion relations calculated for diamond and tantalum provided us with confidence for the phonon calculations of TaC.

Dispersion curves of TaC are shown in figure 5.14. Points indicate calculated values and the lines drawn through the calculated points are a guide to the eye. Experimental values by Smith and Gläser [18] are indicated by squares (transversal modes) and triangles (longitudinal modes). In this figure we can observe a large frequency gap between acoustical and optical branches of about 16 THz. High frequency curves originate mainly from the lower mass of C atoms, while low frequency curves resulted mainly from vibrations of the higher Ta mass atoms. However, Weber [22] states that the very high optic frequencies are due not only to the high mass difference of the atoms, but also to much stronger force constants between nearest neighbor metal and non-metal ions.

As dispersion curves were calculated with wave vectors $q$ at high-symmetry directions, only purely transversal (perpendicular to $q$) and purely longitudinal (parallel to $q$) modes were obtained. Also, the degeneracy of transversal acoustical (TA) and optical (TO) modes is observed at directions $[x00]$ and $[xxx]$. The polarization and degeneracy of dispersion curves are intimately related to the crystal symmetry relative to the direction of propagation.

A number of authors have reproduced the phonon dispersion curves determined by inelastic neutron scattering by Smith and Gläser [18], using phenomenological methods, the shell model or a modified shell model [20, 21, 22, 23].

A third transverse acoustical and optical branches in the $[xx0]$ direction were predicted by Weber and coworkers [21] using an extension of the shell model. These branches also were determined here from first principles calculations. Their model described well the overall shapes of the dispersion curves of some transition metal carbides including TaC.

In addition, Weber [22] describes the sharp minima in most of the acoustic branches as anomalies, and states that these phonon anomalies are caused by the metallic $d$-electron band. Phillips [116] interprets the anomalies in stoichiometric TaC as due to an overscreening of the ion-ion interactions by the electron-ion interactions. On the other hand, Zeller [117] suggests that there is a linear dependence of phonon frequencies on carbon content using a theoretical model. Weber [22] and Verma and Gupta [23] also believe that the anomalous behavior of TaC phonon frequencies is related with the electron-phonon interaction.
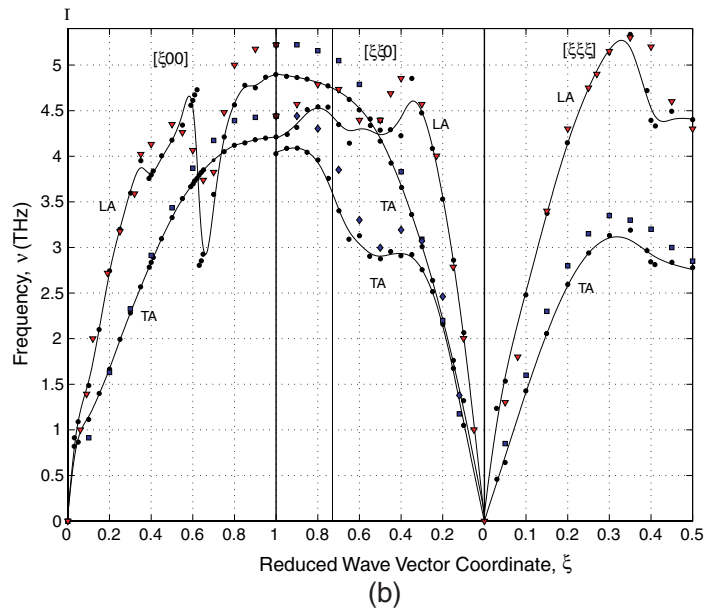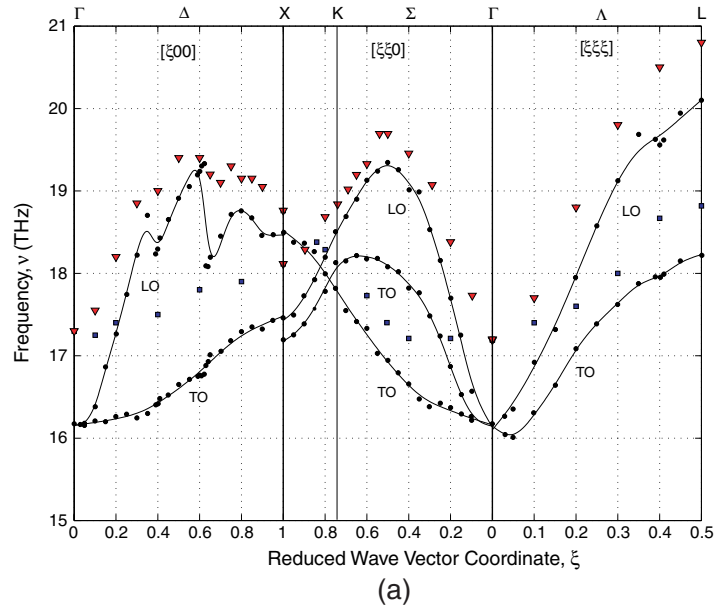
Figure 5.14: Phonon dispersion curves of TaC for the high symmetry directions calculated using the GGA approach: (a) high frequencies and (b) low frequencies. Circles indicate calculated values and lines drawn through calculated points are a guide to the eye. Triangles (longitudinal modes), and squares and diamonds (transversal modes) represent experimental data by Smith and Gläser [18] and Smith [19].

Figura 5.14: *Curvas de dispersión del TaC en las direcciones de alta simetría calculadas con GGA: (a) altas frecuencias y (b) bajas frecuencias. Los círculos indican los valores calculados y las líneas que unen los puntos son una guía para la vista. Los triángulos (modos longitudinales) y los cuadrados y diamantes (modos transversales) representan los valores experimentales obtenidos por Smith y Gläser [18] y Smith [19].*

### 5.2.2   $Ta_2C$

*Ab initio* calculations performed on $Ta_2C$ with the ABINIT code are based on DFT within LDA using a plane-wave basis set. Pseudopotentials provided from the ABINIT data base type Hartwigsen-Goedecker-Hutter [38] for C ($4$ $e^-$) and Ta with semi-core states ($13$ $e^-$) were used. The energy cutoff of $E_{cut}$ =1632.6 eV (60 Hartree) and a $k$-point grid of $8 \times 8 \times 4$ for sampling the Brillouin zone were used. A geometry optimization of the structure produces lattice parameters of $a_0$=3.089 Å (5.84 Bohr) and $c_0$=4.837 Å (9.145 Bohr), with a remaining pressure of $7.1156\text{x}10^{-3}$.

The CASTEP code was used to calculate the elastic properties of $Ta_2C$ using ultrasoft pseudopotentials from the CASTEP/MSI database within the generalized gradient approximation (GGA) and a plane-wave basis set. The kinetic energy cutoff employed was 330 eV (12.12 Hartree) and for the sampling of the Brillouin zone a Monkhorst-Pack grid of $10 \times 10 \times 6$ $k$-points was used. The minimization of the energy with respect to lattice parameters performed with the CASTEP minimizer module determined the equilibrium lattice parameters of $a_0$=3.152 Å (5.958 Bohr) and $c_0$=4.99 Å (9.43 Bohr).

The hexagonal symmetry of $Ta_2C$ allows five independent elastic stiffness coefficients, and those obtained in this calculation are $c_{11}$=445(4), $c_{12}$=172.6(1), $c_{13}$=143.8(1), $c_{33}$=492(4) and $c_{44}$=135.6(1) GPa. The bulk modulus obtained from these coefficients is $B$=256(5) GPa and the Young modulus for each direction are $E_x$=$E_y$=360.5 and $E_z$=425.1 GPa.

Due to its symmetry also, $Ta_2C$ shows six values of Poisson ratio corresponding to the relation of stresses and strains in the $x$, $y$ and $z$ directions, where $x$ and $y$ are equivalent, leading to only three different values of Poisson ratios. These values are $\nu_{xy}$=$\nu_{yx}$=0.32, $\nu_{zx}$=$\nu_{zy}$=0.23 and $\nu_{xz}$=$\nu_{yz}$=0.197. There is not elastic properties data published available for $Ta_2C$ for comparison with the values calculated here.

Table 5.6 shows the calculated values with ABINIT (DFT-LDA) and CASTEP (DFT-GGA) for lattice parameters. It can be observed an overestimation of DFT-GGA lattice parameters of less than 2% for $a_0$ and about 1% for $c_0$ in comparison with experimental values reported by the International Centre for Diffraction Data (ICDD) [32]. On the other hand, the underestimation of lattice parameters calculated by DFT-LDA of less than 1% for $a_0$ and about 2% for $c_0$ is also evident. As no experimental data of mechanical properties of $Ta_2C$ are available, the calculated values mentioned above can be considered as predicted values.

Table 5.6: Lattice parameters $a_0$ and $c_0$ for Ta$_2$C. Experimental values are at room temperature.

Tabla 5.6: *Parámetros de red $a_0$ y $c_0$ del Ta$_2$C. Los valores experimentales son a temperatura ambiente.*

| Reference | $a_0$ (Å) | $c_0$ (Å) |
|---|---|---|
| Lissner & Schleid (ICSD)[26] | 3.1059 | 4.946 |
| Present work from CASTEP (DFT-GGA) | 3.152 | 4.99 |
| Present work from ABINIT (DFT-LDA) | 3.089 | 4.837 |

**Lattice dynamics of Ta$_2$C**

Dispersion relations of phonon frequencies for the high symmetry directions $[xx0]$,$[x00]$ and $[00x]$ (see figure 5.15) were calculated with the ABINIT program using density functional theory and LDA.

Figure 5.16, presents phonon dispersion curves of Ta$_2$C at low (a) and high (b) frequencies. As before, points indicate calculated values and the lines are intended to be a guide to the eye. Because the primitive unit cell of Ta$_2$C has associated three atoms, the dispersion curves generated show 9 branches: 3 acoustical and 6 optical. Figure 5.16 shows the degeneracy of the acoustical and optical branches in the direction $[00x]$ due to symmetry.

Similar to TaC, a large frequency gap separating the branches about 12 THz is found. Again, high frequency curves originate mainly from the lower mass of C atoms, while low frequency curves result mainly from vibrations of the higher Ta mass atoms.

At the time of writing this thesis, we have not found any published data about Ta$_2$C phonon dispersion curves, neither theoretical or experimental. Thus, dispersion curves derived here from calculation can be seen as a prediction.
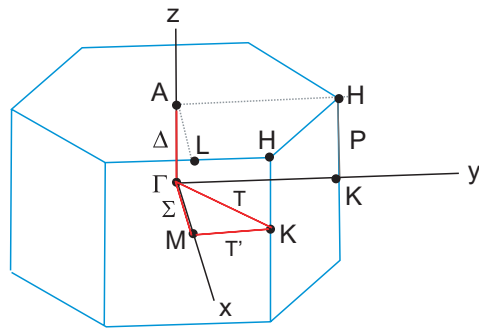
Figure 5.15: First Brillouin zone of the hexagonal lattice showing high symmetry points and lines.

Figura 5.15: *Esquema de la primera zona de Brillouin de una red tipo hexagonal mostrando los puntos y líneas de alta simetría.*
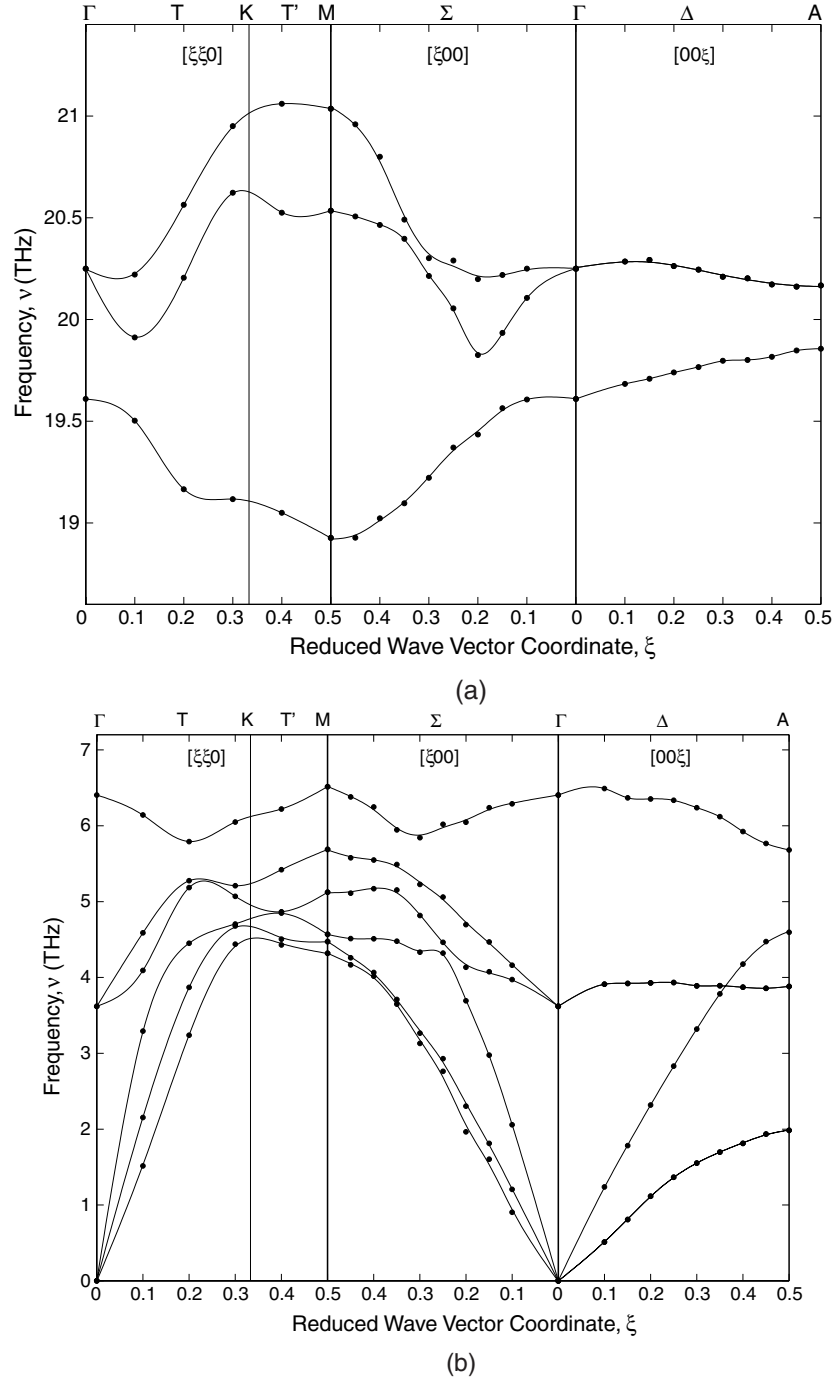
Figure 5.16: Phonon dispersion curves of Ta$_2$C at high symmetry directions calculated with DFT-LDA at: (a) high frequencies and (b) low frequencies. The lines drawn through the calculated points are a guide to the eye.

Figura 5.16: *Curvas de dispersión de fonones del Ta$_2$C en las direcciones de alta simetría calculadas con DFT-LDA: (a) altas frecuencias y (b) bajas frecuencias. Las líneas que unen los puntos calculados son una guía para la vista.*

### 5.2.3  $\delta$-TaN

Elastic properties of cubic tantalum carbide $\delta$-TaN were studied from first principles calcula-
tions. As mentioned above, $\delta$-TaN has a rock-salt crystalline structure and exhibits mechanical
properties similar to those of TaC.

**Elastic properties from calculation for $\delta$-TaN**

Calculations on $\delta$-TaN were performed with the ABINIT code, based on DFT and LDA, using
a plane-wave basis set. Hartwigsen-Goedecker-Hutter type pseudopotentials [38] for N (5 e$^-$)
and with semi-core states for Ta (13 e$^-$) were used. These pseudopotentials were taken from
the ABINIT database. The kinetic energy cutoff $E_{cut}$ =1632.6 eV (60 Hartree) and a grid of
$8 \times 8 \times 8$ to sample the Brillouin zone, which corresponds to 60 $k$-points, were used.

The relation of the lattice parameter and the total energy of the system is shown in figure
5.17. Dots indicate calculated values and the dashed line is a fit with a cubic function in order
to determine the lattice parameter. The lattice parameter that minimizes the energy is $a_0=$
4.329 Å (8.185 Bohr). The geometry optimization performed with ABINIT gives a lattice
parameter of $a_0$=4.3307 Å (8.186 Bohr), with a remaining pressure of $3.84 \times 10^{-4}$ GPa. The
latter lattice parameter was used in the following calculations.

Figure 5.18 shows the pressure-volume relation of the $\delta$-TaN structure. Circles represent
volume as function of pressure, and the dashed line is a fit with a 3rd order Birch-Murnaghan
equation of state. The lattice parameter at zero pressure obtained from this equation is
$a_0$=4.339(6) Å (8.204 Bohr) and the volume $v_0$=81.730(6) Å$^3$. The bulk modulus is $B_0$=373(6)
GPa and the first derivative of the bulk modulus is $B'$=4(1).

The study of elastic properties of $\delta$-TaN were performed using the CASTEP program with
a standard technique based on DFT and GGA. Ultrasoft pseudopotentials for Ta and N were
used from the CASTEP/MSI database in conjunction with a plane-wave basis set. The energy
cutoff of $E_{cut}$=380 eV (13.96 Hartree) was used and, for the sampling of the Brillouin zone, a
Monkhorst-Pack grid of $16 \times 16 \times 16$ $k$-points was employed. From the minimization of energy
performed with CASTEP, the equilibrium lattice parameter of $a_0$=4.4905 Å (8.48 Bohr) was
obtained.

The three independent stiffness coefficients obtained from this calculation are $c_{11}$=700(5),
$c_{12}$=128.8(7) and $c_{44}$=34.7(4) GPa. The bulk and Young moduli obtained from these coeffi-
cients are $B$=319(2) and $E$=659.7 GPa, respectively. The calculated Poisson ratio is $\nu$=0.155.
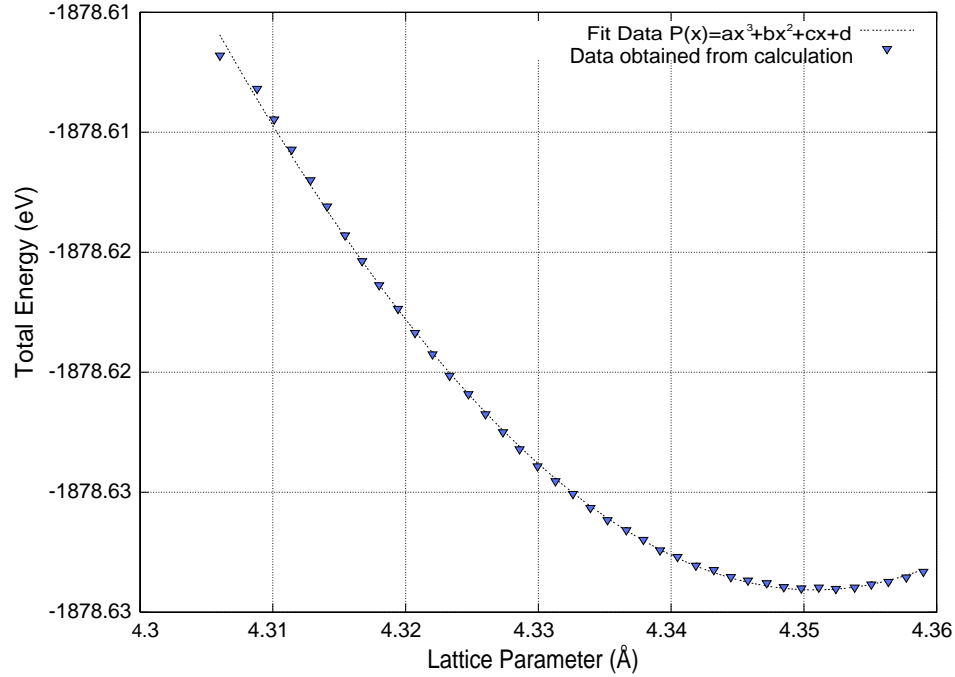
Figure 5.17: Total energy *vs.* lattice parameter of δ-TaN. An energy cutoff of plane waves of 1360.5 eV (50 Hartree) and a k-point grid of $8 \times 8 \times 8$ were used.

Figura 5.17: *Energía total vs. parámetro de red del δ-TaN. Se utilizó una energía de corte para las ondas planas de 1360.5 eV (50 Hartree) y una malla de puntos k de $8 \times 8 \times 8$.*

**δ-TaN Elastic Properties: Results and Discussion**

Table 5.7 shows values of lattice parameter $a_0$ and mass density $\rho$ for δ-TaN. All lattice parameters determined theoretically are in good agreement with the experimental value of $a_0$=4.339 Å by the National Bureau of Standards [32]. However, lattice parameters derived from DFT-LDA calculations performed here and by Sahnoun *et al.* [52] show an underestimation of 1%, while DFT-GGA calculations are overestimated by $\approx 3.5$ and 2%, respectively. As mentioned before, these effects are caused by the overbinding produced with LDA, and the underbinding by GGA. Consequently, mass density computed from DFT-LDA calculated lattice parameters are 1% overestimated in comparison with that determined experimentally of 15.842 $g/cm^3$, and the density computed from DFT-GGA calculated lattice parameters are about 10% underestimated.

Published values of elastic stiffness coefficients of δ-TaN and those obtained in this study are contained in table 5.8. For $c_{11}$, the calculated value of 700(5) GPa agrees better than

3.5% in comparison with the value of 675.95 GPa calculated by Sahnoun *et al.* [52] using the same approximation (DFT-GGA). On the other hand, values calculated with DFT-LDA by Sahnoun (886.9 GPa), and Wu *et al.* [53] (783 GPa), show agreements of 26.7% and 11.85%, respectively. Differences like these between the GGA and LDA approximations were expected. However, the value by Sahnoun is about 100 GPa too large in comparison with that by Wu, calculated also with DFT-LDA. As the values of Sahnoun *et al.* using DFT-GGA, Wu *et al.* and that obtained here are in reasonable agreement, by averaging these values we can predict a likely value of $c_{11}$=720 GPa. In the case of $c_{12}$, all values show a reasonable agreement. Thus, similar to $c_{11}$, a value of $c_{12}$=150 GPa can be predicted.

Although all values shown in table 5.8 were determined theoretically using DFT, serious discrepancies are observed in $c_{44}$ values. Values of Sahnoun *et al.* are some hundreds GPa too
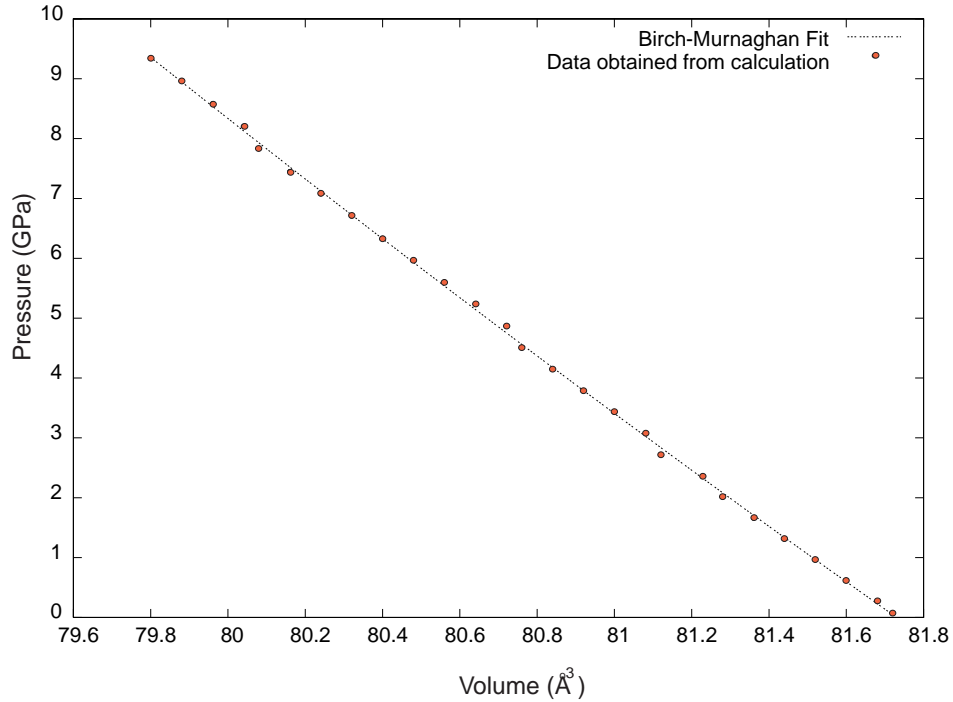


Figure 5.18: Pressure-volume relation of $\delta$-TaN. Circles show data points obtained from ABINIT calculation and the line is the fitting of a 3rd order Birch-Murnaghan equation of state.

Figura 5.18: *Relación presión-volumen del $\delta$-TaN. Los círculos indican los valores obtenidos por el cálculo con ABINIT y la línea es un ajuste a la ecuación de estado de Birch-Murnhagan a tercer orden.*

Table 5.7: Lattice parameter $a_0$ and mass density $\rho$ for $\delta$-TaN. Experimental values are at room temperature.

Tabla 5.7: *Parámetro de red $a_0$ y densidad de masa $\rho$ del $\delta$-TaN. Los valores experimentales son a temperatura ambiente.*

| Reference | $a_0$ (Å) | $\rho$ (g/cm$^3$) |
|---|---|---|
| National Bureau of Standards[32] | 4.339 | 15.842 |
| Sahnoun *et al.*[52] FP-LAPW (DFT-LDA) | 4.33 | ... |
| Sahnoun *et al.*[52] FP-LAPW (DFT-GGA) | 4.42 | ... |
| Present work from CASTEP (DFT-GGA) | 4.4905 | 14.3 |
| Present work ABINIT (DFT-LDA) from cubic fit | 4.329 | 15.96 |
| Present work ABINIT (DFT-LDA) from geometry optimization | 4.3307 | 15.95 |
| Present work ABINIT (DFT-LDA) from EOS | 4.339(6) | 15.85 |

Table 5.8: Elastic stiffness coefficients $c_{ij}$ for $\delta$-TaN.

Tabla 5.8: *Coeficientes de elasticidad $c_{ij}$ del $\delta$-TaN.*

| Reference | $c_{11}$ (GPa) | $c_{12}$ (GPa) | $c_{44}$ (GPa) |
|---|---|---|---|
| Sahnoun *et al.*[52] FP-LAPW (DFT-LDA) | 886.9 | 162.33 | 355.86 |
| Sahnoun *et al.*[52] FP-LAPW (DFT-GGA) | 675.95 | 154.48 | 266.92 |
| Wu *et al.*[53] PW-PP (DFT-LDA) | 783 | 167 | 20 |
| Present work from CASTEP (DFT-GGA) | 700(5) | 128.8(7) | 34.7(4) |

large in comparison with those calculated by Wu *et. al* and this study. As no experimental $c_{44}$ value is available for comparison, and based on the reliability of the agreement found in calculations of TaC with the pseudopotential approach used, a best value of $c_{44}$=27 GPa is predicted. However, an experimental determination of $c_{44}$ is still needed to corroborate this proposed value.

Further elastic properties such as bulk modulus and its first derivative, Young modulus and Poisson ratio, are shown in table 5.9. As all bulk modulus values shown a reasonable agreement, an averaged value of $B$=350 GPa can be taken as a predicted value. For Young modulus, the value of Sahnoun *et al.* [52] from DFT-LDA calculations is too large in comparison with other values calculated with DFT-GGA. Hence, a best value of $E$=640 GPa is preferred. From a similar analysis for Poisson ratio, the most likely value for $\nu$ is 0.165.

Table 5.9: Bulk modulus ($B_0$), first derivative of bulk modulus, Young modulus ($E$), and Poisson ratio ($\nu$) for $\delta$-TaN.

Tabla 5.9: *Módulo de volumen ($B_0$), primera derivada del módulo de volumen, módulo de Young ($E$), y la razón de Poisson ($\nu$) del $\delta$-TaN.*

| Reference | $B_0$ (GPa) | $B'$ | $E$ (GPa) | $\nu$ |
|---|---|---|---|---|
| Kobayashi[118] PW-PP (DFT-LDA) | 341 | ... | ... | ... |
| Sahnoun *et al.*[52] FP-LAPW (DFT-LDA) | 403.85 | 4.28 | 836.8[a] | 0.154[a] |
| Sahnoun *et al.*[52] FP-LAPW (DFT-GGA) | 328.3 | 5.45 | 618.47[a] | 0.186[a] |
| Present work from CASTEP (DFT-GGA) from $c_{ij}$ | 319(2) | ... | 659.7 | 0.155 |
| Present work from ABINIT (DFT-LDA) from EOS | 373(6) | 4(1) | ... | ... |

[a]Calculated from $c_{ij}$.

### 5.2.4   $\epsilon$-TaN

Pseudopotential total energy calculations were performed on $\epsilon$-TaN with the ABINIT code based on DFT within the local density approximation (LDA) in conjuntion a plane-wave basis set. Pseudopotentials taken from the ABINIT database type Hartwigsen-Goedecker-Hutter [38] for N (5 e$^-$), with semi-core states for Ta (13 e$^-$), were used. The cutoff energy of plane-wave basis is $E_{cut}$ =1632.6 eV (60 Hartree) and the sampling the Brillouin zone has been performed with a $k$-point grid of $4 \times 4 \times 8$. A structure optimization performed with the ABINIT code determined lattice parameters $a_0$=5.343 Å (10.1 Bohr) and $c_0$=3.001 Å (5.673 Bohr), with a remaining pressure of $4.8 \times 10^{-3}$ GPa.

Elastic properties of $\epsilon$-TaN were calculated using the CASTEP code within the gradient generalized approximation (GGA) using a plane-wave basis set. Ultrasoft pseudopotentials taken from the CASTEP/MSI database for Ta and N were used. The energy cutoff employed was 330 eV (12.13 Hartree) and for the sampling of the Brillouin zone a Monkhorst-Pack grid of $10 \times 10 \times 6$ $k$-points was used. A full optimization of the cell geometry, with fixed cell parameters, was used to obtain the equilibrium lattice parameters $a_0$=5.4404 Å (10.28 Bohr) and $c_0$=3.1614 Å (5.97 Bohr). Similar to Ta$_2$C, the hexagonal structure of $\epsilon$-TaN shows five independent elastic stiffness coefficients, and those obtained in this calculation are $c_{11}$=294(4), $c_{12}$=239(4), $c_{13}$=170.1(1), $c_{33}$=374(4) and $c_{44}$=95.5(1) GPa. The bulk modulus obtained from these coefficients is $B$=236(2) GPa and the Young modulus for each direction are $E_x$=$E_y$=97.16 and $E_z$=266.17 GPa. Values of Poisson ratio are $\nu_{xy}$=$\nu_{yx}$=0.74, $\nu_{zx}$=$\nu_{zy}$=0.32 and $\nu_{xz}$=$\nu_{yz}$=0.12.

Table 5.10: Lattice parameters $a_0$ and $c_0$ for $\epsilon$-TaN. Experimental values are at room temperature.

Tabla 5.10: *Parámetros de red $a_0$ y $c_0$ del $\epsilon$-TaN. Los valores experimentales son a temperatura ambiente.*

| Reference | $a_0$ (Å) | $c_0$ (Å) |
|---|---|---|
| International Center for Diffraction Data [28] | 5.1910 | 2.908 |
| Present work from CASTEP (DFT-GGA) | 5.4404 | 3.1614 |
| Present work from ABINIT (DFT-LDA) | 5.343 | 3.001 |

Table 5.10 shows the calculated values with ABINIT (DFT-LDA) and CASTEP (DFT-GGA) for lattice parameters $a_0$ and $c_0$. In comparison with experimental values by the International Center for Diffraction Data (ICDD), parameters derived from DFT-LDA calculations show an unexpected overestimation of 3% for both parameters. A reason for this could be a wrong description of the $\epsilon$-TaN structure to the ABINIT code. On the other hand, parameters derived from DFT-GGA calculations agree within 5% for $a_0$ and better than 9% for $c_0$. In the same way as with Ta$_2$C, as no experimental data of mechanical properties of $\epsilon$-TaN is available, the calculated values estimated here can be considered as predicted values.

## Chapter 6

# HEAT CAPACITY

This chapter covers the study of the specific heat of Tantalum, diamond and TaC. The phonon density of states (DOS) and the curve of specific heat as function of temperature were obtained from first principles calculated phonon dispersion relations. In addition, with the help of a differential scanning calorimeter (DSC), the experimental curve of specific heat for $150 \leq$ T $\leq 600$ was determined for a TaC single crystal, complementing the theoretical study.

## 6.1 Fundamental Concepts

The amount of heat necessary to increase the temperature of a certain given mass is different for every material. The relation between the heat supplied to a mass and its corresponding increase of temperature is known as *heat capacity*. The heat capacity per unit of mass is called *specific heat* and is a characteristic of the material [88]. The thermodynamic properties of a solid, such as heat capacity, are determined mostly by the vibrational degrees of freedom of the lattice. However, a complete knowledge of the vibrational spectrum is required for the calculation of these thermodynamic properties. The phonon density of states is determined by the vibrational spectrum, and also is an important piece in the calculation of heat capacity. This section summarizes the basic concepts that relate phonon vibrations with the heat capacity based on the harmonic approximation.

### Phonon Density of states

There are some approximations used to obtain the phonon density of states. A general approximation in three dimensions consists on applying boundary conditions over $N^3$ primitive cells within a cube of side L of a periodic crystal, so that the wave vector **k** is determined by the condition

$$e^{[i(k_x x + k_y y + k_z z)]} \equiv e^{\{i[k_x(x+L) + k_y(y+L) + k_z(z+L)]\}} \quad , \tag{6.1}$$

whence

$$k_x, k_y, k_z = 0; \pm\frac{2\pi}{L}; \pm\frac{4\pi}{L}; ...; \frac{N\pi}{L} \quad , \qquad (6.2)$$

Therefore, there is one allowed value of $\mathbf{k}$ per volume $(2\pi/L)^3$ in $\mathbf{k}$ space, or

$$\left(\frac{L}{2\pi}\right)^3 = \frac{V}{8\pi^3} \qquad (6.3)$$

allowed values of $\mathbf{k}$ per unit volume of $\mathbf{k}$ space, for each polarization and for each branch. The volume of the crystal is $V = L^3$.

The total number of modes $N$ with wave vector less than $k$ is found from equation (6.3) to be $(L/2\pi)^3$ times the volume of a sphere of radius $k$. Thus

$$N = \left(\frac{L}{2\pi}\right)^3 (\frac{4\pi k^3}{3}) \qquad (6.4)$$

for each polarization type. The density of states $g(\omega)$ for each polarization is

$$g(\omega) = \frac{dN}{d\omega} = \left(\frac{Vk^2}{2\pi^2}\right)\left(\frac{dk}{d\omega}\right) = \left(\frac{Vk^2}{2\pi^2}\right)\left(\frac{1}{\frac{d\omega}{dk}}\right) \quad , \qquad (6.5)$$

where we can obtain the group velocity $d\omega/dk$ from the dispersion relation of $\omega$ versus $k$ [94].

In practice, the density of states for a crystal is evaluated by using dispersion relations to calculate a large number of normal mode frequencies, with propagation vectors selected from within the first Brillouin zone. The range of possible frequencies is divided into intervals of width $\Delta\omega$ and a histogram is plotted showing the number of modes obtained in each interval. If $\Delta\omega$ is small and the number of frequencies obtained is large, the histogram approximates $g(\omega)d\omega$ [119, 94].

**Phonon Heat Capacity**

In quantum theory, the energy levels of an N-ion harmonic crystal are described as 3N independent oscillators whose frequencies are those of the 3N classical normal modes. Each particular normal mode with angular frequency $\omega_s(\mathbf{k})$ can have only the discrete set of values

$$(n_{\mathbf{k}s} + \frac{1}{2})\hbar\omega_s(\mathbf{k}) \quad , \qquad (6.6)$$

where $n_{\mathbf{k}s}$ is the excitation number of the normal mode and only can have integer values (0,1,2,...). An energy state of the entire crystal is specified by giving the excitation numbers for each of the 3N normal modes. Then, the total energy is the sum of energies of the individual normal modes:

$$E = \sum_{\mathbf{k}s} (n_{\mathbf{k}s} + \frac{1}{2}) \hbar \omega_s(\mathbf{k}). \tag{6.7}$$

Because an arbitrary number of phonons may occupy a given $\mathbf{k}$ state, one can interpret the excitations of a lattice as particles obeying Bose-Einstein statistics. Then, the probability of exciting a phonon with frequency $\omega_s$ in a particular state $\mathbf{k}$ varies as

$$n_s = \frac{1}{e^{\beta \hbar \omega_s} - 1} \quad, \tag{6.8}$$

where $\beta = 1/(k_B T)$ and $k_B$ is Boltzmann's constant [79].

Substituting equation (6.8) in equation (6.7), the vibrational total energy for a solid at temperature T and angular frequency $\omega_s$ for a mode $s$ has the form

$$E = \sum_s \frac{\hbar \omega_s}{e^{\beta \hbar \omega_s} - 1} + \frac{1}{2} \sum_s \hbar \omega_s \quad. \tag{6.9}$$

This is equivalent to the internal energy; the harmonic model does not allow for thermal expansion, so therefore this function is for constant volume. The constant volume heat capacity, $C_V$, is equal to

$$C_V = \left( \frac{\partial E}{\partial T} \right)_V \tag{6.10}$$

and thus,

$$C_V = \sum_s k_B (\beta \hbar \omega_s)^2 \frac{e^{\beta \hbar \omega}}{(e^{\beta \hbar \omega} - 1)^2} \quad. \tag{6.11}$$

Equation (6.11) for the heat capacity can, in principle, be evaluated directly using a long list of frequency values taken from the dispersion curves calculated over a fine grid of wave vectors within the first Brillouin zone. Since the energy of a vibration depends only on its

frequency, there is some advantage in developing a formalism that relies only in the frequency distribution. Since all solids have a large number of normal modes, closely spaced in frequency, the frequency spectrum can be treated as continuous and the sum in equation (6.9) can be replaced by an integral. As mentioned above, a quantity called the density of states, $g(\omega)$, is defined such that the number of modes with angular frequencies between $\omega$ and $\omega + d\omega$ is equal to $g(\omega)d\omega$. Thus the harmonic phonon energy of the crystal can be written in the new form:

$$E = \int \frac{\hbar\omega}{e^{\beta\hbar\omega} - 1} g(\omega)d\omega + \frac{1}{2} \int \hbar\omega g(\omega)d\omega \quad , \tag{6.12}$$

where each integral is done over the entire frequency spectrum. This equation is valid for both crystalline and amorphous solids. Therefore, from equation (6.10), the heat capacity at constant volume can be written as

$$C_V = 3Nk_B \int\limits_0^{w_{\text{max}}} (\beta\hbar\omega)^2 \frac{e^{\beta\hbar\omega}}{\left(e^{\beta\hbar\omega} - 1\right)^2} \, g(\omega)d\omega \tag{6.13}$$

if the normalization $\int\limits_0^{w_{\text{max}}} g(w)dw = 1$ is used, where N is the number of atoms per unit cell and $\omega_{max}$ is the largest phonon frequency [120, 121, 122, 123]. Equations (6.12) and (6.13) are exact. In order to solve them numerically, we must know the function $g(\omega)$.

## 6.2  Specific Heat of Tantalum

The phonon density of states of tantalum computed from dispersion relations calculated from first principles (see figure 4.7) and normalized as $\int\limits_0^{w_{\text{max}}} g(w)d(w) = 1$ is shown in figure 6.1. A width of 0.15 THz was used as frequency intervals $\omega$ and $\omega + d\omega$. The phonon density of states describes better the phonon frequency distribution if one samples the reciprocal space with several wave vectors and for different directions. Due to limitations in computer time, only phonon calculations of a few wave vectors at high symmetry directions were performed. As a consequence of this simplification, the number of modes at zero frequency influences negatively the expected $\omega^2$ behavior of the DOS curve at low frequencies. This influence is corrected by not considering the number of modes at zero frequency in the density of states.

The DOS curve shown in figure 6.1 reproduces the main features of the frequency distribution function calculated by Woods [45] (see figure 6.2), from a seventh-neighbor general

model fitted to phonon frequencies obtained by inelastic neutron scattering.

The specific heat capacity at constant volume $C_v$ of Ta calculated from computed DOS is shown in figure 6.3. Line represents calculated values, circles show experimental data by White *et al.* [55] at low-temperatures and squares show experimental data at high-temperatures by Milošević *et al.* [124].

At temperatures lower than 25 K (low-temperatures), the calculated specific heat capacity agrees within $\approx 1$ J K$^{-1}$ mol$^{-1}$ with the experimental values of White *et al.*. However, the specific heat approaches the classical value of $3NK_B$ at temperatures higher than 400 K, which in the case of tantalum corresponds to 25 J K$^{-1}$ mol$^{-1}$. Milošević and coworkers [124] explain that according to the Dulong-Petit law, the specific heat of tantalum should enter
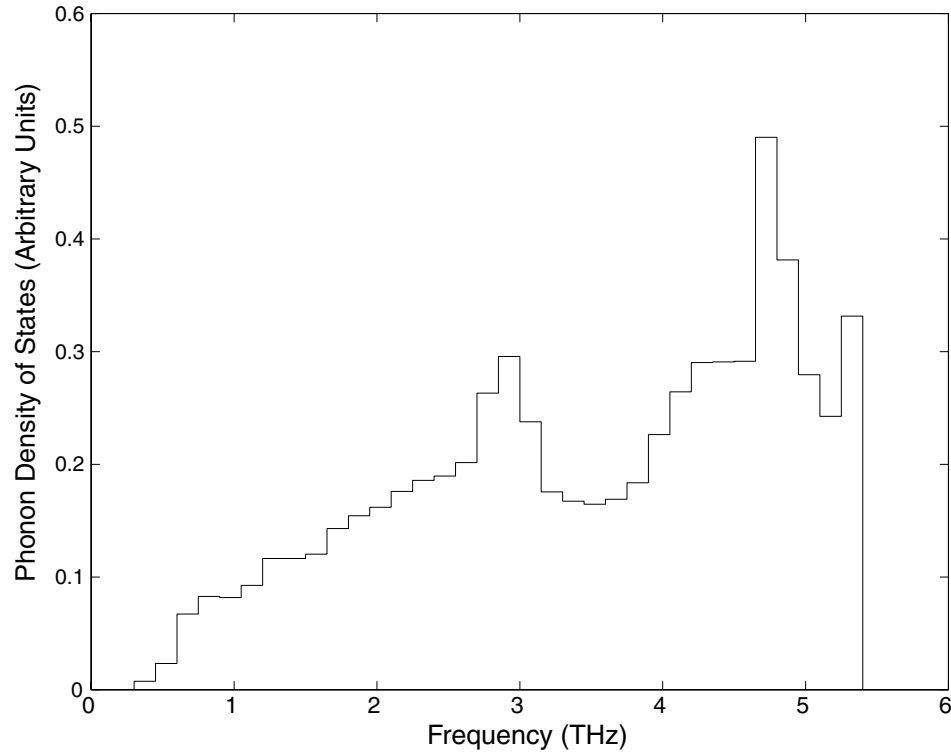
Figure 6.1: Phonon density of states of tantalum obtained from calculated data and normalized as $\int_0^{w_{\max}} g(w)d(w) = 1$.

Figura 6.1: *Densidad de estados de fonones del tantalio obtenida mediante los cálculos y normalizada tal que* $\int_0^{w_{\max}} g(w)d(w) = 1$.

a region of saturation above 230 K. At elevated temperatures, however, the experimental results for tantalum exceeded such a prediction. These higher than predicted values have been attributed to electronic contributions to the specific heat, thermal formation of lattice imperfections at high temperatures and other possible causes.
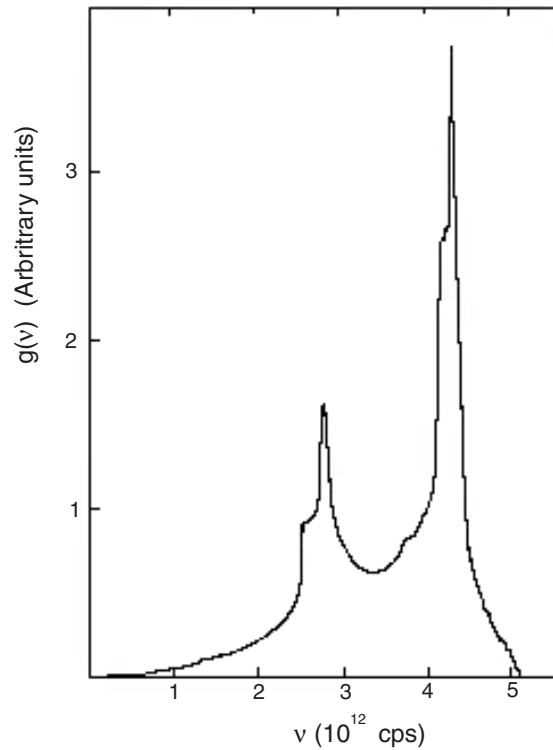


Figure 6.2: Frequency distribution of tantalum calculated by Woods [45] from a seventh-neighbor general force model.

Figura 6.2: *Distribución de frecuencias del tantalio calculada por Woods [45] utilizando un modelo de fuerza general al séptimo vecino.*
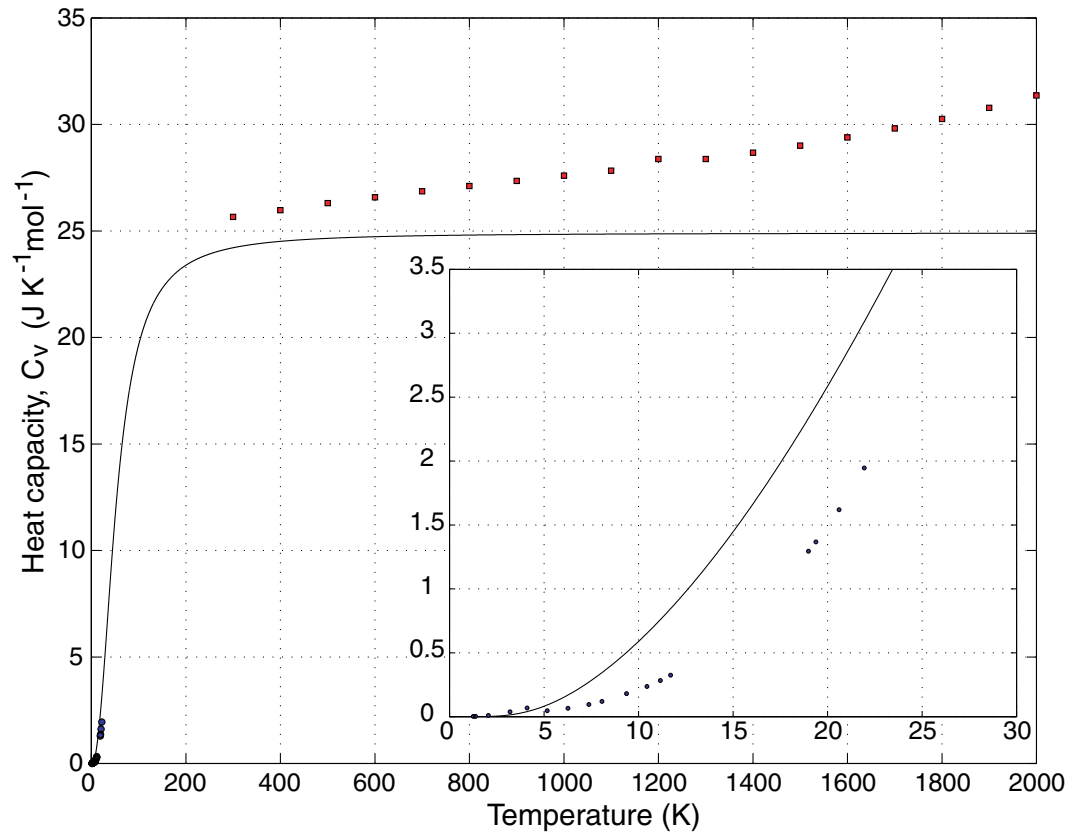
Figure 6.3: Specific heat of tantalum computed from phonon DOS. The line represents calculated values, circles indicate low-temperature experimental data by White *et al.*[55] and squares indicate high-temperature experimental data by Milošević *et al.* [124].

Figura 6.3: *Calor específico del tantalio calculado de la densidad de estados de fonones. La línea representa los valores calculados, los círculos indican los valores experimentales a bajas temperaturas obtenidos por White et al. [55] y los cuadrados indican los valores experimentales a altas temperaturas obtenidos por Milošević et al. [124].*

## 6.3   Specific Heat of Diamond

The phonon density of states of diamond was computed from the dispersion relations calcu-
lated with the ABINIT code shown in figure 4.14 using a frequency width of 0.15 THz. The
obtained DOS curve normalized as $\int_{0}^{w_{\max}} g(w)d(w) = 1$ is shown in figure 6.4. Also, in the same
way as done with tantalum, the number of modes at zero frequency was not considered in
order to keep the $\omega^2$ behavior. Figure 6.5 shows the phonon density of states determined by
Xie and coworkers [56] from *ab initio* pseudopotential calculations in a study about thermo-
dynamic properties of diamond at high pressures. A comparison of the DOS by Xie with that
calculated here shows a noticeable influence of the finite sampling in the DOS curve caused
by the poor frequency data. However, main peaks in the DOS curve are well reproduced.



Figure 6.4: Phonon density of states of diamond obtained from calculation and normalized as
$\int_{0}^{w_{\max}} g(w)d(w) = 1$.

Figura 6.4: *Densidad de estados de fonones del diamante obtenida del cálculo y normalizada
tal que* $\int_{0}^{w_{\max}} g(w)d(w) = 1$.

The specific heat at constant volume ($C_v$) of diamond, shown in figure 6.4 has been calculated from the density of states in a range of temperature from 0 to 1100 K. These theoretical calculations are based on the harmonic approximation and at 0 K. Specific heat measurements are performed at zero pressure and are called $C_p$. In order to compare with experimental data, calculated $C_v$ must be converted to $C_p$ because the harmonic model does not predict the existence of thermal expansion. This conversion can be possible using the relation between $C_v$ and $C_p$ expressed as

$$C_p = C_v + VTB\alpha^2, \tag{6.14}$$

where $V$ is the molar volume, T is temperature, $\alpha$ is the thermal expansion coefficient and $B$ is the bulk modulus or the inverse of compressibility. For the $C_p$ calculation, values of molar volume of $v$=3.415 cm$^3$/mol and bulk modulus of $B$=442 GPa, published by Victor [58], and thermal expansion coefficient values reported by Slack & Bartram [125] were used.

For diamond, $C_p$ and $C_v$ show differences within 1-2%. Hence, the calculated $C_v$ and $C_p$ curves overlapped. In diamond, the higher frequency is so high that at low temperatures the specific heat becomes very small. At temperatures of 100 K and lower, calculated values of $C_p$ agree within 1.5 J K$^{-1}$ mol$^{-1}$ with experimental values by DeSorbo [57]. A better agreement may be obtained with a finer sampling of the Brillouin zone in the calculation of phonon dispersion relations, which would improve the influence of acoustical phonons.
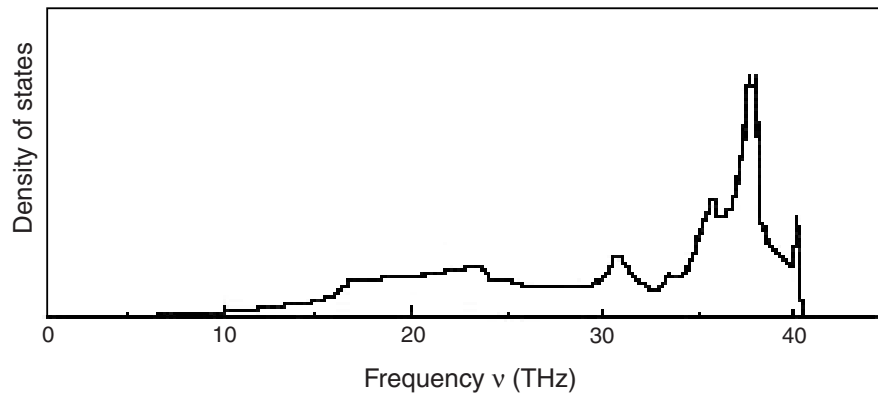


Figure 6.5: Phonon density of states obtained by Xie *et al.* [56] from *ab initio* calculations.

Figura 6.5: *Densidad de estados de fonones obtenida por Xie et al. [56] mediante cálculos ab initio.*
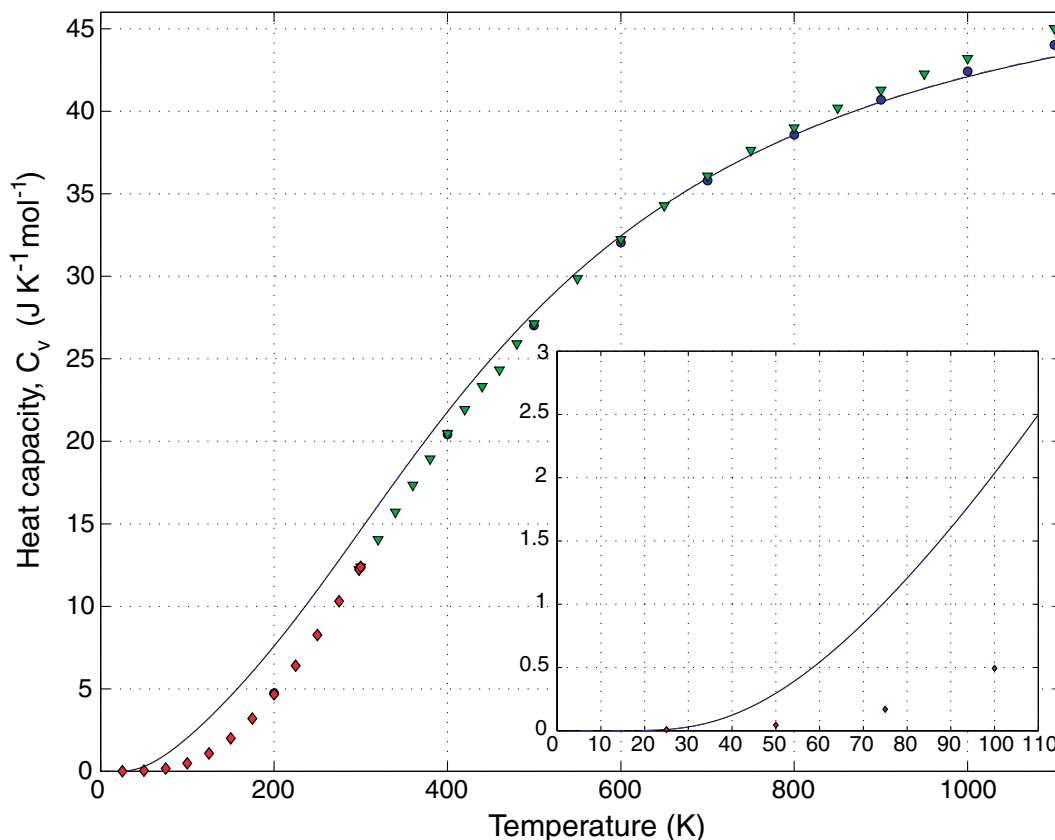
Figure 6.6: Specific heat of diamond. The line represents calculated values of $C_v$ and $C_p$. Circles ($C_p$) and triangles ($C_v$) indicate experimental data by Victor [58] and diamonds represent experimental data of $C_p$ at low-temperatures by DeSorbo [57].

Figura 6.6: *Calor específico del diamante. La línea representa los valores calculados de $C_v$ y $C_p$. Los círculos ($C_p$) y los triángulos ($C_v$) indican los valores experimentales obtenidos por Victor [58] y los diamantes muestran los valores experimentales de $C_p$ a bajas temperaturas obtenidos por DeSorbo [57].*

At high temperatures (T > 700 K), calculated $C_p$ agree within 1 J $K^{-1}$ $mol^{-1}$ with the experimental data of $C_v$ and $C_p$ published by Victor. Figure 6.7 shows this experimental data in comparison with calculated curves at high temperatures. From this figure it can be observed, by comparing experimental $C_p$ with calculated $C_p$, the influence of anharmonicity of about 0.75 J $K^{-1}$ $mol^{-1}$ at 1100 K. In addition, the calculated $C_p$ (dashed line) becomes larger with respect to calculated $C_v$ (solid line) after 500 K, showing a maximum difference of $\approx$ 0.04 J $K^{-1}$ $mol^{-1}$ at 1100 K.
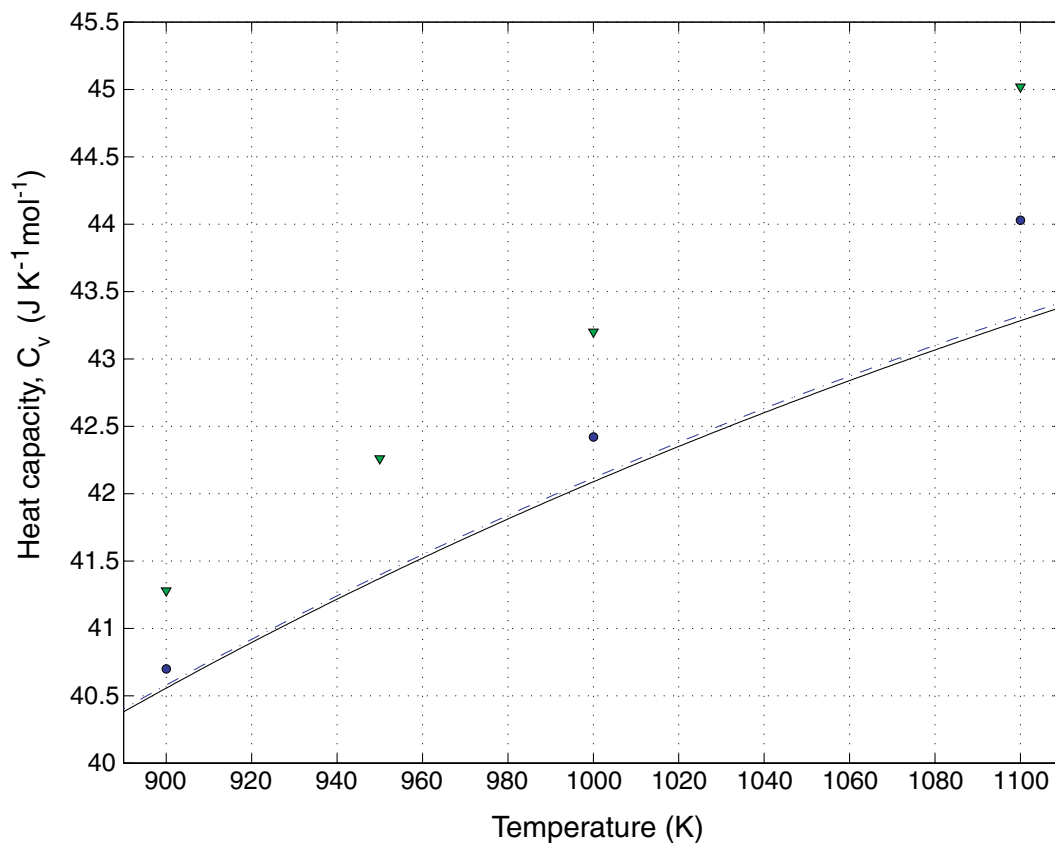
Figure 6.7: Specific heat of diamond at high temperatures. Lines represent calculated values of $C_v$ (solid) and $C_p$ (dashed). Circles ($C_p$) and triangles ($C_v$) indicate experimental data by Victor [58].

*Figura 6.7: Calor específico del diamante a altas temperaturas. La línea representa los valores calculados de $C_v$ (sólida) y $C_p$ (punteada). Los círculos ($C_p$) y triángulos ($C_v$) indican los valores experimentales obtenidos por Victor [58].*

## 6.4   Specific Heat of TaC

The specific heat for tantalum carbide (TaC) was determined both theoretically and experimentally. Descriptions of these procedures are given in this section.

### 6.4.1   TaC Specific Heat from Experiment

The specific heat as function of temperature was measured for a TaC single crystal disc, cut from a single crystal rod, purchased from Applied Physics Technologies Inc., using a differential scanning calorimeter (DSC) type Netzsch DSC F1 Phoenix 204. The specific heat was determined in a temperature range of 150 to 500 K.

A general brief description of the DSC technique is the following. Differential scanning calorimetry is a technique for measuring the energy necessary to establish a nearly zero temperature difference between a substance and an inert reference material that can be air. The calorimeter contains a furnace in which usually two identical crucibles, one for the sample and one as reference, are subjected to identical temperature regimes in an environment heated or cooled at a controlled rate.

Because sample and reference have different thermal characteristics, one of them will need more heat to reach the same temperature. Particularly, if the reference crucible is empty, the sample will take more heat. By measuring how much more heat the sample needs to be at the same temperature as the reference, the DSC determines the difference in heat as function of the increasing temperature, this is, the heat absorbed by the sample in a certain temperature range. On the other hand, as mentioned above, the specific heat is the heat necessary to increase the temperature in a certain amount of mass. Consequently, the specific heat can be determined from a DSC measurement.

For the heat capacity measurement for TaC, the first step consisted of performing a calibration by using two identical Ti crucibles with both lids empty, sample and reference. This was done under the required conditions for the TaC measurement. This specific heat determination on the crucibles has the purpose of determining their contribution in later measurements, allowing us to subtract their signal from the data measured for TaC. In subsequent measurements, is essential to keep the crucibles in the place they where during calibration. Any change of place will be reflected on the new data acquired.

Afterwards, the relation of specific heat as function of temperature for a sapphire standard was measured in order to calibrate the DSC with a well known material. The crucible taken

as reference was empty and both crucibles kept their lids. The signal obtained before for the empty crucibles is subtracted from the sapphire signal.

Finally, a measurement of the heat for a TaC single crystal of 289.15 mg at zero pressure with the reference crucible empty was made. The temperature range was from 150 to 500 K, increasing the temperature at a rate of 5 K/min. The TaC data were corrected with the information obtained before for the crucibles and the sapphire sample. The resulting curve is shown and discussed in the next section.

### 6.4.2 TaC Specific Heat from Calculation

The phonon density of states $g(\omega)$ of TaC was determined as a frequency histogram, using a frequency width of 0.3 THz, from the phonon dispersion relations of TaC (see figure 5.14) obtained with DFT-GGA calculations performed with the ABINIT code. The phonon DOS was normalized so that $\int_{0}^{w_{max}} g(w)dw = 1$ and is shown in figure 6.8.

The molar specific heat at constant volume ($C_v$) of TaC calculated from equation (6.13) using the phonon density of states obtained above is shown in figure 6.9, along with the experimental data determined using a differential scanning calorimeter (DSC). Equation (6.13) was used considering one TaC primitive cell with two atoms, so that $N=2$. In figure 6.9, the line represents calculated $C_v$ and circles experimental values determined here. Diamonds show experimental data of $C_p$ by Kelley [59].

Calculated values of $C_v$ agree within 3 J K$^{-1}$ mol$^{-1}$ with values of C$_p$ by Kelley, and within 2.4 J K$^{-1}$ mol$^{-1}$ in comparison with the experimental values determined here. It is noticeable in figure 6.9 that the calculated $C_v$ shows values larger than the experimental ones. A reason for this may be the non-stoichiometry of TaC samples used for the measurements. In these calculations we considered a perfect crystal (no defects) with stoichiometry Ta$_1$C$_1$. In practice, conventional methods applied for the synthesis of tantalum carbide produce mainly non-stoichiometric samples. Usually, impurities as carbon or metallic tantalum are contained in samples, influencing the results of measurements.

### 6.5 Specific Heat for Ta$_2$C

Figure 6.10 presents the phonon density of states of Ta$_2$C computed from calculated dispersion curves using DFT-LDA (figure 5.16). A frequency width of 0.5 THz were used in this calculation. The phonon DOS was normalized so that $\int_{0}^{w_{max}} g(w)dw = 1$.

The calculated specific heat of Ta$_2$C is shown in figure 6.11. The curve reaches the pre-dicted classical value of 74.7 J K$^{-1}$ mol$^{-1}$ after a temperature of 800 K. As no experimental data is available for the specific heat of Ta$_2$C, this theoretical result can be taken as a predic-tion for future measurements.
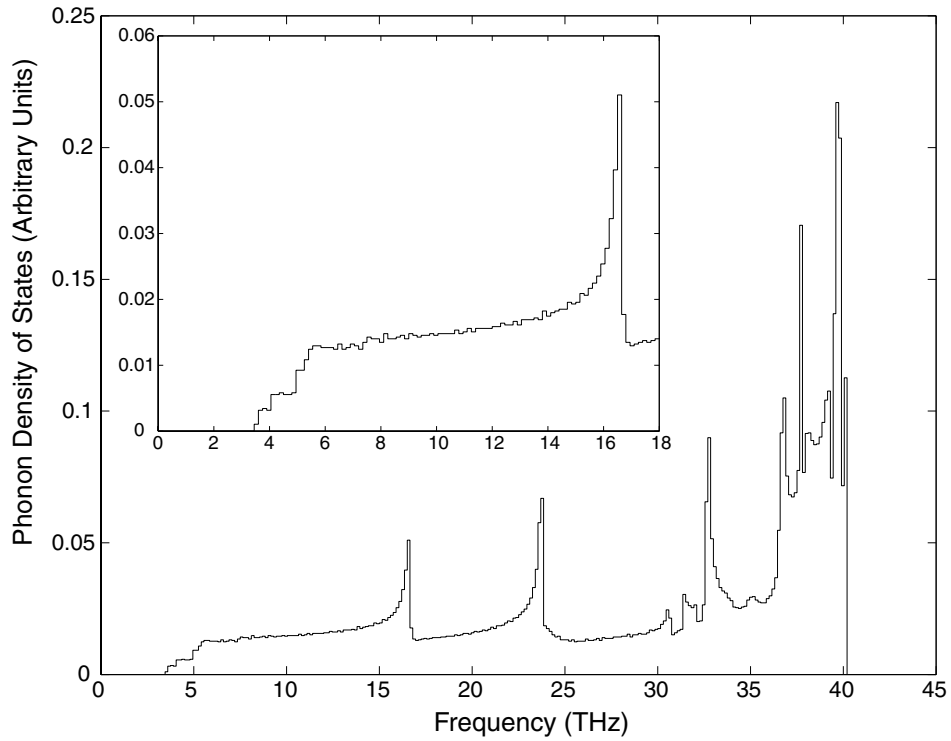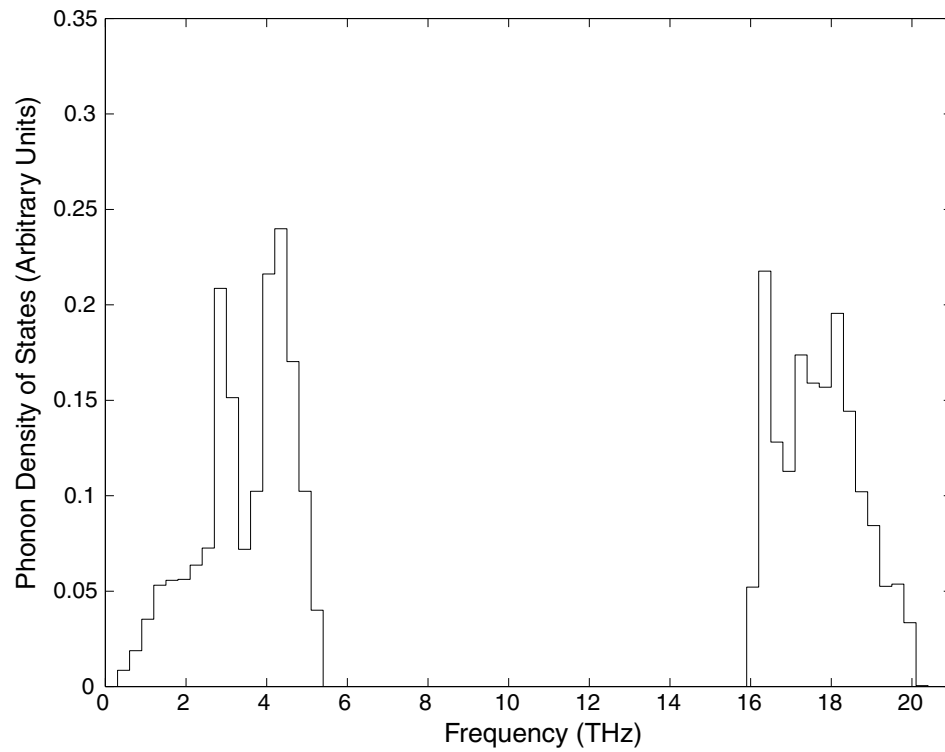


Figure 6.8: Phonon density of states of TaC obtained from calculation and normalized as $\int_0^{w_{\max}} g(w)d(w) = 1$.

Figura 6.8: *Densidad de estados de fonones del TaC obtenida mediante el cálculo y normal-izada tal que* $\int_0^{w_{\max}} g(w)d(w) = 1$.
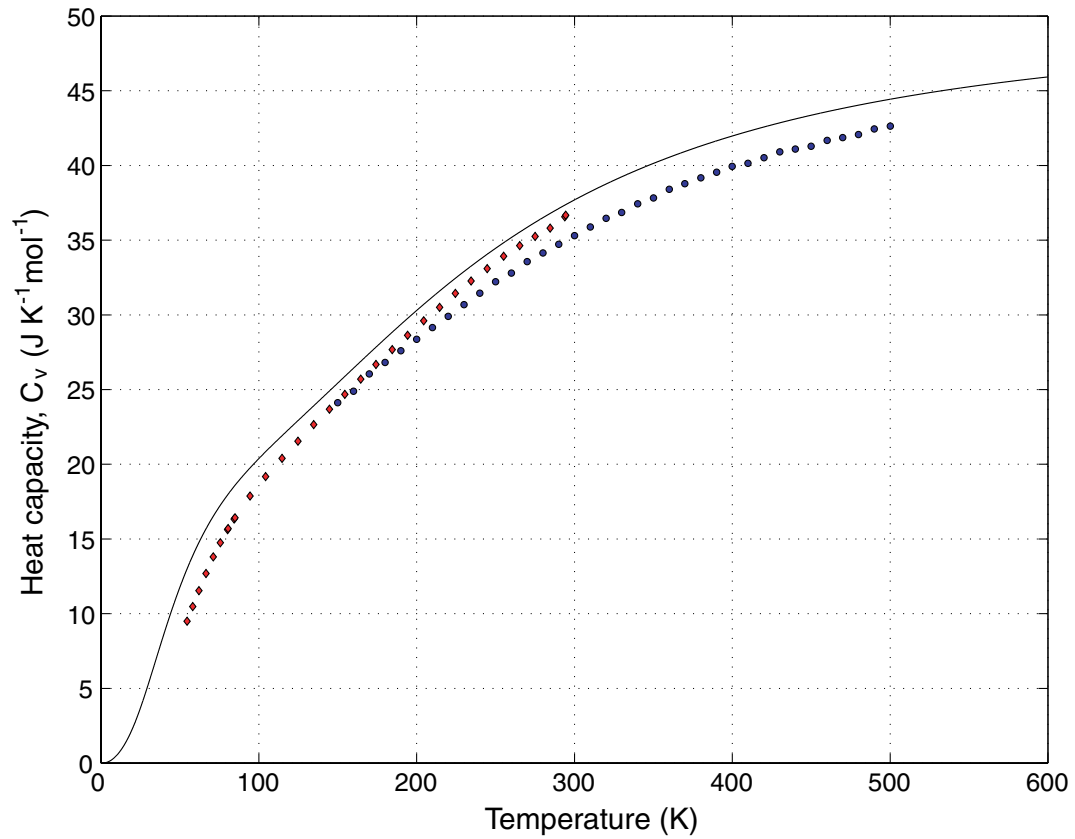
Figure 6.9: Experimental and calculated specific heat of TaC. Circles indicate experimental data determined here and the line represents calculated values. Diamonds show experimental values by Kelley [59].

Figura 6.9: *Valores experimentales y calculados del calor específico del TaC. Los círculos indican los valores experimentales obtenidos aquí y la línea representa los valores calculados. Los diamantes muestran los valores experimentales obtenidos por Kelley [59].*
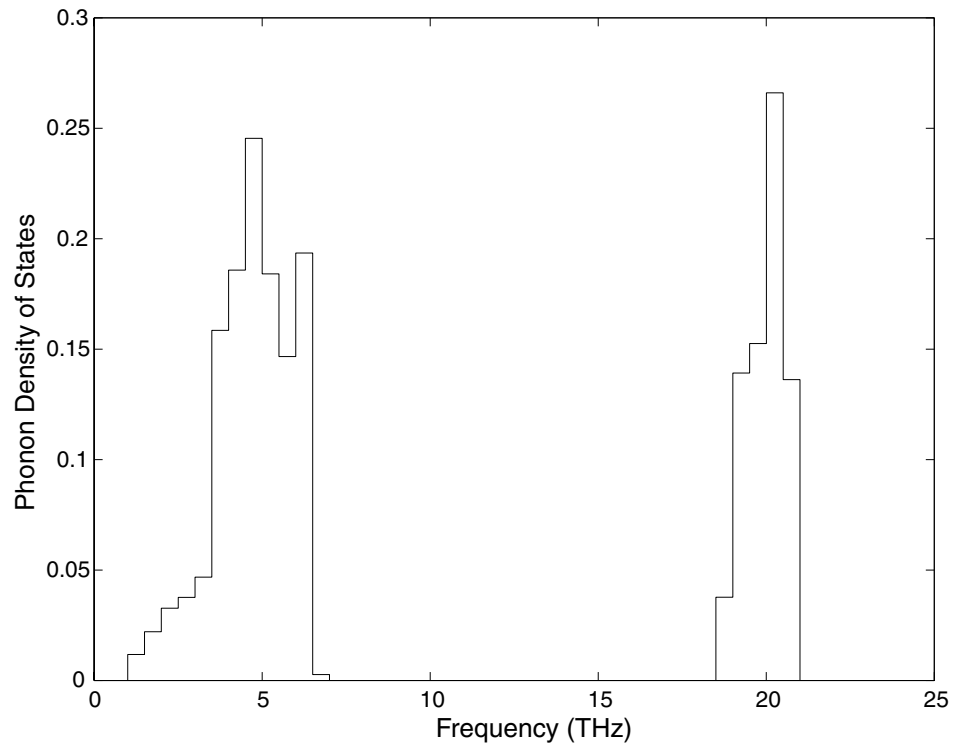
Figure 6.10: Phonon density of states of Ta$_2$C obtained from calculation and normalized as $\int_{0}^{w_{\max}} g(w)d(w) = 1$.

Figura 6.10: *Densidad de estados de fonones del Ta$_2$C obtenida mediante el cálculo y normalizada tal que $\int_{0}^{w_{\max}} g(w)d(w) = 1$.*
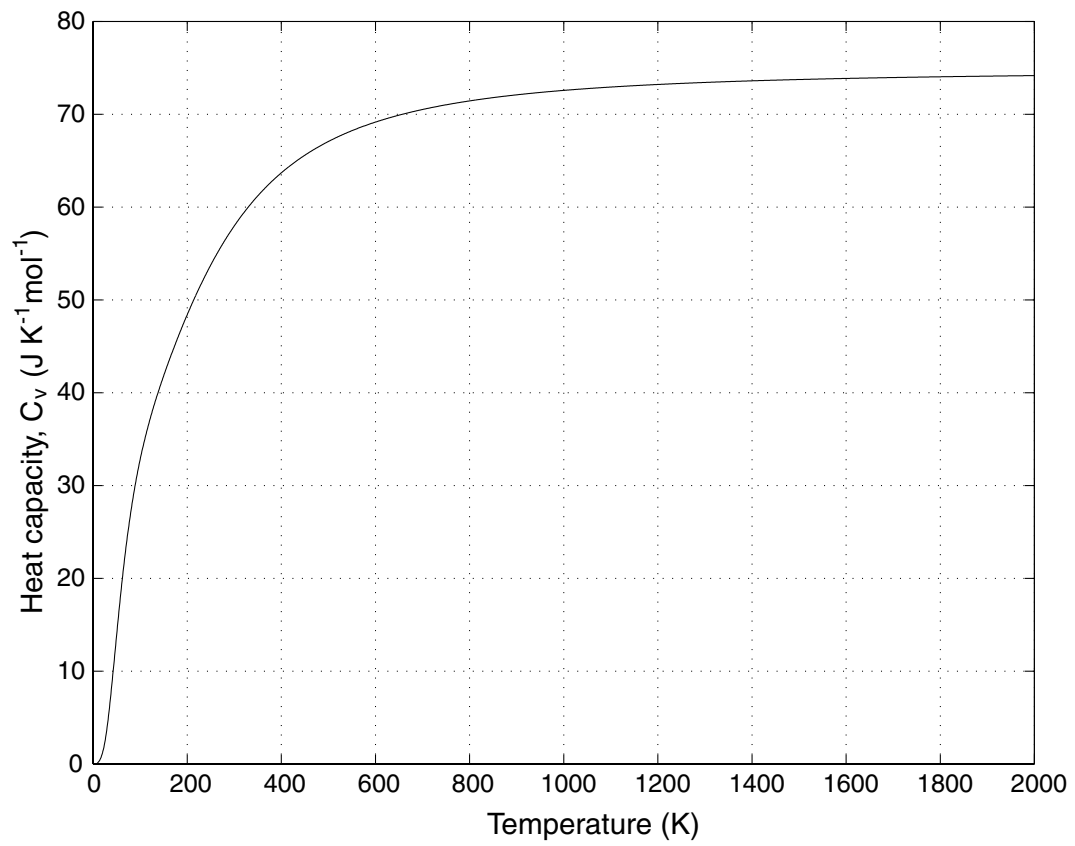
Figure 6.11: Calculated specific heat of Ta$_2$C.

Figura 6.11: *Curva teórica del calor específico del Ta$_2$C.*

# Chapter 7

# CONCLUSIONS

This thesis has described the application of density functional theory to predict macroscopic mechanical properties of binary tantalum carbides and nitrides. These calculations have shown good agreement with published experimental data and provide reliable values for properties not measured yet.

## Mechanical properties

The structural properties and the pressure-volume relation (except for $Ta_2C$ and $\epsilon$-TaN) have been calculated for tantalum, diamond, TaC, $Ta_2C$, $\delta$-TaN and $\epsilon$-TaN, with the ABINIT code using DFT and norm-conserving pseudopotentials with a plane-wave basis set. The LDA approach was used for all the compounds, and the GGA approach was used only for TaC.

In addition, the lattice parameter, elastic stiffness coefficients, bulk and Young moduli, and Poisson ratio for TaC, $Ta_2C$, $\delta$-TaN and $\epsilon$-TaN have been obtained from DFT-GGA calculations using pseudopotentials in conjunction with a plane-wave basis set. These calculations were performed with the CASTEP code. Results have been compared to earlier published values, when available, and a preferred set of values has been obtained for each compound.

The elastic stiffness coefficients $c_{11}$ and $c_{44}$ were determined experimentally for a TaC single crystal sample using a plane-wave ultrasound method. These values agree better than 8% with values obtained from the calculation.

## Lattice dynamics

Dispersion relations have been determined from first principles calculations for tantalum, diamond, TaC and $Ta_2C$ at high symmetry directions. For tantalum, diamond and TaC, phonon frequencies are within a few percent with respect to experimental data reported. The main dispersion relations features were well reproduced. In the case of TaC, a phonon transversal optical branch, which have not been measured yet but predicted by other theoretical models was obtained in the $[xx0]$ direction.

For $Ta_2C$ no published data about dispersion relations was available at the time of writing this thesis. Thus, calculated dispersion curves of $Ta_2C$ can be considered as a prediction for experimental studies.

## Heat capacity

Phonon density of states and specific heat capacities were computed from phonon dispersion relations of tantalum, diamond TaC and $Ta_2C$. For tantalum, the calculated specific heat curve agrees within $\approx 1$ J K$^{-1}$ mol$^{-1}$ with experimental values at temperatures lower than 25 K. However, at high temperatures the calculated curve behaves as predicted classically.

The agreement of the calculated specific curve of diamond in comparison with experimental published data are within 1.5 J K$^{-1}$ mol$^{-1}$ at temperatures of 100 K and lower, and within 1 J K$^{-1}$ mol$^{-1}$ for 700 K and higher.

The specific heat of a TaC single crystal was determined experimentally for temperatures from 150 to 600 K. The calculated specific heat agrees within 2.4 J K$^{-1}$ mol$^{-1}$ with those experimental data determined here, and within 3 J K$^{-1}$ mol$^{-1}$ with respect to published experimental data.

For $Ta_2C$ there is not experimental data available. Thus, the theoretical heat capacity obtained from this study can be taken as a prediction in future measurements.

# Bibliography

[1] Louis E. Toth. *Transition metal carbides and nitrides*. Academic Press, New York, 1971.

[2] S. H. Jhi, S. G. Louie, M. L. Cohen, and J. Ihm. "Vacancy hardening and softening in transition metal carbides and nitrides". *Physical Review Letters*, 86(15):3348–3351, 2001.

[3] Y. J. Chen, J. B. Li, and H. Z. Zhai. "Preparation and growth mechanism of $TaC_x$ whiskers". *Journal of Crystal Growth*, 224:244–250, 2001.

[4] J. E. Field. *The properties of diamond*. Academic Press, Great Britain, 1979.

[5] A. Katz, S. J. Pearton, S. Nakahara, F. A. Baiocchi, E. Lane, and J. Kovalchick. "Tantalum nitride films as resistors on chemical vapor deposition". *Journal of Applied Physics*, 73(10):5208–5211, 1993.

[6] S. T. Oyama. Introduction to the chemistry of transition metal carbides and nitrides. In S. T. Oyama, editor, *Introduction to the chemistry of transition metal carbides and nitrides*. Blackie Academic & Professional, 1996.

[7] J. Chan and S. M. Kauzlarich. "Rare-earth halides as fluxes for the synthesis of tantalum and niobium carbide". *Chemistry of Materials*, 9:531–534, 1997.

[8] PDF-2 database, entry 35-801. *National Bureau Standards (U.S.) Monograph 25*, 21:124, 1984.

[9] O.Yu. Khyzhun. "XPS, XES, and XAS studies of the electronic structure of substoichiometric cubic $TaC_x$ and hexagonal $Ta_2C_y$ carbides". *Journal of Alloys and Compounds*, 259:47–58, 1997.

[10] J. G. Choi. "The influence of surface properties on catalityc activities of tantalum carbides". *Applied Catalysis A*, 184:189–201, 1999.

[11] L. Trignan-Piot, M. Brardo, J. Gastaldi, and S. Giorgio. "Influence of plasma spraying parameters on the carbon content and porosity of TaC coatings". *Surface and Coatings Technology*, 79:113–118, 1996.

[12] A. Krajewski, L. D'Alessio, and G. De Maria. "Physico-chemical and thermophysical properties of cubic binary carbides". *Crystal Research Technology*, 33(3):341–374, 1998.

[13] D. J. Rowcliffe and W. J. Warren. "Structure and properties of tantalum carbide crystals". *Journal of Materials Science*, 5:345–350, 1970.

[14] M. Khusainov, G. Demyshav, and M. Myshlyaev. Mechanical properties and structure of carbide coatings of niobium and tantalum on graphite. *Russian Metallurgy*, 1990:139, 1990.

[15] R. W. Bartlett and C. W. Smith. "Elastic constants of tantalum monocarbide, $TaC_{0.90}$". *Journal Applied Physics*, 38:5428–5429, 1967.

[16] H. L. Brown, P. E. Armstrong, and C. P. Kempter. "Elastic properties of some policrystalline transition-metal monocarbides". *Journal of Chemical Physics*, 45(2):547–549, 1966.

[17] C. K. Jun and P. T. B. Shaffer. "Elastic moduli of niobium carbide and tantalum carbide at high temperature". *Journal of the Less-Common Metals*, 23:367–373, 1971.

[18] H. G. Smith and W. Gläser. "Phonon spectra in TaC and HfC". *Physical Review Letters*, 25(23):1611–1613, 1970.

[19] H. G. Smith. "Phonon anomalies in transition-metal carbides". *Physical Review Letters*, 29(6):353–354, 1972.

[20] M. Mostoller. "Phonon spectra of some transition metal carbides from a simple pseudopotential approach". *Physical Review B*, 5(4):1260–1265, 1972.

[21] W. Weber, H. Bilz, and U. Schröder. "Resonant electronic polarization in the lattice dynamics of transition-metal compounds". *Physical Review Letters*, 28(10):600–603, 1972.

[22] W. Weber. "Lattice dynamics of transition-metal carbides". *Physical Review B*, 8(11):5082–5092, 1973.

[23] M. P. Verma and B. R. K. Gupta. "Three-body-force shell-model study on phonon dispersion in the transition-metal carbides TaC and HfC". *Physical Review B*, 12(4):1314–1318, 1975.

[24] A. L. Bowman, T. C. Wallace, J. L. Yarnell, R. G. Wenzel, and E. K. Storms. "The crystal structures of $V_2C$ and $Ta_2C$". *Acta Crystallographica*, 19(6):6–9, 1965.

[25] F. Donald Bloss. *Crystallography and crystal chemistry.* Mineralogical Society of America, Washington, D.C., 1994.

[26] F. Lissner and T. Schleid. *Zeitschrift fuer Kristallographie*, 216:329–330, 2001.

[27] K. Wakasugi, M. Tokunaga, T. Sumita, H. Kubota, M. Nagata, and Y. Honda. "Superconductivity of reactively sputtered TaN film for ULSI process". *Physica B*, 239:29–31, 1997.

[28] W. Wong-Ng and *et al. Powder Diffraction*, 3:120, 1988.

[29] K. Reichelt, W. Nellen, and G. Mair. "Preparation and compositional analysis of sputtered TaN films". *Journal Applied Physics*, 49(10):5284–5287, 1978.

[30] E.G. Gillan and R.B. Kaner. "Rapid solid-state synthesis of refractory nitrides". *Inorganic Chemistry*, 33:5693–5700, 1994.

[31] A. N. Christensen and B. Lebech. "A reinvestigation of the structure of $\delta$-tantalum nitride". *Acta Crystallographica*, B34:261–263, 1978.

[32] T. Mashimo and *et al. Journal of Materials Science*, 28:3439, 1993.

[33] S. V. Popova. "The crystal structures of new superconducting materials obtained by high pressure treatment". *Acta Crystallographica A*, 31:S99, 1978.

[34] P. Hohenberg and W. Kohn. "Inhomogeneous electron gas". *Physical Review*, 136(3B):B864–B871, 1964.

[35] W. Kohn and L. J. Sham. "Self-consistent equations including exchange and correlations effects". *Physical Review*, 140(4A):A113–A1138, 1965.

[36] J. P. Perdew, K. Burke, and M. Ernzerhof. "Generalized gradient approximation made simple". *Physics Review Letters*, 77(18):3865–3868, 1996.

[37] *www.abinit.org.* The ABINIT Program is a common project of the Université Catholique of Louvain, Corning Incorporated, and other contributors,1991.

[38] C. Hartwigsen, S. Goedecker, and J. Hutter. "Relativistic separable dual-space gaussian pseudopotential from H to Rn". *Physics Review B*, 58(7):3641, 1998.

[39] N. Troullier and L. Martins. "Efficient pseudopotentials for plane-wave calculations". *Physical Review B*, 43(3):1993–, 1991.

[40] M. D. Segall, P. L. D. Lindan, M. J. Probert, C. J. Pickard, P. J. Hasnip, S. J. Clark, and M. C. Payne. "First-principles simulation: ideas, illustrations and the CASTEP code". *Journal of Physics: Condensed Matter*, 14(11):2717–2743, 2002.

[41] D. Vanderbilt. "Soft self-consistent pseudopotentials in generalized eigenvalue formalism". *Physical Review B*, 41:7892, 1990.

[42] H. E. Swanson and E. Tatge. "Standard X-ray diffraction powder patterns I". *National Bureau of Standards (U.S.), Circular (1953)*, 359:1–95, 1953.

[43] H. Cynn and C. S. Yoo. "Equation of state of tantalum to 174 GPa". *Physical Review B*, 59(13):8526–8529, 1999.

[44] K. W. Katahara, M. H. Manghnani, and E. S. Fisher. "Pressure derivatives of the elastic moduli of niobium and tantalum". *Journal of Applied Physics*, 47(2):434–439, 1976.

[45] A. D. Woods. "Lattice dynamics of tantalum". *Physical Review*, 136(3A):A781–A783, 1985.

[46] M. E. Straumanis and E. Z. Aka. "Precision determination of lattice parameter, coefficient of thermal expansion and atomic weight of carbon in diamond". *Journal of the American Chemical Society*, 73:5643–5646, 1951.

[47] H. J. McSkimin, P. Andreatch Jr., and P. Glynn. "The elastic stiffness moduli of diamond". *Journal of Applied Physics*, 43(3):985–987, 1972.

[48] J. L. Warren, R. G. Wenzel, and J. L. Yarnell. *Inelastic Scattering of Neutrons.* International Atomic Energy Agency, Vienna, 1965.

[49] J.L. Warren, J.L. Yarnell, G. Dolling, and R.A. Cowley. "Lattice dynamics of diamond". *Physical Review*, 158(3):805–808, 1967.

[50] H. J. Monkhorst and J. D. Pack. "Special points for the Brillouin-zone integrations". *Physical Review B*, 13(12):1260–1265, 1976.

[51] M. Sahnoun, C. Daul, J. C. Parlevas, C. Demangeat, and M. Driz. "Electronic structure and optical properties of TaC from first principles calculation". *The European Physical Journal B*, 44:281–286, 2005.

[52] M. Sahnoun, C. Daul, M. Driz, J. C. Parlevas, and C. Demangeat. "FP-LAPW investigation of electronic structure of TaN and TaC compounds". *Computational Materials Science*, 33:175–183, 2005.

[53] Z. Wu, X. J. Chen, V. V. Struzhkin, and R. E. Cohen. "Trends in elasticity and electronic structure of transition-metal nitrides and carbides from first principles". *Physical Review B*, 71:214103, 2005.

[54] S. P. Dodd, M. Cankurtaran, and B. James. "Ultrasonic determination of the elastic and nonlinear acoustic properties of transition-metal carbide ceramics: TiC and TaC". *Journal of Material Science*, 38:1107–1115, 2003.

[55] D. White, C. Chou, and H. L. Johnston. "Heat capacity in the normal and superconducting states and critical field of tantalum". *Physical Review*, 109(3):797–802, 1958.

[56] J. Xie, S. P. Chen, J. S. Tse, S. de Gironcoli, and S. Baroni. "High-pressure thermal expansion, bulk modulus, and phonon structure of diamond". *Physical Review B*, 60(13):9444–9449, 1999.

[57] W. DeSorbo. "Specific heat of diamond at low temperatures". *Journal of Chemical Physics*, 21:876–880, 1953.

[58] A. C. Victor. "Heat capacity of diamond at high temperatures". *The Journal of Chemical Physics*, 36(7):1903–1911, 1962.

[59] K. K. Kelley. "The specific heats at low temperatures of tantalum oxide and tantalum carbide". *Journal of the American Chemical Society*, 62(4):818–819, 1940.

[60] M. Sôb, M. Friák, D. Legut, J. Fiala, and V. Vitek. "The role of ab initio electronic structure calculations in studies of the strength of materials". *Materials Sciencie and Engineering A*, 387-389:148–157, 2004.

[61] J. Grossman, A. Mizel, M. Côté, M. Cohen, and S. Louie. "Transition metals and their carbides and nitrides: trends in electronic and structural properties". *Physical Review B*, 60(9):6343–6347, 1999.

[62] M. Khusainov, G. Demyshav, and M. Myshlyaev. "Mechanical properties and structure of carbide coatinigs of niobium and tantalum carbide". *Russian Metallurgy*, 5:144–146, 1990.

[63] W. S. Williams. "Electrical properties of hard materials". *International Journal of Refractory Metals and Hard Materials*, 17:21–26, 1999.

[64] Q. Y. Zhang, X. X. Mei, D. Z. Yang, F. X. Chen, T. C. Ma, Y. M. Wang, and F. N. Teng. "Preparation, structure and properties of TaN and TaC films obtained by ion beam assisted deposition". *Nuclear Instruments and Methods in Physics Research B*, 127/128:664–668, 1997.

[65] T. Kim and M. Wooldrige. "Catalytically assisted self-propagating high-temperature synthesis of tantalum carbide powders". *Journal of the American Ceramic Society*, 84(5):976–982, 2001.

[66] R. Marchand, F. Tessier, and F.J. DiSalvo. "New routes to transition metal nitrides: preparation and characterization of new phases". *Journal of Materials Chemistry*, 9:297–304, 1999.

[67] M.H. Tsai, S.C. Sun, C.P. Lee, H.T. Chiu, C.E. Tsai, S.H. Chuang, and S.C. Wu. "Metal-organic chemical vapor deposition of tantalum nitride barrier layers for ULSI applications". *Thin Solids Films*, 270:531–536, 1995.

[68] A. M. Nartowski, I.P. Parkin, A.J. Craven, and M. MacKenzie. "Rapid solid-state metathesis routes to metal carbides". *Advance Materials*, 10(10):805–808, 1998.

[69] H. B. Nie, S. Y. Xu, S. J. Wang, L. P. You, Z. Yang, C. K. Ong, J. Li, and T. Y. F. Liew. "Structural and electrical properties of tantalum nitride thin films fabricated by using reactive radio-frequency magnetron sputtering". *Applied Physics A*, 73:229–236, 2001.

[70] J.L. O'Loughlin, C.H. Wallace, M.S. Knox, and R.B. Kaner. "Rapid solid-state synthesis of tantalum, chromium, and molibdenum nitrides". *Inorganic Chemistry*, 40:2240–2245, 2001.

[71] L. Yu, D. Marshall, T. Eshrich, V. Narayanan, J.M. Rowell, N. Newman, and A.J. Freeman. "Mechanism and control of the metal-to-insulator transition in rocksalt tantalum nitride". *Physical Review B*, 65:245110, 2002.

[72] M. C. Payne, M. P. Teter, D. C. Allan, T. A. Arias, and J. D. Joannopoulos. "Iterative minimization techniques for *ab initio* total-energy calculations: molecular dynamics and conjugate gradients". *Reviews of Modern Physics*, 64(4):1045–1047, 1992.

[73] Martin Dove. *Introduction to lattice dynamics*. Cambridge University Press, Cambridge, Great Britain, 1993.

[74] R. M. Martin. *Electronic structure*. Cambridge University Press, 2004.

[75] D. M. Ceperly and B. J. Alder. "Ground state of the electron gas by a stochastic method". *Physics Review Letters*, 45:566–, 1980.

[76] J. P. Perdew and A. Zunger. "Self interaction correction to density functional approximations for many electrons system". *Physics Review B*, 23:5048–, 1981.

[77] A. P. Sutton. *Electronic structure of materials*. Oxford University Press, New York, 1993.

[78] J. P. Perdew, J. A. Chevary, S. H. Vosko, K. A. Jackson, M. R. Pederson, D. J. Singh, and C. Fiolhais. "Atoms, molecules, solids, and surfaces: Applications of the generalized gradient approximation for exchange and correlation". *Physics Review B*, 49(11):6671–6687, 1992.

[79] N. Aschcroft and D. Mermin. *Solid state physics*. Saunders College Publishing, USA, 1976.

[80] Michael Marder. *Condensed Matter Physics*. John Wiley & Sons, Inc., USA, 1993.

[81] D. R. Hamman, M. Schluter, and C. Chiang. "Norm-conserving pseudopotentials". *Physical Review Letters*, 43:1494–1497, 1979.

[82] S. Baroni, S. de Gironcoli, A. Dal Corso, and P. Gianozzi. "Phonons and related crystal properties from density-functional perturbation theory". *Review of Modern Physics*, 73:515–562, 2001.

[83] X. Gonze, J.-M. Beuken, R. Caracas, F. Detraux, M. Fuchs, G.-M. Rignanese, L. Sindic, M. Verstraete, G. Zerah, F. Jollet, M. Torrent, A. Roy, M. Mikami, P. Ghosez, J. Raty, and D. Allan. "First-principles computation of material properties: the ABINIT software project". *Computational Materials Science*, 25:478–492, 2002.

[84] X. Gonze, G. Rignanese, M. Verstraete, J.M. Beuken, Y. Pouillon, R. Caracas, F. Jollet, M. Torrent, G. Zerah, M. Mikami, P. Ghosez, M. Veithen, J. Raty, V. Olevano, F. Bruneval, L. Reining, R. Godby, G. Onida, D. Hamman, and D. Allan. "A brief introduction to the ABINIT software package". *Zeitschrift fur Kristallographie*, 220:558–562, 2005.

[85] M. A. White. *Properties of Materials*. Oxford University Press, New York, 1999.

[86] J. F. Nye. *Physical Properties of Crystals*. Oxford University Press, Oxford, Great Britain, 1985.

[87] R. J. Angel. *Equations of state*, volume 41 of *Reviews in Mineralogy and Geochemistry*, pages 35–59. Mineralogical Society of America, 2000.

[88] R. Resnick, D. Halliday, and K. Krane. *Physics, Volume one*. John Wiley and Sons, Inc., USA, 1992.

[89] Q. He and Z. T. Yan. "Study of temperature dependence of bulk modulus and interatomic separation of ionic solids". *Physica Status Solidi (b)*, 223:767–771, 2001.

[90] Y. Makino and S. Miyake. "Estimation of bulk moduli of compounds by empirical relations between bulk modulus and interatomic distance". *Journal of Alloys and Compounds*, 313:235–241, 2000.

[91] S. Raju, K. Sivasubramanian, and E. Mohandas. "On the thermodynamic interrelationship between enthalpy, volume thermal expansion and bulk modulus". *Scripta Materialia*, 44:269–274, 2001.

[92] H. Ledbetter. "Relationship between bulk-modulus temperature dependence and thermal expansivity". *Physica Status Solidi (b)*, 181:81–85, 1994.

[93] K. Chen, L. R. Zhao, and J. S. Tse. "Ab initio study of elastic properties of Ir and $Ir_3X$ compounds". *Journal of Applied Physics*, 93(5):2414–2417, 2003.

[94] C. Kittel. *Introduction to solid state physics*. John Wiley and Sons, Inc., 1996.

[95] H. Bilz and W. Kress. *Phonon dispersion realtions in insulators*. Springer Verlag, Berlin, 1979.

[96] K. S. Upadhyaya, Ajar Kumar Singh, A. Pandey, S. N. Pathak, and A. K. Singh. "Lattice vibrational properties of transition metal carbides (TiC, ZrC and HfC)". *Pramana-Journal of Physics*, 64(2):299–304, 2005.

[97] L. Pintschovius, W. Reichardt, and B. Scheerer. "Lattice dynamics of TiC". *Journal of Physics C: Solid State Physics*, 11:1557–1562, 1978.

[98] P. T. Jochym, K. Parlinski, and M. Sternik. "TiC lattice dynamics from *ab initio* calculations". *The European Physical Journal B*, 10:9–13, 1999.

[99] P. T. Jochym and K. Parlinski. "*Ab initio* lattice dynamics and elastic constants for ZrC". *The European Physical Journal B*, 15:265–268, 2000.

[100] S. Y. Savrasov. "Linear-response theory and lattice dynamics: A mufin-tin-orbital approach". *Physical Review B*, 54(23):16470–16486, 1996.

[101] V. Milman, B. Winkler, J. A. White, J. Pickard, M. C. Payne, E. V. Akhmatskya, and R. H. Nobes. "Electronic structure, properties, and phase stability of inorganic crystals: A pseudopotential plane-wave study". *International Journal of Quantum Chemistry*, 77(5):895–910, 2000.

[102] B. Winkler, M. Hytha, M. C. Warren, V. Milman, J. D. Gale, and J. Schreuer. "Calculation of the elastic constants of the $Al_2SiO_5$ polymorphs andalusite, sillimanite and kyanite". *Zeitschrift fuer Kristallographie*, 216:67–70, 2001.

[103] S. Q. Wang and H. Q. Ye. "Plane-wave pseudopotential study on mechanical and electronic properties for IV and III-V crystalline phases with zinc-blende structure". *Physics Review B*, 66:235111, 2002.

[104] S. Q. Wang and H. Q. Ye. "First-principles study on elastic properties and phase stability of III-V compounds". *Physics Status Solidi B*, 240(1):45–54, 2003.

[105] R. P. Bajpai and K. Neelakandan. "Lattice dynamics of transition metals". *Il Nuovo Cimento*, 7 B(2):177–184, 1972.

[106] S. Haussühl. Plate modes. In *Handbook of elastic properties of solids, liquids, and gases. Volume I.* Academic Press, San Diego, 2001.

[107] H. Nowotny and H. Auer-Welsbach. "The variation of lattice parameter with carbon content of tantalum carbide". *Journal of Physical Chemistry*, 65:1596–1598, 1961.

[108] P. M. McKenna. "Tantalum carbide: its relation to other hard refractory compounds". *Industrial and Engineering Chemistry*, 28:767–772, 1936.

[109] FIZ Karlsruhe, Inorganic crystal structure database (2004).

[110] R. D. Shannon. "Revised effective ionic radii and systematic studies of interatomic distances in halides and chalcogenides". *Acta Crystallographica A*, 32:751–767, 1976.

[111] D. L. Anderson and O. L. Anderson. "The bulk modulus-volume relationship for oxides". *Journal of Geophysical Research*, 75:3494–3500, 1970.

[112] Calculated from ICSD using POWD-12++, (1997).

[113] Y. Kumashiro, H. Tokumoto, E. Sakuma, and E. Itho. "The elastic constants of TiC, VC, and NbC single crystals". *Internal Friction and Ultrasonic Attenuation in Solids*, 6:395–399, 1977.

[114] H. M. Ledbetter, S. Chevacharoenkul, and R.F. Davis. "Monocrystal elastic constants of NbC". *Journal of Applied Physics*, 60:1614–1617, 1986.

[115] J. Schreuer. "Elastic and piezoelectric properties of $La_3Ga_5SiO_{14}$ and $La_3Ga_{5.5}Ta_{0.5}SiO_{14}$: an application of resonant ultrasound spectroscopy". *IEEE Transactions on Ultrasonics, Ferroelectrics, and Frequency Control*, 49:1474–1479, 2002.

[116] J. C. Phillips. "Lattice instabilities and high-temperature superconductivity". *Physical Review B*, 26(10):543–546, 1971.

[117] H. R. Zeller. "Effect of lattice instabilities on superconducting and other properties of $TaC_x$". *Physical Review B*, 5(5):1813–1817, 1972.

[118] K. Kobayashi. "First-principles study of the electronic properties of transition metal nitride surfaces". *Surface Science*, 493:665–670, 2001.

[119] Richard Christman. *Fundamentals of solid state physics*. John Wiley and Sons, Inc., 1989.

[120] R. Roadhammer, W. Weber, E. Gmelin, and K. H. Rieder. "Low temperature specific heat and phonon anomalies in transition metal compounds". *The Journal of Chemical Physics*, 64(2):581–585, 1976.

[121] C. Lee and X. Gonze. "Ab initio calculation of the thermodymic properties and atomic temperature factors of $SiO_2$ $\alpha$-quartz and stishovite". *Physical Review B*, 51(13):8610–8613, 1995.

[122] A. Bosak and M. Krisch. "Phonon density of states probed by inelastic x-ray scattering". *Physical Review B*, 72(224305), 2005.

[123] X. Gonze, G. Rignanese, and R. Caracas. "First-principle studies of the lattice dynamics of crystals, and related properties". *Zeitschrift fur Kristallographie*, 220:458–472, 2005.

[124] N. D. Milošević, G. S. Vuković, D. Z. Pvičić, and K. D. Maglić. "Thermal properties of tantalum between 300 and 2300 K". *International Journal of Thermophysics*, 20(4):1129–1136, 1999.

[125] G. A. Slack and S. F. Bartram. "Thermal expansion of some diamondlike crystals". *Journal of Applied Physics*, 46(1):89–98, 1975.

# Appendix A

# TRANSFORMATION OF THE COORDINATES OF WAVE VECTORS $q$ OF THE CONVENTIONAL CELL TO COORDINATES OF THE PRIMITIVE CELL

In the ABINIT program the coordinates of wave vectors $\mathbf{q}$ are used as coordinates in the primitive cell in calculations of phonons. However, the description of crystalline structures are made using coordinates in the conventional cell. Thus, the wave vectors must be transformed to the primitive cell coordinates. To do this, the primitive vectors of the crystalline structure forming a matrix are used as a transformation operator.

## Body-centered cubic

In the case of tantalum, which shows a body-centered cubic structure, the transformations for the three general directions $[xxx]$, $[xx0]$ and $[x00]$, using Eq. (A.1) as the transformation operator, are the following.

$$
\begin{pmatrix} \frac{-1}{2} & \frac{1}{2} & \frac{1}{2} \\ \frac{1}{2} & \frac{-1}{2} & \frac{1}{2} \\ \frac{1}{2} & \frac{1}{2} & \frac{-1}{2} \end{pmatrix}.
\tag{A.1}
$$

For a general wave vector $\mathbf{q}$ with direction $[xxx]$,

$$
\begin{pmatrix} \frac{-1}{2} & \frac{1}{2} & \frac{1}{2} \\ \frac{1}{2} & \frac{-1}{2} & \frac{1}{2} \\ \frac{1}{2} & \frac{1}{2} & \frac{-1}{2} \end{pmatrix} \begin{pmatrix} x \\ x \\ x \end{pmatrix} = \begin{pmatrix} \frac{x}{2} \\ \frac{x}{2} \\ \frac{x}{2} \end{pmatrix}.
\tag{A.2}
$$

For a general wave vector $\mathbf{q}$ with direction $[xx0]$,

$$
\begin{pmatrix} \frac{-1}{2} & \frac{1}{2} & \frac{1}{2} \\ \frac{1}{2} & \frac{-1}{2} & \frac{1}{2} \\ \frac{1}{2} & \frac{1}{2} & \frac{-1}{2} \end{pmatrix} \begin{pmatrix} x \\ x \\ 0 \end{pmatrix} = \begin{pmatrix} 0 \\ 0 \\ x \end{pmatrix}.
\tag{A.3}
$$

And finally, a general wave vector $\mathbf{q}$ with direction $[x00]$ will be as

$$\begin{pmatrix} \frac{-1}{2} & \frac{1}{2} & \frac{1}{2} \\ \frac{1}{2} & \frac{-1}{2} & \frac{1}{2} \\ \frac{1}{2} & \frac{1}{2} & \frac{-1}{2} \end{pmatrix} \begin{pmatrix} x \\ 0 \\ 0 \end{pmatrix} = \begin{pmatrix} \frac{-x}{2} \\ \frac{x}{2} \\ \frac{x}{2} \end{pmatrix}. \tag{A.4}$$

**Face-centered cubic**

For face-centered cubic structures such as TaC and diamond, a similar procedure as above is applied using the primitive vectors forming the following matrix,

$$\begin{pmatrix} 0 & \frac{1}{2} & \frac{1}{2} \\ \frac{1}{2} & 0 & \frac{1}{2} \\ \frac{1}{2} & \frac{1}{2} & 0 \end{pmatrix}. \tag{A.5}$$

For a general wave vector $\mathbf{q}$ with direction $[xxx]$,

$$\begin{pmatrix} 0 & \frac{1}{2} & \frac{1}{2} \\ \frac{1}{2} & 0 & \frac{1}{2} \\ \frac{1}{2} & \frac{1}{2} & 0 \end{pmatrix} \begin{pmatrix} x \\ x \\ x \end{pmatrix} = \begin{pmatrix} x \\ x \\ x \end{pmatrix}. \tag{A.6}$$

For a general wave vector $\mathbf{q}$ with direction $[xx0]$,

$$\begin{pmatrix} 0 & \frac{1}{2} & \frac{1}{2} \\ \frac{1}{2} & 0 & \frac{1}{2} \\ \frac{1}{2} & \frac{1}{2} & 0 \end{pmatrix} \begin{pmatrix} x \\ x \\ 0 \end{pmatrix} = \begin{pmatrix} \frac{x}{2} \\ \frac{x}{2} \\ x \end{pmatrix}. \tag{A.7}$$

For a general wave vector $\mathbf{q}$ with direction $[x00]$,

$$\begin{pmatrix} 0 & \frac{1}{2} & \frac{1}{2} \\ \frac{1}{2} & 0 & \frac{1}{2} \\ \frac{1}{2} & \frac{1}{2} & 0 \end{pmatrix} \begin{pmatrix} x \\ 0 \\ 0 \end{pmatrix} = \begin{pmatrix} 0 \\ \frac{x}{2} \\ \frac{x}{2} \end{pmatrix}. \tag{A.8}$$

**Hexagonal structure**

For hexagonal structure phonon calculations, such as $Ta_2C$, there is no $\mathbf{q}$ wave vector transformation and the directions and paths desired for calculation are used directly.

## Appendix B

# RELATION BETWEEN COMPLIANCE $s_{ij}$ AND STIFFNESS $c_{ij}$ COEFFICIENTS

The explicit general equations for the compliance coefficients $s_{ij}$ in terms of the stiffness coefficients $c_{ij}$ are derived here for the cubic system, from the stiffness coefficients expressions shown in Eq. (B.1), (B.2) and (B.3) [86],

$$c_{11} = \frac{s_{11} + s_{12}}{(s_{11} - s_{12})(s_{11} + 2s_{12})},$$
(B.1)

$$c_{12} = \frac{-s_{12}}{(s_{11} - s_{12})(s_{11} + 2s_{12})}.$$
(B.2)

$$c_{44} = \frac{1}{s_{44}}.$$
(B.3)

From Eq. (B.1),

$$(s_{11} - s_{12})(s_{11} + 2s_{12}) = \frac{s_{11} + s_{12}}{c_{11}}.$$
(B.4)

Substituting Eq. (B.4) in Eq. (B.2),

$$c_{12} = \frac{-c_{11}}{\frac{s_{11}}{s_{12}} + 1}.$$
(B.5)

Obtaining $s_{12}$ from Eq. (B.5),

$$s_{12} = \frac{-s_{11}c_{12}}{c_{11} + c_{12}}.$$
(B.6)

Substituting Eq. (B.6) in Eq. (B.2),

$$c_{12} = \frac{s_{11}c_{12}}{(c_{11} + c_{12})s_{11}^2(1 + \frac{c_{12}}{c_{11}+c_{12}})(1 - \frac{2c_{12}}{c_{11}+c_{12}})}. \tag{B.7}$$

We obtained $s_{11}$ from Eq. (B.7),

$$s_{11} = \frac{c_{11} + c_{12}}{(c_{11} - c_{12})(c_{11} + 2c_{12})}. \tag{B.8}$$

And replacing Eq. (B.8) in Eq. (B.6) we get $s_{12}$,

$$s_{12} = \frac{-c_{12}}{(c_{11} - c_{12})(c_{11} + 2c_{12})}. \tag{B.9}$$

Finally,

$$s_{44} = \frac{1}{c_{44}}. \tag{B.10}$$

# Appendix C

# CRYSTALLOGRAPHIC DATA

The crystallographic data used in calculations, such as lattice parameters and atomic positions, was taken from the International Centre of Diffraction Data (ICDD) and Inorganic Crystal Structure Database (ICSD). In this appendix, the crystallographic data for tantalum, diamond and the binary tantalum compounds are summarized.

## Ta

```
04-0788                                              Wavelength= 1.54056        *
Ta                                          2θ     Int   h  k  l

Tantalum                                    38.472  100   1  1  0
                                            55.549   21   2  0  0
                                            69.581   38   2  1  1
                                            82.461   13   2  2  0
Rad.: CuKa1   λ: 1.5405   Filter: Ni   Beta    d-sp:  94.936   19   3  1  0
                                           107.640    7   2  2  2
Cut off:          Int.: Diffract.      I/Icor.:  4.44  121.349   29   3  2  1
Ref: Swanson, Tatge, Natl. Bur. Stand. (U.S.), Circ. 539, I, 29  137.491    4   4  0  0
(1953)

Sys.: Cubic                      S.G.: Im3̄m  (229)
a: 3.3058      b:        c:          A:          C:
α:             β:        γ:          Z: 2        mp:
Ref: Ibid.

Dx: 16.634     Dm:         SS/FOM: F 8 = 109(.0092 ,  8 )

Color: Gray
Pattern taken at 26 C. Sample procured from Johnson Matthey
Company, Ltd., London, England, UK. CAS #:  7440-25-7. The
material contained dissolved gases which caused broadening of
diffraction peaks, and TaH, which contributed extra reflections.
After annealing at 1500 C in vacuum for 30 minutes in a tantalum
boat, the sample gave very sharp reflections including only traces
of the hydride. Spectroscopic analysis shows faint traces of Nb, Al,
Si, Fe, Mn. Color from Merck Index, 8th Ed., p. 1012. W type. PSC:
cI2. Mwt: 180.95. Volume[CD]: 36.13.
```
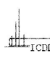
```
*data for   ICSD #76152
Coll Code   76152
Rec  Date   2000/12/16
Chem Name   Tantalum
Structured  Ta
Sum         Ta1
ANX         N
D(calc)     16.63
Title       Standard X-ray diffraction powder patterns I
Author(s)   Swanson, H.E.;Tatge, E.
Reference   National Bureau of Standards (U.S.), Circular
            (1953), 359, 1-95
Unit Cell   3.3058 3.3058 3.3058 90. 90. 90.
Vol         36.13
Z           2
Space Group I m -3 m
SG Number   229
Cryst Sys   cubic
Pearson     cI2
Wyckoff     a
Red Cell    I  2.862 2.862 2.862 109.471 109.471 109.471 18.063
Trans Red   0.500 0.500 -0.500 / -0.500 0.500 0.500 / 0.500 -0.500 0.500
Comments    The structure has been assigned a PDF number: 4-788
            Temperature in Kelvin: 298
            No R value given in the paper.
            At least one temperature factor missing in the paper.
Atom  #   OX   SITE      x           y          z          SOF      H
 Ta   1  +0    2 a   0           0          0          1.        0
*end for    ICSD #76152
```

# Diamond

| 79-1467 | | | | | Wavelength= 1.54056 | | H |
|---|---|---|---|---|---|---|---|

| C | | 2θ | Int | h | k | l |
|---|---|---|---|---|---|---|
| Carbon | | 43.933 | 999* | 1 | 1 | 1 |
| | | 75.30 | 266 | 2 | 2 | 0 |

Diamond 3C

Rad.: CuKa1   λ: 1.54060   Filter:                    d–sp: Calculated

Cut off: 17.7    Int.: Calculated        I/Icor.:   1.10
Ref: Calculated from ICSD using POWD-12++. (1997)
Ref: Ownby, P.D., Yang, X., Liu. J., J. Am. Ceram. Soc., 75,
1876 (1992)

Sys.: Cubic                    S.G.: Fd$\bar{3}$m (227)

| a: 3.5667 | b: | c: | A: | C: |
|---|---|---|---|---|
| α: | β: | γ: | Z: 8 | mp: |

Ref: Ibid.

Dx:  3.517       Dm:

Peak height intensity. C type. PSC: cF8. See PDF 6–675 and
PDF 75–0220. No R value given. At least one TF missing. Mwt:
12.01. Volume[CD]: 45.37.

```
COL   ICSD Collection Code 28863
DATE  Recorded Jan 1, 1980; updated Jun 26, 1998
NAME  Carbon
MINR  Diamond - from Belgian Congo, gray boart
FORM  C
      = C
TITL  Precision Determination of Lattice Parameter, Coefficient of
      Thermal Expansion and Atomic Weight of Carbon in Diamond
REF   Journal of the American Chemical Society
      JACSA 73 (1951) 5643-5646
AUT   Straumanis M E, AkaEZ
CELL  a=3.567(0) b=3.567(0) c=3.567(0) =90.0 =90.0 =90.0
      V=45.4 Z=8
SGR   F d -3 m S    (227) - cubic
CLAS  m-3m  (Hermann-Mauguin) - Oh  (Schoenflies)
PRS   cF8
ANX   N
PARM  Atom__No OxStat  Wyck -----X----- -----Y----- -----Z-----   -SOF-
      C      1  0.000    8a  0.          0.          0.
WYCK  a
REM   TEM 293
REM   M PDF 6-675
TEST  No R value given in the paper. (Code 51)
TEST  At least one temperature factor missing in the paper. (Code 53)
```

# TaC

       Wavelength= 1.54056    *

| 2θ | Int | h | k | l |
|---|---|---|---|---|
| 34.855 | 100 | 1 | 1 | 1 |
| 40.460 | 70 | 2 | 0 | 0 |
| 58.559 | 41 | 2 | 2 | 0 |
| 70.003 | 41 | 3 | 1 | 1 |
| 73.609 | 14 | 2 | 2 | 2 |
| 87.501 | 6 | 4 | 0 | 0 |
| 97.842 | 10 | 3 | 3 | 1 |
| 101.311 | 12 | 4 | 2 | 0 |
| 115.777 | 3 | 4 | 2 | 2 |
| 127.916 | 5 | 5 | 1 | 1 |

TaC

Tantalum Carbide

Tantalcarbide, syn

Rad.: CuKa1   λ: 1.540598   Filter: Graph Mono    d-sp: Diff.

Cut off:    Int.: Diffract.      I/Icor.:

Ref: Natl. Bur. Stand. (U.S.) Monogr. 25, 21, 124 (1984)

Sys.: Cubic       S.G.: Fm3m (225)

a: 4.4547(2)   b:    c:    A:    C:

α:    β:    γ:    Z: 4    mp:

Ref: Ibid.

Dx: 14.498    Dm:    SS/FOM: $F_{10}$ = 98(.0102 . 10)

Color: Dark brownish gray
Peak height intensity. The mean temperature of data collection
was 24.0 C. The sample was obtained from Aesar Division of
Johnson Matthey, Inc., Seabrook, New Hampshire, USA. CAS #:
12070-06-3. $\sigma(I_{obs})$= ±0.01. Cl Na type. Halite Group, carbide
Subgroup. Silver used as an internal stand. PSC: cF8. To replace
19-1292. Mwt: 192.96. Volume[CD]: 88.40.

```
COL   ICSD Collection Code 38239
DATE Recorded Jan 1, 1980; updated Jun 13, 1985
NAME Tantalum carbide (1/1)
FORM Ta C
     = C Ta
TITL Die Kristallstruktur von Tantalkarbid
REF  Metallwirtschaft, Metallwissenschaft, Metalltechnik
     METWA 12 (1933) 298
AUT  Schwarz M von, Summa0
CELL a=4.446(1) b=4.446 c=4.446 =90.0 =90.0 =90.0
     V=87.9 Z=4
SGR  F m -3 m       (225) - cubic
CLAS m-3m  (Hermann-Mauguin) - Oh  (Schoenflies)
PRS  cF8
ANX  NO
PARM Atom__No OxStat  Wyck -----X----- -----Y----- -----Z-----   -SOF-
     Ta    1  4.000   4a  0.            0.           0.
     C     1 -4.000   4b  1/2           1/2          1/2
WYCK b a
REM  XDP (X-ray diffraction from a powder)
TEST No R value given in the paper. (Code 51)
TEST At least one temperature factor missing in the paper. (Code 53)
```

# Ta$_2$C

| | | | | |
|---|---|---|---|---|
| Ta2C | | | | |
| | 2θ | Int | h k l | |
| Tantalum Carbide | 33.292 | 19 | 1 0 0 | |
| | 36.296 | 17 | 0 0 2 | |
| | 38.066 | 100 | 1 0 1 | |
| | 50.077 | 25 | 1 0 2 | |

| 2θ | Int | h | k | l |
|---|---|---|---|---|
| 33.292 | 19 | 1 | 0 | 0 |
| 36.296 | 17 | 0 | 0 | 2 |
| 38.066 | 100 | 1 | 0 | 1 |
| 50.077 | 25 | 1 | 0 | 2 |
| 59.471 | 31 | 1 | 1 | 0 |
| 66.493 | 45 | 1 | 0 | 3 |
| 69.877 | 6 | 2 | 0 | 0 |
| 71.714 | 45 | 1 | 1 | 2 |
| 72.868 | 25 | 2 | 0 | 1 |
| 77.175 | 5 | 0 | 0 | 4 |
| 81.419 | 10 | 2 | 0 | 2 |
| 86.711 | 10 | 1 | 0 | 4 |
| 95.453 | 23 | 2 | 0 | 3 |
| 98.603 | 7 | 2 | 1 | 0 |
| 101.513 | 45 | 2 | 1 | 1 |
| 105.811 | 35 | 1 | 1 | 4 |
| 110.234 | 16 | 2 | 1 | 2 |
| 112.409 | 21 | 1 | 0 | 5 |
| 115.798 | 8 | 2 | 0 | 4 |
| 118.628 | 20 | 3 | 0 | 0 |
| 126.027 | 70 | 2 | 1 | 3 |
| 132.361 | 45 | 3 | 0 | 2 |
| 138.799 | 6 | 0 | 0 | 6 |
| 150.846 | 65 | 2 | 0 | 5 |
| 156.476 | 32 | 3 | 0 | 3 |
| 157.774 | 48 | 2 | 1 | 4 |
| 166.20 | 85 | 2 | 2 | 0 |

Rad.:   λ:   Filter:   d-sp:

Cut off:   Int.: Diffract.   I/Icor.:

Ref: Korolev, M. et al., Russ. J. Inorg. Chem. (Engl. Transl.), 20, 159 (1975)

Sys.: Hexagonal      S.G.: P$\bar{3}$m1 (164)

a: 3.1046   b:   c: 4.9444   A:      C: 1.5926

α:   β:   γ:   Z: 1   mp:

Ref: Ibid.

Dx: 15.044   Dm:   SS/FOM: F$_{27}$ = 7(0.118 , 35)

Cell parameters generated by least squares refinement. Schonberg, Acta Chem. Scand., 8 620 (1954) found parameters to vary between a=3.094, c=4.918, C=1.590 and a=3.111, c=4.948, C=1.590, while Mirnova, S., Orment, Dokl. Akad. Nauk SSSR, 96 577 (1954) found them to increase from a=3.101, c=4.937, C=1.592 ( Ta C0.38 ) to a=3.104, c=4.941, C=1.592 ( Ta C0.59 ). Reference reports: a=3.1028, c=4.9374. Cd I2 type. PSC: hP3. To replace 18-1296. Mwt: 373.91. Volume[CD]: 41.27.

```
COL   ICSD Collection Code 409555
DATE  Recorded Sep 5, 2002;
NAME  Tantalum carbide (2/1)
FORM  Ta2 C
      = C1 Ta2
TITL  Refinement of the crystal structure of ditantalum monocarbide
REF   zeitschrift fuer kristallographie - New Crystal Structures
      (2001), 216, 329-330
AUT   Lissner, F.; Schleid, T.
CELL  a=3.1059(5) b=3.1059(5) c=4.9464(9) =90.0 =90.0 =120.0
      V=41.32 Z=1
SGR   P -3 m 1      (164) - trigonal/rhombohedral
CLAS  -3m1  (Hermann-Mauguin) - Oh  (Schoenflies)
PRS   hP3
ANX   NO
PARM  Atom__No OxStat  Wyck -----X----- -----Y----- -----Z-----  -SOF-
      C     1 -4.000   1a  0.          0.          0.            1.0
      Ta    1  2.000   2d  1/3         2/3         0.25201(8)    1.0
WYCK  d a
REM   XDP (X-ray diffraction from a powder)
TEST  No R value given in the paper. (Code 51)
TEST  At least one temperature factor missing in the paper. (Code 53)
```

# $\delta$-TaN

| | | | Wavelength= 1.54056 | | | |
|---|---|---|---|---|---|---|

TaN

Tantalum Nitride

| $2\theta$ | Int | h | k | l |
|---|---|---|---|---|
| 35.830 | 100 | 1 | 1 | 1 |
| 41.605 | 68 | 2 | 0 | 0 |
| 60.257 | 43 | 2 | 2 | 0 |
| 72.123 | 45 | 3 | 1 | 1 |
| 75.878 | 13 | 2 | 2 | 2 |
| 90.447 | 4 | 4 | 0 | 0 |
| 101.377 | 14 | 3 | 3 | 1 |
| 105.070 | 25 | 4 | 2 | 0 |

Rad.: CuKa   $\lambda$: 1.5418   Filter: Mono   d-sp: Diff.

Cut off:   Int.: Diffract.   I/Icor.:

Ref: Mashimo, T et al., J. Mater. Sci., 28, 3439 (1993)

Sys.: Cubic   S.G.: Fm$\bar{3}$m (225)

a: 4.3399(2)   b:   c:   A:   C:

$\alpha$:   $\beta$:   $\gamma$:   Z: [4]   mp:

Ref: Ibid.

Dx: 15.842   Dm:   SS/FOM: F$_8$ = 90(.0111 , 8)

Tantalum powder was nitrided at high temperature, then powdered,
sintered and enclosed in an iron capsule.  The sample was
shock-loaded using a tungsten flat-flyer plate. Composition
estimated from Ta N0.96 to Ta N0.99. Cell parameter generated by
least squares refinement. Reference reports: a=4.33635(16). Cl Na
type. Silicon. PSC: cF8. To replace 32-1283. Mwt: 194.95.
Volume[CD]: 81.74.

```
COL  ICSD Collection Code 76457
DATE Recorded Dec 16, 2000
NAME Tantalum Nitride - Hp, Epsilon
FORM Ta N
     N1 Ta1
TITL Ta N, eine neue Hochdruckform von Tantalnitrid
REF  Monatshefte fuer Chemie (-108,1977)
     (1972), 103, 794-798
     Journal of Solid State Chemistry
     (1977), 20, 205-207
AUT  Brauer, GP.;Mohr, E.;Neuhaus, A.;Skogan, A.
CELL a=5.186(1) b=5.186 c=2.913 =90.0 =90.0 =120.0
     V=67.85 Z=3
SGR  P 6/m m m      (191) - hexagonal
CLAS m-3m  (Hermann-Mauguin) - Oh  (Schoenflies)
PRS  hP6
ANX  AX
PARM Atom__No OxStat  Wyck -----X----- -----Y----- -----Z-----  -SOF-
     Ta    1 +3.000   3f  1/2        0.          0.
     N     1 -3.000   1a  0.         0.          0.
     N     1 -3.000   2d  0.3333     0.6667      0.5
WYCK f d a
REM  XDP (X-ray diffraction from a powder)
TEST No R value given in the paper. (Code 51)
TEST At least one temperature factor missing in the paper. (Code 53)
```

# $\epsilon$-TaN

Wavelength= 1.54056

| TaN | | | |
|---|---|---|---|

Tantalum Nitride

| $2\theta$ | Int | h | k | l |
|---|---|---|---|---|
| 30.705 | 4 | 0 | 0 | 1 |
| 34.522 | 100 | 1 | 1 | 0 |
| 36.772 | 78 | 1 | 0 | 1 |
| 46.877 | 12 | 1 | 1 | 1 |
| 51.332 | 28 | 2 | 0 | 1 |
| 61.855 | 14 | 3 | 0 | 0 |
| 63.345 | 23 | 2 | 1 | 1 |
| 63.989 | 5 | 0 | 0 | 2 |
| 70.649 | 2 | 3 | 0 | 1 |
| 72.812 | 8 | 2 | 2 | 0 |
| 74.800 | 13 | 1 | 1 | 2 |
| 76.270 | <1 | 3 | 1 | 0 |
| 81.057 | 1 | 2 | 2 | 1 |
| 84.483 | 7 | 3 | 1 | 1 |
| 94.551 | 3 | 4 | 0 | 1 |
| 95.138 | 7 | 3 | 0 | 2 |
| 103.458 | 4 | 4 | 1 | 0 |
| 104.805 | 5 | 3 | 2 | 1 |
| 105.211 | 3 | 0 | 0 | 3 |
| 105.415 | 4 | 2 | 2 | 2 |
| 108.761 | 2 | 1 | 0 | 3 |
| 111.881 | 1 | 4 | 1 | 1 |
| 116.028 | <1 | 1 | 1 | 3 |
| 119.835 | 3 | 2 | 0 | 3 |
| 125.794 | 2 | 3 | 3 | 0 |
| 127.374 | 2 | 5 | 0 | 1 |
| 132.374 | 3 | 2 | 1 | 3 |

Rad.: CuKa1    λ: 1.540598    Filter: Graph Mono    d-sp: Diff.

Cut off:   5.0    Int.: Diffract.    I/Icor.:

Ref: Wong-Ng, W., McMurdie, H., Paretzkin, B., Hubbard, C.,
Dragoo, A., NBS (USA), ICDD Grant-in-Aid, (1987)

Sys.: Hexagonal    S.G.: P6/mmm (191)

a: 5.1918(3)    b:    c: 2.9081(2)    A:    C: 0.5601

α:    β:    γ:    Z: 3    mp:

Ref: Wong-Ng, W et al., Powder Diffraction, 3, 120 (1988)

Dx: 14.306    Dm:    SS/FOM: $F_{27}$ = 60(.0116 , 39)

Color: Black
Peak height intensity. The mean temperature of data collection
was 23.7 C. The sample was obtained from Johnson Matthey,
Incorporated, Seabrook, New Hampshire, USA. CAS #:  12033-62-4. The
sample contained a small amount of Ta5 N4. The structure of TaN
was studied by Brauer and Zapp (1). Co Sn type. Silicon,
fluorophlogopite used as an internal stands. PSC: hP6. To replace
9-257, Brauer and Zapp (1). Mwt: 194.95. Volume[CD]: 67.89.

```
COL   ICSD Collection Code 76456
DATE Recorded Dec 16, 2000
NAME Tantalum Nitride - Ht, Delta
FORM Ta N
   TITL Das kubische Tantalmononitrid (B1-Typ) und seine Mischbarkeit mit den
       isotypen Uebergangsmetallnitriden und -carbiden
REF  Monatshefte fuer Chemie (-108,1977)
     (1975), 106, 1137-1147
     Fizika Metallov i Metallovedenie
     (1975), 40, 177-179
     Acta Crystallographica A (24,1968-38,1982)
     (1975), 31, 99-99
AUT  Gatterer, J.;Dufek, G.;Ettmayer, P.;Kieffer, R.
CELL a=4.331 b=4.331 c=4.331 =90.0 =90.0 =90.0
     V= 81.24 Z=4
SGR  F m -3 m         (225) - cubic
CLAS 23    (Hermann-Mauguin) - T   (Schoenflies)
PRS  cF12
ANX  AX
PARM Atom__No OxStat  Wyck -----X----- -----Y----- -----Z-----   -SOF-
     Ta   1  3.000   4b  1/2         1/2         1/2
     N    1 -3.000   4a  0.          0.          0.
WYCK b a
REM  XDP (X-ray diffraction from a powder)
TEST No R value given in the paper. (Code 51)
TEST At least one temperature factor missing in the paper. (Code 53)
```

# Appendix D

# ABINIT FILES

As examples, some input files for the ABINIT code are shown. These calculations are about the ABINIT geometry optimization of the phases $\delta$ and $\epsilon$ of TaN, and the calculation of phonons at the $\Gamma$ point and one specific wave vector for TaC and Ta$_2$C.

## $\delta$-TaN

```
#####################################################################
# TaN-d (cubic) : optimization of cell parameter,
# ngkpt 8x8x8, ecut 60.0 Ha, nband 12, nshift 4,
# acell 8.1867  value obtained from Geo. opt. by Abinit
#####################################################################

ndtset 20
acell:  7.81 7.81 7.81 acell+ 0.03 0.03 0.03

########### Specific to ground state calculation
  kptopt   1             # Automatic generation of k points, taking
                         # into account the symmetry
  tolvrs   1.0d-16       # SCF stopping criterion
  iscf     5             # Self-consistent calculation, using algorithm 5

#####################################################################
#Common input variables

#######  Definition of the unit cell

rprim   0.0  0.5  0.5   # this matrix converts the atoms positions
        0.5  0.0  0.5   # from the crystalline system to the lattice
        0.5  0.5  0.0   # system.

#Definition of the atom types
ntype 2                # two type of atoms
zatnum 73  7           # The keyword "zatnum" refers to the atomic number of the
                       # possible type(s) of atom. The pseudopotential(s)
                       # mentioned in the "files" file must correspond
                       # to the type(s) of atom. Here, type 1 is Ta and type 2 is N.


#Definition of the atoms
natom 2                # There are two atom
type 1  2              # The type 1 is (Ta), and type 2 (N)
xred                   # This keyword indicate that the location of the atoms
                       # will follow, one triplet of number for each atom
   0.5  0.5  0.5       # Triplet giving the REDUCED coordinate of atom 1. (Ta)
   0.0  0.0  0.0       # Triplet giving the REDUCED coordinate of atom 2. (N)
```

```
#Gives the number of band, explicitely (do not take the default)
nband  12              # number of bands (Ta has 13 -e, and N has 5-e, and there are 1 atom
                       # of each one, so we need a minimun of more of 8 bands)
occopt  3              # d-TaN is metallic
tsmear 0.01


#Definition of the planewave basis set

ecut   60.0    # Maximal kinetic energy cut-off, in Hartree

ngkpt 8 8 8

nshift 4
shiftk 0.5 0.5 0.5
       0.5 0.0 0.0
       0.0 0.5 0.0
       0.0 0.0 0.5

#Definition of the SCF procedure
nstep 50               # Maximal number of SCF cycles
diemac 1.0d+6          # Although this is not mandatory, it is worth to
                       # precondition the SCF cycle. The model dielectric
prtwf  0               # No will print the wave functions files.
```

## $\epsilon$-TaN

```
########################################################################
# TaN-e: Geometry optimization by ABINIT.
#        acell a=b= 9.8034, c=5.5066 Bohr
#        ecut  Ha, ngkpt x x , nband 40, nshift 1.
#        Hexagonal P6/mm (191).
########################################################################


##########   Automatic geometry optimization

optcell  1
ionmov   3
ntime    50
dilatmx  1.05
ecutsm   0.5


##########   Specific to ground state calculation
  kptopt   1              # Automatic generation of k points, taking
                          # into account the symmetry
  tolvrs   1.0d-16        # SCF stopping criterion
  iscf     5              # Self-consistent calculation, using algorithm 5


########################################################################
#Common input variables

#--------- Definition of the unit cell --------
acell 2*9.8034 5.5066   #

angdeg 90 90 120         # definition of hexagonal lattice

#--------- Definition of the atom types --------
ntypat 2                 # Two type of atoms.
zatnum 73  7             # The keyword "zatnum" refers to the atomic number of the
                         # possible type(s) of atom. The pseudopotential(s)
                         # mentioned in the "files" file must correspond
                         # to the type(s) of atom. Here, type 1 is the tantalum and 2 is N.


#--------- Definition of the atoms --------
natom 6                  # There are 6 atoms.
typat 1 1 1 2 2 2        # The type 1 is Ta, and type 2 is N.
xred                     # This keyword indicate the location of the atoms
   0.5    0.0     0.0  # Ta atom
   0.0    0.5     0.0  # Ta atom
   0.5    0.5     0.0  # Ta atom
   0.0    0.0     0.0  # N atom
   1/3    2/3     0.5  # N atom
   2/3    1/3     0.5  # N atom

nband  40                # number of bands (Ta has 13 -e, and N has 5-e, and there are 4 atoms.
                         # of each one, so we need minimun 34 bands)
occopt  3                # TaN-e is a metal.
tsmear 0.01

#--------- Exchange-correlation functional--------
ixc 1                    # LDA HGH.

#---------- Definition of the planewave basis set -------------
ecut   60.0    # Maximal kinetic energy cut-off, in Hartree.
```

```
#--------- Definition of the k-point grid set ------
ngkpt 4 4 8                # This is a grid based on the primitive vectors
                          # of the reciprocal space
                          # repeated one time, with differents shifts.
nshift 1                  # nshift and shift values recommended in the ABINIT list of variables
shiftk 0.0 0.0 0.5

#--------- Definition of the SCF procedure --------
nstep 100                 # Maximal number of SCF cycles.
diemac 1.0d+6             # Although this variable is not mandatory, it is worth to
                          # precondition the SCF cycle.
# -------- Use of memory -----------------------
mkmem  0
mkqmem 0
mk1mem 0
```

# TaC

```
#######################################################################
# TaC : computation of the dynamical matrix at gamma  q=(0 0 0)
#######################################################################

#Response Function calculation for the gamma point------------
  rfphon   1                # Activate the calculation of the atomic dispacement perturbations
 rfatpol   1 2              # All the atoms will be displaced
   rfdir   1 1 1            # Need to consider the perturbation in the z-direction only

    nqpt   1
     qpt   0.0 0.0 0.0

  irdwfk   1                # Uses as input wfs the output wfs of the dataset 1

  kptopt   2                # Automatic generation of k points.

    iscf   5                # Self-consistent calculation, using algorithm 5.
  tolvrs   1.0d-8

#######################################################################
#Common input variables

#--------  Definition of the unit cell
acell  3*8.5566            # Value obtained from geo. opt. by abinit.
rprim   0.0  0.5  0.5      # This matrix converts the atoms positions
        0.5  0.0  0.5      # from the crystalline system to the lattice
        0.5  0.5  0.0      # system.

#-------   Definition of the atom types
ntypat 2                   # Two type of atoms.
znucl 73  6                # The keyword "zatnum" refers to the atomic number of the
                           # possible type(s) of atom. The pseudopotential(s)
                           # mentioned in the "files" file must correspond
                           # to the type(s) of atom. Here, type 1 is Ta and type 2 is C.

#--------- Definition of the atoms
natom 2                    # There are 2 atoms.
typat 1  2                 # The type 1 is Ta, and type 2 C.
xred                       # This keyword indicate that the location of the atoms
   0.0  0.0  0.0           # will follow, one triplet of number for each atom.
   0.5  0.5  0.5           # Triplet giving the REDUCED coordinate of atom 1.
                           # Triplet giving the REDUCED coordinate of atom 2.

#Gives the number of band, explicitely (do not take the default)
nband  20                  # Number of bands (Ta has 13 -e, and C has 4-e, and there are 2 atoms
                           # of each one, so we need a minimun of 9 bands).
occopt  3                  # TaC is a metal.
tsmear  0.01
#--------- Exchange-correlation functional--------
ixc 11                     # GGA, Perdew-Burke-Ernzerhof GGA functional.

#--------- Definition of the planewave basis set
ecut   50.0                # Maximal kinetic energy cut-off, in Hartree.


#--------- Definition of the k-point grid set ----
```

```
ngkpt 8 8 8              # This is a grid based on the primitive vectors
                         # of the reciprocal space (that form a FCC laticce!),
                         # repeated one time, with differents shifts.
nshift 4
shiftk 0.5 0.5 0.5
       0.5 0.0 0.0
       0.0 0.5 0.0
       0.0 0.0 0.5

#--------- Definition of the SCF procedure --------
nstep 100                # Maximal number of SCF cycles.
diemac 1.0d+6            # Although this is not mandatory, it is worth to
                         # precondition the SCF cycle.

# -------- Use of memory ------------------------
mkmem  0
mkqmem 0
mk1mem 0
```

```
########################################################################
# TaC : computation of the dynamical matrix at q=[xxx]=(0.5 0.5 0.5)
########################################################################

ndtset 3

#-------------------------------------------------------------------
#Specific to ground state calculation-----DATASET 1------------------

  kptopt1   1                 # Automatic generation of k points, taking
                              # into account the symmetry.
    iscf1   5                 # Self-consistent calculation, using algorithm 5.
  tolvrs1   1.0d-18           # SCF stopping criterion.
  prtden1   1                 # Will be needed for dataset 2.
#-------------------------------------------------------------------

#Response Function calculation for --------DATASET 2 ----------------

#Non-self consistent ground-state calculation, with q=(0.5 0.5 0.5)
    nqpt2   1
     qpt2   0.5 0.5 0.5 #

  getwfk2   1                 # Uses as input wfs the output wfs of the dataset 1.
  getden2   1                 # Uses as input density the output density of the dataset 1.

  kptopt2   3                 # Automatic generation of k points,
                              # no use of symetries to decrease
                              # the size of the k-point set.
    iscf2  -3                 # Non-self-consistent calculation.
  tolwfr2   1.0d-16

 #Response Function calculation for --------DATASET 3----------------
  rfphon3   1                 # Activate the calculation of the atomic dispacement perturbations.
 rfatpol3   1 3               # All the atoms will be displaced.
   rfdir3   1 1 1             # Need to consider the perturbation in the x-direction only.

    nqpt3   1
     qpt3   0.5 0.5 0.5 #

  getwfk3   1                 # Uses as input wfs the output wfs of the dataset 1.
  getwfq3   2                 # Uses as input ddk wfs the output of the dataset 2.

  kptopt3   3                 # Automatic generation of k points,
                              # no use of symetries to decrease
                              # the size of the k-point set.
    iscf3   5                 # Self-consistent calculation, using algorithm 5.
  tolvrs3   1.0d-8


########################################################################
#Common input variables

#-------- Definition of the unit cell
acell  3*8.5566         # Value obtained from geo. opt. by abinit.
rprim   0.0  0.5  0.5   # This matrix converts the atoms positions
        0.5  0.0  0.5   # from the crystalline system to the lattice
        0.5  0.5  0.0   # system.

#-------   Definition of the atom types
```

```
ntypat 2                 # Two type of atoms.
znucl 73  6              # The keyword "zatnum" refers to the atomic number of the
                         # possible type(s) of atom. The pseudopotential(s)
                         # mentioned in the "files" file must correspond
                         # to the type(s) of atom. Here, type 1 is Ta and type 2 is C.


#--------- Definition of the atoms
natom 2                  # There are 2 atoms.
typat 1  2               # The type 1 is Ta, and type 2 C.
xred                     # This keyword indicate that the location of the atoms
   0.0  0.0  0.0         # will follow, one triplet of number for each atom.
   0.5  0.5  0.5         # Triplet giving the REDUCED coordinate of atom 1.
                         # Triplet giving the REDUCED coordinate of atom 2.


#Gives the number of band, explicitly (do not take the default)
nband  20                # Number of bands (Ta has 13 -e, and C has 4-e, and there are 2 atoms
                         # of each one, so we need a minimun of 9 bands).
occopt  3                # TaC is a metal.
tsmear  0.01
#--------- Exchange-correlation functional--------
ixc 11                   # GGA, Perdew-Burke-Ernzerhof GGA functional.


#--------- Definition of the planewave basis set
ecut   50.0              # Maximal kinetic energy cut-off, in Hartree.



#--------- Definition of the k-point grid set ----
ngkpt 8 8 8              # This is a grid based on the primitive vectors
                         # of the reciprocal space (that form a FCC laticce!),
                         # repeated one time, with differents shifts.
nshift 4
shiftk 0.5 0.5 0.5
       0.5 0.0 0.0
       0.0 0.5 0.0
       0.0 0.0 0.5


#--------- Definition of the SCF procedure --------
nstep 100                # Maximal number of SCF cycles.
diemac 1.0d+6            # Although this is not mandatory, it is worth to
                         # precondition the SCF cycle.


# -------- Use of memory ------------------------
mkmem  0
mkqmem 0
mk1mem 0
```

# Ta$_2$C

```
###################################################################
# Ta2C(trigona\rhombohedral): computation of the dynamical matrix at gamma  q=(0 0 0)
###################################################################

ndtset 2

#Response Function calculation for the gamma point------------
  rfphon   1                # Activate the calculation of the atomic dispacement perturbations
 rfatpol   1 2              # All the atoms will be displaced
   rfdir   1 1 1            # Need to consider the perturbation in the z-direction only

    nqpt   1
     qpt   0.0 0.0 0.0

  irdwfk   1                # Uses as input wfs the output wfs of the dataset 1

  kptopt   2                # Automatic generation of k points.

    iscf   5                # Self-consistent calculation, using algorithm 5.
  tolvrs   1.0d-8

####################################################################
#Common input variables

#--------- Definition of the unit cell------

acell 2*5.84 9.145

spgroup 164              # Space group.
spgaxor 1                # Orientation of the unit cell axis: 1 hexagonal axes.
brvltt  1                # Type of Bravais lattice, primitive with no associative translation.
angdeg 90 90 120         # Definition of hexagonal lattice. "Replaces rprim".

#---------- Definition of the atom types -----------
ntypat 2                 # Two type of atoms.
znucl  73  6             # The keyword "zatnum" refers to the atomic number of the
                         # possible type(s) of atom. The pseudopotential(s)
                         # mentioned in the "files" file must correspond
                         # to the type(s) of atom. Here, type 1 is Ta and type 2 is C.

#---------- Definition of the atoms------------------
natom 3                  # There are 3 atoms.
typat 1 1 2              # The type 1 is C, and type 2 Ta.
xred                     # This keyword indicate that the location of the atoms:
   0.33333333333333333333  0.66666666666666666667  0.2520   # Ta
   0.66666666666666666667  0.33333333333333333333 -0.2520   # Ta
   0.0     0.0     0.0        # C

#Gives the number of band, explicitely (do not take the default)
nband  20                # number of bands (Ta has 13 -e, and C has 4-e, and there are 2 Ta atoms.
                         # and 1 C atoms, so we need a minimun of 15 bands).
occopt  3                # Ta2C is a metal.
tsmear 0.01
#--------- Exchange-correlation functional--------
ixc 1                    # LDA.
```

```
#--------- Definition of the planewave basis set
ecut    50.0                # Maximal kinetic energy cut-off, in Hartree.

#--------- Definition of the planewave basis set -------------------

ngkpt 8 8 4                 # This is a grid based on the primitive vectors
                           # of the reciprocal space
                           # repeated one time, with differents shifts:
nshift 1                    # nshift and shift values recommended in the ABINIT list of variables.
shiftk 0.0 0.0 0.5

#--------- Definition of the SCF procedure-------------------------
nstep 100                   # Maximal number of SCF cycles.
diemac 1.0d+6               # For metals this should be large.

# -------- Use of memory -----------------------
mkmem   0
mkqmem 0
mk1mem 0
```

```
####################################################################
# Ta2C(trigona\rhombohedral) :computation of the dynamical matrix at q=[00x]
#                              =(0 0 0.2)
####################################################################

ndtset 3

#-------------------------------------------------------------------
#Specific to ground state calculation-----DATASET 1------------------

  kptopt1   1               # Automatic generation of k points, taking
                            # into account the symmetry.
    iscf1   5               # Self-consistent calculation, using algorithm 5.
  tolvrs1   1.0d-18         # SCF stopping criterion.
  prtden1   1               # Will be needed for dataset 2.
#-------------------------------------------------------------------

#Response Function calculation for --------DATASET 2 -----------------

#Non-self consistent ground-state calculation, with q=(0 0 0.2)
    nqpt2   1
     qpt2   0 0 0.2

  getwfk2   1               # Uses as input wfs the output wfs of the dataset 1.
  getden2   1               # Uses as input density the output density of the dataset 1.

  kptopt2   3               # Automatic generation of k points,
                            # no use of symetries to decrease
                            # the size of the k-point set.
    iscf2  -3               # Non-self-consistent calculation.
  tolwfr2   1.0d-16

 #Response Function calculation for --------DATASET 3----------------
  rfphon3   1               # Activate the calculation of the atomic dispacement perturbations.
 rfatpol3   1 3             # All the atoms will be displaced.
   rfdir3   1 1 1           # Need to consider the perturbation in the x-direction only.

    nqpt3   1
     qpt3   0 0 0.2

  getwfk3   1               # Uses as input wfs the output wfs of the dataset 1.
  getwfq3   2               # Uses as input ddk wfs the output of the dataset 2.

  kptopt3   3               # Automatic generation of k points,
                            # no use of symetries to decrease
                            # the size of the k-point set.
    iscf3   3               # Self-consistent calculation, using algorithm 3.
  tolvrs3   1.0d-8

#####################################################################

#Common input variables
#--------- Definition of the unit cell------

acell 2*5.84 9.145

spgroup 164          # Space group.
spgaxor 1            # Orientation of the unit cell axis: 1 hexagonal axes.
brvltt 1             # Type of Bravais lattice, primitive with no associative translation.
```

```
angdeg 90 90 120       # Definition of hexagonal lattice. "Replaces rprim".


#---------- Definition of the atom types -----------
ntypat 2               # Two type of atoms.
znucl  73  6           # The keyword "zatnum" refers to the atomic number of the
                       # possible type(s) of atom. The pseudopotential(s)
                       # mentioned in the "files" file must correspond
                       # to the type(s) of atom. Here, type 1 is Ta and type 2 is C.


#---------- Definition of the atoms------------------
natom 3                # There are 3 atoms.
typat 1 1 2            # The type 1 is C, and type 2 Ta.
xred                   # This keyword indicate that the location of the atoms:
   0.33333333333333333333   0.66666666666666666667   0.2520   # Ta
   0.66666666666666666667   0.33333333333333333333  -0.2520   # Ta
   0.0      0.0      0.0  # C

#Gives the number of band, explicitely (do not take the default)
nband  20              # number of bands (Ta has 13 -e, and C has 4-e, and there are 2 Ta atoms.
                       # and 1 C atoms, so we need a minimun of 15 bands).
occopt  3              # Ta2C is a metal.
tsmear 0.01
#--------- Exchange-correlation functional--------
ixc 1                  # LDA.


#--------- Definition of the planewave basis set
ecut   50.0              # Maximal kinetic energy cut-off, in Hartree.


#--------- Definition of the planewave basis set -------------------

ngkpt 8 8 4              # This is a grid based on the primitive vectors
                        # of the reciprocal space
                        # repeated one time, with differents shifts:
nshift 1                # nshift and shift values recommended in the ABINIT list of variables.
shiftk 0.0 0.0 0.5


#--------- Definition of the SCF procedure-------------------------
nstep 100               # Maximal number of SCF cycles.
diemac 1.0d+6           # For metals this should be large.

# -------- Use of memory ------------------------
mkmem  0
mkqmem 0
mk1mem 0
```